SPECTRUM SHARING IN COGNITIVE RADIO NETWORKS

Waqas Ahmed
MS Systems Eng.

CENTRE FOR TELECOMMUNICATIONS AND MICRO-ELECTRONICS,
FACULTY OF HEALTH, ENGINEERING AND SCIENCE,
VICTORIA UNIVERSITY

SUBMITTED IN FULFILLMENT OF THE
REQUIREMENTS OF THE DEGREE OF
DOCTOR OF PHILOSOPHY

JUNE 2012

VICTORIA UNIVERSITY

"I, Waqas Ahmed, declare that the PhD thesis entitled 'THESIS TITLE' is no more than 100,000 words in length including quotes and exclusive of tables, figures, appendices, bibliography, references and footnotes. This thesis contains no material that has been submitted previously, in whole or in part, for the award of any other academic degree or diploma. Except where otherwise indicated, this thesis is my own work."

Signature: ______________________
Waqas Ahmed

Date: ______________________

Abstract

Years of growth in wireless communication services and conservative spectrum allocation policies by government regulators have led to spectrum scarcity. On the other hand, spectrum measurement campaigns have indicated that the actual occupancy of most licensed frequency bands is quite low. In recent years, Cognitive radio has emerged as a promising solution to increase spectrum occupancy and tackle spectrum scarcity. Cognitive radio enables the unlicensed (secondary) user to establish a communication link in licensed spectrum on the condition that there is no or minimal interference to the licensee (primary user).

In this thesis, the two main facets of spectrum sharing in cognitive radio networks are investigated; interweave access and underlay access. The former is an orthogonal scheme, where the secondary user only transmits in white space (idle primary user spectrum). The latter is a shared scheme in which concurrent primary and secondary transmission is allowed, subject to any co-channel interference at the primary being below an acceptable limit. In the first part of the thesis, the quality of service for a group of secondary users is analysed in an interweave access

senario. A continuous time Markov model is used to calculate the forced termination probability, blocking probability and throughput. The impact of spectrum handoff and channel reservation is investigated and the optimal operating regions are identified. Spectrum handoff gave the largest throughput improvement. The analysis was further extended to study the airtime fairness between two secondary user groups with different traffic statistics. At this juncture, the assumption of orthogonality between the primary and secondary transmissions was relaxed leading to the underlay spectrum access paradigm.

In the second part of the thesis, an underlay sensing and access architecture is proposed based on the measurements carried out in our laboratory. This architecture empowers a secondary femtocell to coexist in the downlink channels of a primary macrocell. The distance dependent and average cell-wide outage probabilities of the primary macrocell user are derived. Situations where the femtocell sensing and transmission paths are not co-located can cause a doubling of the primary macrocell user's additional outage. The effectiveness of the femtocell transmission is also investigated and cell sizes between $20 - 50$m are possible. As a byproduct of this analysis, it was shown that the femtocell transmission opportunities can be modelled by a Log-Skew normal distribution for a shadow fading environment.

The final part of the thesis addresses a fundamental problem in underlay access network; the quantification of the Signal to Interference plus Noise distribution. Bounds of the distribution are derived using Steffensen's inequality. It is shown that the possibility of obtaining trivial bounds can be circumvented by exploiting the unimodality of the interfering path's probability density function. The effectiveness of the bounds is demonstrated on a gamma-gamma wireless fading channel.

This thesis can be very useful in understanding the performance limits of interweave and underlay access modes. Several interesting, accurate and previously unknown results are presented, which can be beneficial for cognitive radio network analysis and design. In addition, the concepts of underlay transmission exploiting duplexing features and integral inequalities to quantify physical layer performance can motivate further research.

Acknowledgements

First of all, I thank Almighty ALLAH for giving me strength and ability to complete this thesis. I would like to thank my supervisor, Prof. Michael Faulkner, for his guidance and support during my PhD studies. This dissertation would never have been possible without his belief in my abilities. I admire his dedication, and hard work.

I would like to express my deep and sincere gratitude to Dr. Jason Gao, with whom I spent countless hours discussing and refining my ideas. I am grateful to Dr. Himal Suraweera and Dr. Mansoor Shafi for their technical guidance. I would also like to give thanks to Dr Daniel Lai. Despite his busy schedule he has spent lots of time to review and critique my thesis. My deepest gratitude to Prof. Stephen Collins, Prof. Aladdin Zayegh, Dr. Philip Conder and Lance Linton for their support in my research. I am thankful to the administrative staff of CTME, Office of Postgraduate Research and Faculty of Health Engineering and Science, in particular, Shukonya Benka, Elizabeth Smith, Lesley Birch, Sue Davies, Natalie Gloster and Angela Rojter.

I would like to thank all the past and present CTME students and my warmest wishes to all those who have encouraged me during this tough time. So a big thank you to Micheal, Vandana Rizwan, Robab, Mustafa, Shabbir, Shahryar, Kevin, Alamgir, Venkat, Rahele, Reza, Hadi, Hojjat, Zaheer, Faizan and Asyik. Finally, I would like to thank my family; parents, wife, brothers, and sisters for their love, encouragement and support.

To my loving wife Nabia and my son Hashim

Table of Contents

List of Figures

List of Tables

List of Abbreviations

3G	Third Generation
4G	Fourth Generation
BAS	Basic Access Scheme
CEFC	Cognitive Radio Empowered Femtocell
CDF	Cumulative Distribution Function
CR	Cognitive Radio
CRN	Cognitive Radio Network
CTMC	Continuous Time Markov Chain
DL	Downlink
FCC	Federal Communications Commission
FDD	Frequency Division Duplex
FC	Femtocell
GHQ	Gaussian Hermite Quadrature
GMQ	Gaussian Moment Quadrature
GSM	Global System for Mobile Communications
HA	Heuristic Approximation
IEEE	Institute of Electrical and Electronics Engineering
i.i.d	independent and identically distributed
KS	Kolmogorov-Smirnov
LTE	3GPP Long Term Evolution
MHz	Mega Hertz
ND	Normal Distribution
Ofcom	Office of Communications
OFDM	Orthogonal Frequency Division Multiplexing

OSA	Opportunistic Spectrum Access
PAS	Probabilistic Access Scheme
PBS	Primary Base Station
PDF	Probability Density Function
PPP	Poisson Point Process
PU	Primary User
PUE	Primary User Equipment
QoS	Quality of Service
RB	Resource Blocks
REM	Radio Environment Map
SBS	Secondary Base Station
SINR	Signal to Interference plus Noise Ratio
SIR	Signal to Interference Ratio
SND	Skew Normal Distribution
SNR	Signal to Noise Ratio
SU	Secondary User
SUE	Secondary User Equipment
TDD	Time Division Duplex
TDMA	Time Division Multiple Access
TV	Television
UL	Uplink
US	United States
UWB	Ultra Wide Band

Chapter 1

Introduction

Reliable and fast wireless data transmission is emerging as a global phenomenon and becoming a major consideration in our lives such as internet, online shopping, and social networking. This has caused an exponential increase in the demand for the radio frequency spectrum. However, conservative spectrum allocation policies have created a shortage of vacant spectrum bands (channels). The US frequency allocation given in [1] indicates that there is little room for any new allocation in the most useful frequency bands (<3GHz) for wireless communications. On the other hand, recent studies conducted by the Federal Communications Commission (FCC) in the United States [2] and Ofcom in the United Kingdom [3] have found that the average utilization in licensed frequency bands is as low as 5%. This is also indicated by the spectrum measurements carried out in our laboratory within a range of 1MHz to 1Ghz, which show large swathes of inactive spectrum (Fig. 1.1).

Based on these measurements [2], FCC concluded that there are two basic scenarios to improve the spectrum efficiency of the licensed bands. In the first scenario, where the spectrum is fully utilised, the spectrum efficiency can be improved in terms of bits per second per Hertz (bps/Hz), by using better radio access technologies. In

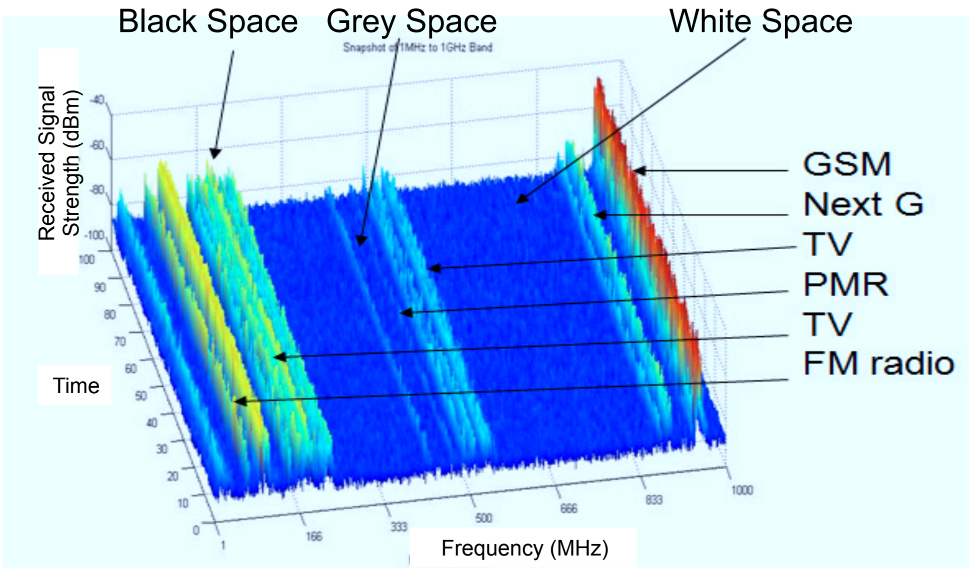

Figure 1.1: Spectrum measurements.

the second scenario, where the spectrum usage is relatively low over time, the spectrum efficiency can be improved by increasing the access efficiency i.e. allowing access of unlicensed (secondary) devices to the licensed (primary) frequency bands.

Up until recently, most research has been concentrated on improving spectrum efficiency in bps/Hz. There has, however, been an increase in research effort directed towards increasing access efficiency through spectrum sharing. One of the key enabling technologies in this push is cognitive radio (CR), which was originally proposed by Mitola [4]. CR enables the secondary user (SU) to build transmission links in vacant PU channels such that there is no/minimum interference to PUs. Realisation of such an operation requires the CR to have the following functionalities: spectrum sensing; spectrum access; spectrum allocation and management among different SUs; and a reconfigurable hardware [4]-[7].

Although various SU transmission modes of SU have been discussed/proposed in the literature, they can be broadly categorized into two modes: interference avoidance (white space) mode and the interference management (black and grey space) mode [5].

1.0.1 Interference Avoidance

The interference avoidance mode is often termed as interweave access. In interweave access, the SU finds spectrum holes (white space) by sensing the radio frequency spectrum. The presence of spectrum holes in the PU channels are highlighted in Fig. 1.2. These spectrum holes are used by the SU for its transmission. This scheme is often referred to as opportunistic spectrum access (OSA). No concurrent transmission of the PU and the SU is allowed. The SU must vacate the channel as soon as the PU reappears, which leads to the forced termination of the SU connection (if there is no other available channel for the SU). Since the SU has no control over the resource availability, the transmission of the SU is blocked when the channel is occupied by the PU. The forced termination and blocking of a SU connection is shown in Fig. 1.3. The forced termination probability and blocking probability are the key parameters which determine the throughput of the SU, and thus its viable existence. The forced termination depends on the traffic behaviour of the PUs and the SUs (e.g. arrival rates, service time etc.). In the case of multiple SU groups with different traffic statistics, the forced termination and blocking probabilities lead to unfairness among the SU groups. The QoS provisioning task becomes difficult.

1.0.2 Interference Management

The interference management mode in a CR can be categorized as overlay and underlay. Both these techniques allow concurrent transmission. The *Overlay mode*

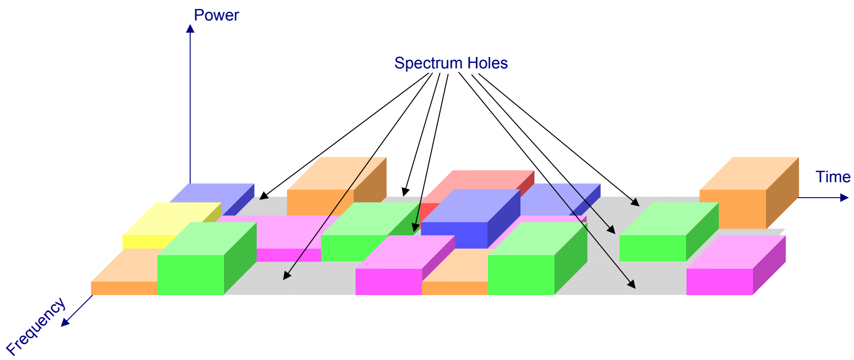

Figure 1.2: Conceptual view of spectrum holes for interweave approach.

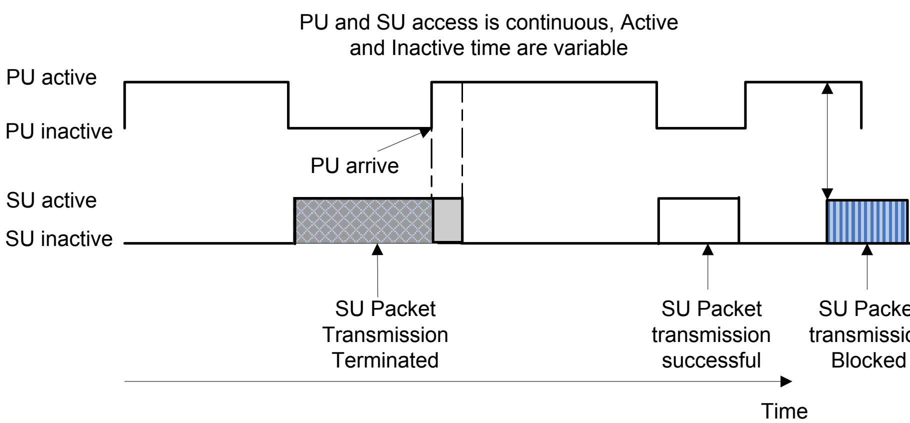

Figure 1.3: Illustration of forced termination and blocking.

refers to a technique in which the SU exploits additional knowledge of the PU transmissions. It increases its transmission opportunities by enhancing the PU messages, and relies on dirty paper coding techniques to mitigate interference at its own receiver [8]. This access mode has also been studied under the heading of CR enabled cooperative relaying [9].

The *Underlay mode* refers to a technique in which the SU can only share the spectrum, as long as its signal remains below the acceptable interference limit of the PU. This threshold is the peak or average power that can be tolerated by the PU receiver [10][11]. This constraint is useful when the signal variation at the PU receiver is quasi-static, such as Television unit. However, when signal variations from the PU transmitter to the PU receiver are random, outage probability is a better measure. Outage at the PU receiver occurs when the Signal Interference plus Noise Ratio (SINR) falls below a certain threshold (different from the interference threshold). The spectrum sharing constraint in this scenario is based on the long term outage or short term outages acceptable to the PU network. The SU transmit power is a key factor which determines its coexistence in an underlay mode. Due to the strict transmit power constraint, the coverage area of the secondary network in an underlay mode is very restricted [8]. Generally, the calculation of SU transmit power requires the knowledge of PU receiver location and the channel gains between the SU transmitter-PU receiver and PU transmitter- PU receiver. Since the SU operates independently of the PU network, these parameters are often unknown to the SU transmitter and must be estimated. This comes at a cost of increased signalling overhead.

In recent years, it has been envisaged that the potential of the CR underlay paradigm can be applied for interference management by the PU itself, such as femtocells [12][13]. The possibility of a CR empowered femtocell (FC) has also been considered as a viable solution [14] to increase spectrum availability for cellular operators. In short, a FC enables the reuse of macrocell (coverage area of primary base station) frequencies in a cellular network over a small range with the primary aim of improving indoor coverage [15]. The FC consists of a low power femtocell base station which is connected to a backbone network by DSL or cable internet. In the case of multiple FCs, the interference problem becomes two tier [16] i.e, macrocell to FC (cross-tier) and FC to FC (inner-tier). By introducing additional information through a sensing phase (similar to a CR), two-tier interference can be avoided in FC deployments.

In underlay mode it is often necessary to derive the SINR distribution, in order to calculate practical performance measures such as capacity and SINR outage [17] [18]. The propagation channel between the PU and the SU is generally subject to fading which is traditionally modelled by a gamma or lognormal distribution [19]. The cumulative distribution function (CDF) for the SIR is often known in closed form [11]. However, in the case of SINR, which include the effect of noise, these models yield integrals for which closed form expressions are not known. Although integral inequalities [20] have successfully been applied to obtain bounds on capacity problems [21]-[22], their application to SINR have been almost non-existent.

1.1 Thesis Contributions and Organisation

The motivation and key concepts which instigated this research are highlighted in the previous section. The thesis deals with aspects of interweave and underlay based spectrum sharing techniques. The selection of topics are based on research opportunities; where contributions can be made to an existing body of literature. In addition, the diverse nature of topics covered here do share a common objective: to address inefficient utilization of the licensed spectrum by CR enabled secondary access. This thesis consists of three major parts, and each part is compiled as a Chapter. In what follows, we present the organisation of the thesis and its main contributions.

- Chapter 2 provides the necessary background information that will be further used in this thesis. It highlights the key research areas in CRN and presents a summary of relevant existing literature.

- Chapter 3 is the first technical part of thesis. Using spectrum spooling as a base model (originally proposed by Weiss [23]) we analyse and quantify the SU QoS parameters such as forced termination probability, blocking probability and throughput in a multiple PU channel scenarios. The effect of horizontal spectrum handoff and channel reservation is investigated. The impact of spectrum sharing among two SU groups is discussed in the light of their traffic parameters.

- Chapter 4 presents a novel access scheme for FC coexistence in the DL channels of a cellular network. It exploits the interweave aspect of spectrum sharing to facilitate FC transmissions in an underlay mode. An example of a GSM-like network is used to illustrate the scheme by exploiting its duplexing features. The PU's probability of detection, the distribution functions for interference power and the signal to interference plus noise ratio (SINR) are derived. The effect of different parameters on the outage probability of the PU and the SU are discussed. The analysis relies heavily on the numerical integration techniques (Gaussian quadratures) to obtain the SINR distributions.

- Chapter 5 revisits the SINR distribution, which is a fundamental problem in many wireless systems, in addition to the underlay scenario considered here. A unique bounding approach is developed using Steffensen's inequality. It uses simple integral manipulations and utilizes the knowledge of the primary and the interfering paths' probability density function (PDF). It is shown that if the interfering path is unimodal, then the possibility of trivial bounds can be avoided. We demonstrate the effectiveness of the derived bounds in a gamma-gamma fading environment for medium to high SINR values, which are of practical interest in wireless systems.

- Chapter 6 concludes the work and indicates possible future research opportunities. These include QoS analysis of variable bandwidth users in interweave CRN, and the incorporation of fast fading and multiple FCs in the underlay approach.

1.2 Research Contributions

This work has lead to the following contributions

1. W. Ahmed, J. Gao, and M. Faulkner, " Comments on "Analysis of Cognitive Radio Spectrum Access with Optimal Channel Reservation"," *IEEE Transactions on Wireless Communications.*, pp. 4488-4491, vol. 8, no. 9, Sept. 2009.

2. W. Ahmed, M. Faulkner, and J. Gao, "Opportunistic Spectrum Access in Cognitive Radio Network," *Chapter 9 in Foundation of Cognitive Radio Systems*, pp. 189-214, 2012, ISBN 978-953-307-643-0.

3. W. Ahmed, M. Faulkner, J. Gao, and S. Saleem, "An Access Architecture for Secondary Femtocells in Downlink channels," *To be Submitted in IEEE Transactions on Wireless Communications.*

4. W. Ahmed, and M. Faulkner, "An Approximate PDF of the Distance Between Uniformly Distributed Points in a Circle," *To be Submitted in Institute of Engineering and Technology Letter.*

5. W. Ahmed, J. Gao, D. Lai, and M. Faulkner, "On Generalized SINR bounds: A Steffensen's Inequality Approach," *To be Submitted in IEEE Transactions on Wireless Communications*

6. W. Ahmed, J. Gao, S. Saleem, and M. Faulkner, "An Access Technique for Secondary Network in Downlink Channels," *Proceedings of IEEE Personal Indoor and Mobile Radio Communication (PIMRC)*, pp. 423-427, Sept. 2011.

7. W. Ahmed, J. Gao, M. Faulkner, "Channel Allocation for Fairness in Opportunistic Spectrum Access Networks," in *Proceedings of IEEE Wireless Communications and Networking Conference (WCNC), 2010*, pp. 1-6, 18-21 Apr. 2010.

8. W. Ahmed, J. Gao, H. Zhou and M. Faulkner, "Throughput and Proportional Fairness in Cognitive Radio Network", in *Proceedings of Advanced Technologies for Communications (ATC)*, pp. 248-252, 12-14 Oct. 2009.

9. W. Ahmed, J. Gao, H. Zhou and M. Faulkner, "Goodput and Channel allocation," in *Proceedings Personal Indoor and Mobile Radio Communications (PIMRC)*, pp. 476-480, 13-16 Sept. 2009.

10. W. Ahmed, J. Gao, and M. Faulkner, "Performance Evaluation of a Cognitive Radio Network with Exponential and Truncated Usage Models," in *Proceedings International Conference on Wireless and Pervasive Computing (ISWPC)*, pp. 1-5, 11-13 Feb. 2009.

11. J. Gao, W. Ahmed, J. Yang, and M. Faulkner, "Throughput Comparison in Cognitive Radio Networks," in *Proceedings of Electrical Engineering/Electronics Computer Telecommunications and Information Technology (ECTI-CON)*, pp. 748-751, 19-21 May 2010.

Other Contributions

1. R. Berangi, S. Saleem, M. Faulkner, W. Ahmed, "TDD Cognitive Radio Femtocell Network (CRFN)," *Proceedings of Personal Indoor and Mobile Radio Communication*, pp. 482-486, 2011.

2. S. Saleem, W. Ahmed, "Transmission in Black Space: A Paradigm in Cognitive Radio Networks," Presented by S. Saleem at ARC Cognitive and Multihop Wireless Networking Workshop, 2010.[Online]: `http://www.acorn.net.au/event/mwnworkshop10/`

3. W. Ahmed, "Optimal Allocation of Secondary Users in a Multi-Channel Cognitive Radio Network," Presented at ARC Communications Research Network (ACoRN): Multihop Wireless Networking Workshop, 2009. [Online]: `http://www.acorn.net.au/event/mwnworkshop08/`

4. W. Ahmed, "Aspects of QoS for Opportunistic Spectrum Access Networks," Presented at ARC Communications Research Network (ACoRN): Multihop Wireless Networking Workshop, 2008. [Online]: `http://www.acorn.net.au/event/mwnworkshop09/`

Chapter 2

Literature Review

The main aim of this Chapter is to provide an overview of the recent developments, issues and future trends in CRN research, with emphasis on the interweave and underlay spectrum sharing modes. In Section 2.1 we discuss the main functionalities of the CRN. This is followed by a review of the interweave mode (Section 2.2) and its performance aspects. Section 2.3 details an underlay spectrum sharing problem. Section 2.4 discusses the application of the interweave and underlay spectrum sharing modes to CR enabled FC.

2.1 Basic Functionalities of CR

CR technology is an innovative concept introduced by Mitola [4]. A CR must be highly adaptive to the needs of the SU and its surrounding radio environment. It has the potential to dramatically increase the efficiency of spectrum usage. IEEE 1900.1 has the following working definition of a CR [7]:

> *A type of radio that can sense and autonomously reason about its environment and adapt accordingly. This radio could employ knowledge representation, automated reasoning and machine learning mechanisms in establishing, conducting, or terminating communication or networking*

functions with other radios. Cognitive radios can be trained to dynamically and autonomously adjust its operating parameters.

There are four main functionalities in the IEEE definition. The first functionality requires sensing of the radio frequency environment, which includes detection of spectrum holes (unused), estimation of channel state information and PU traffic statistics. In reality, sensing imperfections (misdetection and false alarm) occur due to channel impairments and limited observation times. The misdetection leads to interference between the PU and the SU, whereas a false alarm results in lost opportunities and hence lower spectrum utilization.

The second functionality enables the SU to access a best available channel for its transmissions based on sensing information. The access modes of the SU are classified as interweave, underlay, and overlay [24] as described previously in Chapter 1. The third functionality highlights the need for spectrum sharing mechanisms to achieve fairness among multiple or dissimilar SUs. The final functionality identifies a reconfigurable hardware architecture which will adapt its operating parameters to suit the current radio frequency environment.

To understand the system-wide benefits it is pertinent to analyse the access modes of the SU in PU channels. The next few sections present a literature survey of coexistence analysis in an interweave and underlay mode.

2.2 Interweave Spectrum Sharing Model

In an interweave mode (often refereed as opportunistic spectrum access (OSA)), the SU accesses the spectrum in an opportunistic manner. Due to this secondary nature, the QoS in the CRN is dependent on the PU traffic parameters. For example, in the case when a PU access is unslotted and perfect sensing information is available at all times, the SU must vacate the channel as soon as the PU reappears to ensure no/minimum interference to the PU. This phenomena is called the forced termination. Similarly, the SU is blocked from accessing the channel when it finds the PU active.

In the existing literature, several authors [23]-[63] have studied the forced termination and blocking probabilities for one and two groups of SUs. In these papers, spectrum pooling [23] is used as a base system model. Spectrum pooling refers to an interweave paradigm which enables the PU network to rent out its idle spectrum bands to the SU group. It is assumed that the SU group will be able to perform wideband sensing and during their transmissions will introduce spectral nulls in the frequency bands where they find the PU active. It is suggested that in order to accommodate simultaneous SU connections, a wideband PU channel can be divided into multiple narrowband subchannels for SU access. The Continuous Time Markov Chain (CTMC) [25] is extensively used in modelling spectrum sharing scenarios based on interweave access. To simplify mathematical analysis it is commonly assumed that the traffic behaviour of the PU and the SU groups obey a Markov (memoryless) property i.e. the arrival rates follow a Poisson distribution and the service rates follow an exponential distribution. In addition, the SU connections are coordinated through a central entity (centralised secondary network) which ensures no collision between the SU connections i.e, no concurrent SU connections on the same frequency band or subchannel. The SU connections have negligible access, switching delays and perfect sensing information is available to them at all times. The papers dealing with QoS analysis can be divided into two scenarios: without forced termination; with forced termination, described in the following.

2.2.1 Without Forced Termination

The main aim in this type of system model is to understand the blocking probability tradeoff between two users with different bandwidth requirements. In [26] while investigating the blocking probability tradeoff between equal priority users, the authors concluded that the blocking probability of the wideband user is lower bounded by the blocking probability of the narrowband user. The best probability tradeoff can only be achieved by changing the arrival rates of both the wideband and the narrowband user [27]. This fact is used in [28] where it is shown that the optimal arrival rates which achieve airtime fairness can be derived using the Homo-Egualis model. Furthermore, the blocking probability in the network can be reduced when the narrowband users pack the channels [28, Fig. 6] by employing spectrum handoff[1]. The authors in [29] developed an upper bound on the throughput that can be achieved using spectrum agility with a listen before talk rule[2]. It was found that a fixed channel assignment strategy yields better results than spectrum agility under heavy load conditions.

Although, the above mentioned schemes provide a fair understanding of the blocking probability and airtime behaviour in a CRN, these analyses are only applicable to users in open unlicensed networks (e.g. ISM bands in 900MHz, 2.4 GHz and 5GHz), when the SU group utilizes the unlicensed channels for coordination or backup (in case the PU channels are fully occupied [28]).

[1]Spectrum handoff allows the SU connection to move to another vacant frequency channel during its transmission.

[2]Spectrum agility refers to the ability of a user to access multiple channels. Please note that spectrum agility is a stepping stone for spectrum handoff.

2.2.2 With Forced Termination

Initial investigation carried out in [30], focused on the advantages of primary assisted SU spectrum sharing; termed controlled spectrum sharing. In controlled spectrum sharing, the PU network assigns channels to its users (PUs) so as to avoid termination of SU connections. It is concluded that this approach increases bandwidth utilization without causing any significant increase in the blocking probability of the SU connections. No analytical expressions were derived for the forced termination probability and the throughput. In another controlled spectrum sharing scenario [31][32], a number of channels are allocated for SU connections by the PU network. Under saturated condition an incoming PU connection can also occupy the secondary allocated channels. Although this scheme decreases the forced termination probability, it comes with a cost of an increased SU blocking probability. To counter the effect of the forced termination the authors in [33] have proposed and analyzed random access schemes employing different sensing and backoff mechanisms. However, the analysis is limited to a single channel and saturated SU traffic conditions.

To avoid this foreseeable termination, spectrum handoff techniques have also been investigated from the forced termination and blocking probability perspective. Generally, spectrum handoff techniques can be categorised as either reactive or proactive. In the reactive approach, the SU moves to another vacant channel only when the current channel is reoccupied by a PU, whereas in the proactive approach the SU avoids collision and switches to another vacant channel before a PU reappears. The channel switching is performed based on the observed statistics of the PU channels[3]. To further ensure the continuity of SU transmission, inband

[3]This thesis only considers reactive spectrum handoff techniques. Some interesting proactive spectrum handoff strategies are provided in [34]-[37].

channel reservation (number of channels are reserved exclusively for handoff calls within the primary channels) and out-of-band channel reservation have also been suggested [38][39].

2.2.2.1 Reactive Spectrum Handoff

In [38], authors investigated the impact of spectrum handoff and channel reservation on the forced termination and blocking probabilities. However, the paper presented an incomplete CTMC analysis. In addition the expressions are derived based on a false assumption of completion probability from each Markov state. The corrections on this work is provided in [40][41][42]. The work in [40] forms part of this thesis and discussed in Chapter 3. Although, the authors in [41] included the queuing of SU connections, the analysis is limited to only handoff scenario. The investigations in [41][42] do not address the incomplete Markov analysis and throughput. The approach presented in [40] (Chapter 3) can be scaled to address the inaccurate probability analysis in [39]. It has been shown in [43] that an adaptive channel reservation scheme gives better performance than the fixed reservation policy. This adaption is based on traffic statistics of the PU. A relatively similar conclusion has been drawn in [44]. Extending the work in [38]-[43], the authors in [45] showed that the forced termination probability can be reduced by assigning multiple subchannels to each SU connection (reducing their transmission time). The forced termination probability expression derived in this paper is the termination probability seen by an incoming SU (an incoming SU call may be blocked) rather than the termination probability on the channel. The throughput in [42]-[45] is defined as the average completion rate of SU connections which does not include the average duration of completed SU connections. In order to address this problem, the duration of completed SU connections is calculated in [46], however, the analytical results derived are not very accurate. A more compact and accurate expression of throughput is derived in [40] (Chapter 3). The authors in [47] consider a PU network which has three different user classes. The users are admitted into the network based on a Guarded Threshold channel reservation Policy [48]. One of the classes is treated as a SU group, while the remaining two have PU status. The results indicate that such a scheme is only useful when the collision probability between the SU class and the two PU classes is high.

Based on a simplified system model, the link maintenance probability and the forced termination probability of delay sensitive SU connections are discussed in [49]-[52]. Including imperfect sensing, the probability derivations have been carried out in [50], where authors derive the collision probability rather than the forced termination probability[4]. In [51][52] it has been found that reactive spectrum handoff based on dynamic channel selection is a better strategy than the static strategy, however, it results in an increased sensing overhead. To decrease this overhead, a handoff reduction policy is proposed in [53] using connection success rate as a key metric [54]. Based on our findings [40], the authors in [55] proposed a channel allocation technique which yields almost similar performance to a spectrum handoff system.

From the perspective that CRN will be able to support multiple SU services, call admission control is investigated in [56]-[61]. The authors in [56] derived optimal access probabilities to achieve proportional fairness among two SU groups. These

[4]Without spectrum handoff the collision probability and forced termination probability is the same. However in the case of spectrum handoff, the SU connection can collide with the PU multiple times without being terminated. In essence collision probability calculation is performed on the basis of a single PU arrival, whereas the forced termination calculation are performed on the basis of multiple PU arrivals in the SU connection's life time [40][41]

results are derived based on a loose definition of throughput without considering the forced termination. A channel packing scheme which provides 10%- 15% gain over random channel access has been presented in [57]. The optimal access rates are derived only for a single wideband channel and three different type of users: one wideband PU: one wideband SU group; and one narrowband SU group. Although overall forced termination probability is also shown, it is strictly numerical and does not provide any insight into the individual forced termination probabilities of the two SU groups. A fair opportunistic spectrum access scheme with emphasis on two SU groups has been presented in [58]. Although the effect of collision probability is included, the results are only valid when the SU groups have the same connection length. The prioritisation among SU traffic from a physical layer and network integration perspective have been studied in [59][60]. Moreover, as identified in [61], these works do not include the effect of spectrum handoff. The probability aspects of prioritisation between two SU groups have been recently analyzed in [61]. Subchannel reservation policies were investigated to achieve the QoS of the prioritised SU group. The probability derivations were very similar to those previously presented by us in [62][63] and now described in Chapter 3.

In the literature summary presented so far, it is assumed that the PU group follows an ON/OFF process and sensing information is available to the SU group through a centralised entity at all times. This facilitates the SU in maintaining orthogonality with the PU transmissions; avoiding interference. However, in the case when such sensing information is not available, the SU has to perform sensing before its transmission, the outcome of which is a function of its vicinity to the PU transmitter and the channel gain. The SU may not be able to detect any PU transmissions due to its limited receiver sensitivity. Any subsequent SU transmission will generate interference at the PU receiver and vice versa, causing an outage. However, most wireless systems are designed to tolerate a certain amount of outage to accomodate the unknown variations in signal (due to fading etc.). Therefore it is possible to relax the orthogonality condition, transforming the interweave mode to an underlay mode, while still maintaining an acceptable performance. Underlay networks are discussed in the next section.

2.3 Underlay Spectrum Sharing Model

In a secondary underlay approach the possibility of spectrum sharing depends on the PU receiver's acceptable interference limit. The acceptable interference model was introduced by regulators to enable the reuse of TV spectrum frequencies in geographical locations, outside the TV coverage zone [2]. Generally, underlay spectrum sharing is not confined to TV bands[5]. For example the coexistence of FCs in a cellular network [12] can also involve underlay transmissions. Fig. 2.1 shows the two tier network architecture of a macrocell containing multiple FCs. The PU transceivers are denoted by PBS and PUE, and FC transceivers are denoted by SBS and SUE. The corresponding interference paths on the UL and the DL channels are highlighted in Fig. 2.2 for an FDD cellular network. Additional outage in the macrocell network (PBS and PUE) can occur due to cross-tier interference, whereas the outage at FCs can occur due to both cross-tier and inner-tier interference. In the following we present a literature summary of interference and outage analysis in a generalised secondary underlay model. We further expand this review to include interference avoidance and management techniques in a CR enabled FC.

[5]Another example of underlay spectrum sharing is Ultra Wide Band (UWB) radios in 3.1 to 10.6 GHz spectrum [64].

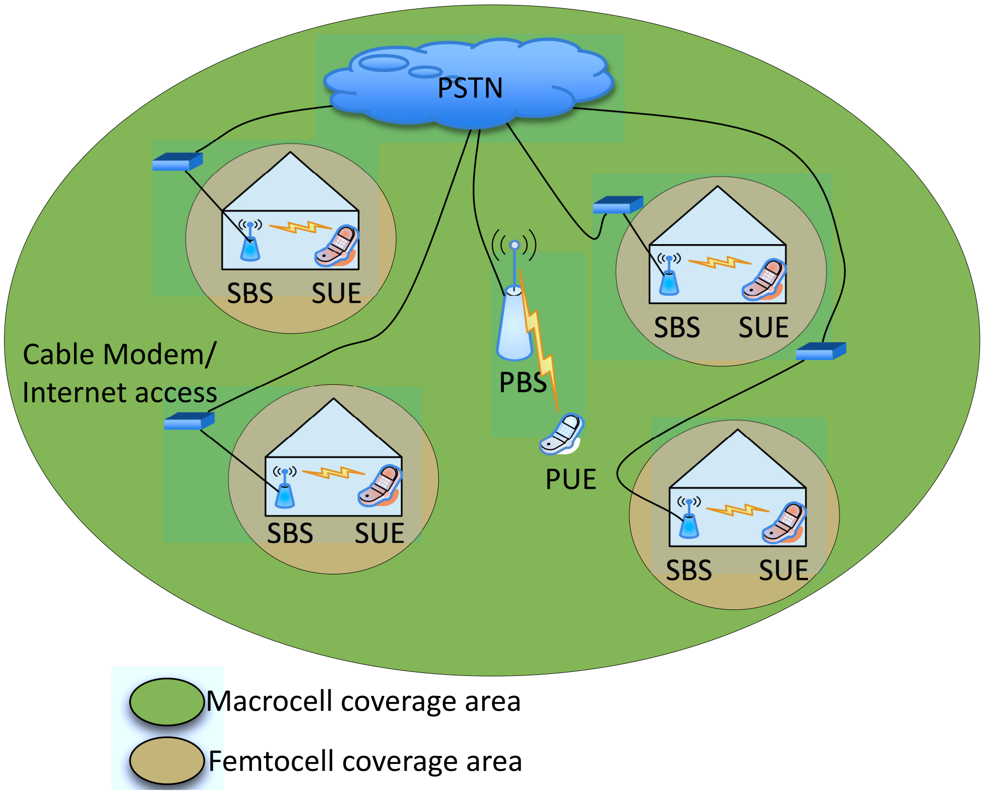

Figure 2.1: Existence of multiple femtocells in a macrocell coverage area.

2.3.1 Exclusion Zone Method

One of the most celebrated methods for managing interference in underlay networks is the exclusion zone method. This exclusion zone (a physical separation) provides a buffer to the PUE. Any SBS within that exclusion zone is not allowed to access the channel. The acceptable interference temperature of the PUE determines the exclusion zone area. For this the modelling of the aggregate interference (the sum interference from multiple SBSs) remains a key research area in cognitive underlay networks. The aggregate interference statistics are used to calculate SINR or SIR at the PUE. Generally, the aggregate interference is based on the random distribution of the SBSs around the PUE and the lognormal or gamma propagation model. Such an assumption is suitable to characterise interference in large wireless network [65].

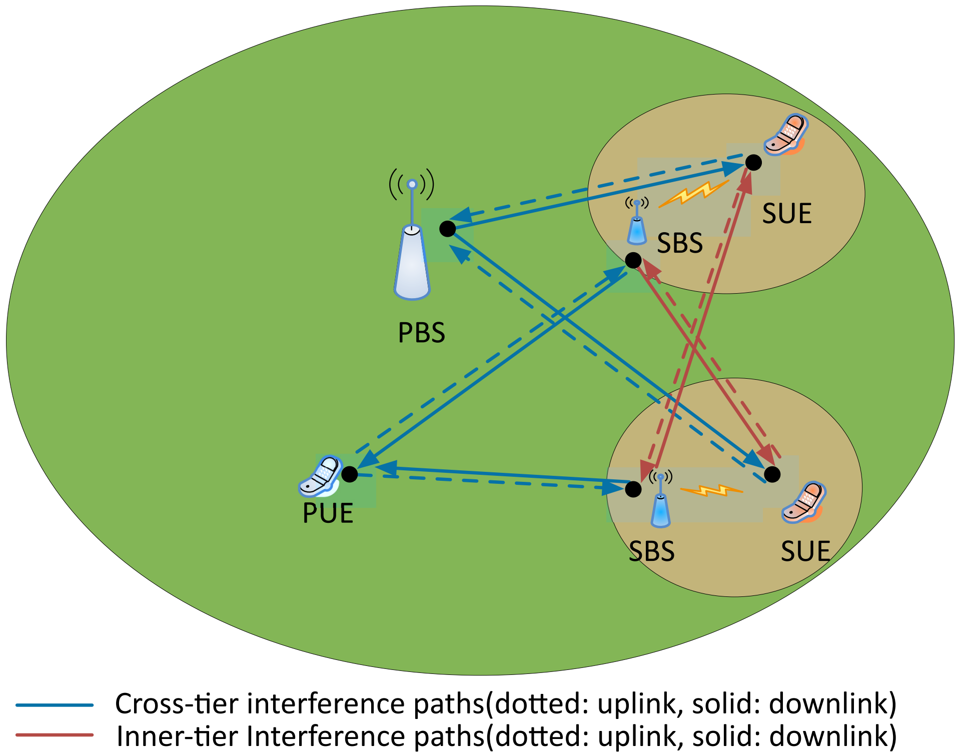

Figure 2.2: Cross-tier and inner-tier interference scenarios in a FDD cellular network. FDD eliminates the interference paths between the BSs and between the UEs.

2.3.1.1 Aggregate Interference Modelling

The calculation of aggregate interference statistics is often mathematically intractable. Various methods, such as moment matching, cummulant matching, and series approximations are envisaged. For example in [65], the authors presented a cummulant based approach to classify the underlying Gaussian and non-Gaussian nature of aggregate interference. It is concluded that when the exclusion radius is large, the aggregate interference tends to a Gaussian distribution, whereas in smaller exclusion radii the behaviour is skewed (generally non-Gaussian) and governed by the distribution of dominant interferers. Similar observations are also reported in [66][67]. To address the skewness [68], the authors in [69] modelled the aggregate interference as a shifted lognormal distribution. The intuitive result which indicates that the dominant region from Non-Gaussian interference increases with the exclusion radius and decreases with the pathloss exponent is derived in [70]. An interesting work in which multiple SBSs adapt their transmit power based on the received signal from the PUE is presented in [71]. The interference cummulants are derived to show that aggregate interference can be modelled by an unconventional truncated-stable distribution [72]. Taking into account the irregular shape of the exclusion zone in a shadow fading environment, the results in [73] show that the aggregate interference can be approximated by a lognormal distribution.

An alternative approach which augments the exclusion zone approach is known as the Radio Environment Map (REM) [74]. REM is proposed as an integrated database that characterises information such as geographical features, available services, spectral regulations, locations and activities of radios, relevant policies, and experiences. The results in [75][76] show that under the aggregate interference constraint a greater number of SBSs can be operated in the PUE vicinity by including the REM information. However, REM comes with a cost of increased signalling overhead [77].

2.3.1.2 Outage Probability

The modelling of aggregate interference enables the calculation of PUE outage probability. The outage probability is calculated on the basis of Signal to Interference Ratio (SIR) or SINR, when both the PBS and the PUE are static. Considering only a pathloss model the bounds on the exclusion radius are derived in [78]. In addition, the power scaling of multiple SBSs is derived to meet the PUE outage requirement. Using a similar pathloss model, the authors in [79][80] showed reduced PUE outage probability, when the SBSs spread their transmission power over the entire available bandwidth (Ultra Wide Band (UWB)).

2.3.1.3 Fading and Density of SBSs

The tradeoff between the density of SBSs and PUE outage probability has been recently studied in [81]. It was shown that the SBS density can be significantly increased, when dominant SBSs are suppressed either by sensing or interference cancellation techniques. Extending these results, the authors in [82] derived approximate expressions for the PUE outage by classifying the aggregate interference statistics in terms of SBS density. In a simplified scenario of Rayleigh fading, the optimal SBS density for maintaining predefined outage probability is calculated in [83]. The literature dealing with the fundamental effects of fading and SBS density on the exclusion zone and the outage probability can be found in [84]-[87] .

2.3.2 Interference Avoidance in FC

CR functionalities have been recently proposed to avoid the cross tier and inner-tier interference on the basis of Received Interference Power (RIP) [88]. This is achieved by incorporating a sensing phase in the existing FC which can learn about the channel condition between neighbouring FCs and PUEs [13]. This framework is used in [89] to avoid interference between a macrocell and a FC in an LTE network [90]. In this scheme, the SBS estimates the UL energy of the PUEs in its proximity. It allocates the best spectrum resource to the SUE by avoiding channels with strong UL energy. Similar techniques have also been discussed in [91][92], where the authors propose that the unique interference signature of PUEs can be used to avoid interference in the DL of 3G and UL of LTE networks, respectively. A distance dependent path loss channel model was used and no fading or shadowing effects were taken into consideration in the simulations. The authors in [93] have discussed dynamic resource block allocation in FCs of LTE networks based on RIP to the PUEs in DL channels.

2.3.3 Existence of CR empowered FC

In the current literature, a CR empowered FC (CEFC) has been treated as a device which has the ability to access both the licensed and the unlicensed band. Generally, the information about the network state, policies and interference conditions in the licensed bands is treated from two perspectives: Centralised and Decentralised. In a centralised approach, this information is fed to the CEFC by a dedicated universal channel called the cognitive pilot channel [94]. This centralised approach can avoid cross-tier interference. However, for inner-tier interference avoidance the universal control channel must carry global scheduling information. In a dense deployment of CEFCs the increase in the bandwidth of the cognitive pilot channel (due to global scheduling overhead) can outweigh its benefits [95].

In a decentralised approach, the CEFC collects network information through localised spectrum sensing. Two possible CEFC architectures have been presented in the literature so far:

2.3.3.1 Overlay Architecture

In an overlay architecture, the SBS schedules transmission for both the conventional and other low priority secondary devices [14]. The SBS acts as a conventional femtocell base station when serving the SUE (by connecting the SBS to the IP backhaul network). To schedule transmissions for the low priority secondary devices, the SBS must perform sensing to identify the spectrum holes. The signalling information between the SBS and the low priority secondary devices can be carried out in open unlicensed networks. Similar CEFC overlay models in both the UL and DL of a

WiMAX network have been investigated by the authors in [96], assuming that the PBS is also equipped with CR capabilities (such as sensing and dynamic spectrum access). Recently authors in [97] proposed that a SBS can increase its transmission opportunities in a PBS retransmission scenarios (due to collision or interference in initial transmission). When the PBS retransmits, the knowledge of the initial primary transmission can be used to mitigate interference at the SUE, provided that the SUE has decoded the initial transmission properly. Although this scheme can increase SBS transmission opportunities, it can also cause a significant increase in the number of PBS retransmissions.

2.3.3.2 Underlay Architecture

In [98] the authors propose to exploit the user level scheduling information or location information of the PUE to determine the set of resource blocks (RBs) [90] that can be used without causing interference. A Time Division Duplex (TDD) based CEFC scheme operating in UL spectrum was proposed in [99]. UL spectrum is used because the position of the PUE is unknown and so interference avoidance could not be guaranteed. The PBS position is known and so interference to the PBS can be controlled. Their simulations assumed that PBS interference was negligible, and therefore SBS must be positioned far from the PBS (>1.5km), which is a fairly restrictive constraint. Very recently in [100], the authors propose that DL control information (from the PBS) can be used to schedule the SBS and SUE transmission in both the UL and the DL of the primary network. The authors argue that by placing multiple antennas and applying beam forming duality, the SUE near the PBS will be able to transmit in UL by steering a null. However, this conclusion is oversimplified due to the assumptions in their simulations; the PBS distance is known apriori and the Rayleigh fading is independent of the duplex links.

2.4 SINR Bounds

The quantification of SINR statistics is a critical component in determining outage probability. It is also used in many other applications such as handover calculations in cellular system, diversity combining systems and capacity calculations. The fading distributions which characterise signal propagation through a wireless medium do not yield closed form solutions for the integrals governing the calculation of the SINR's CDF or SINR's PDF. Conditional solutions have been obtained by neglecting the noise component (in which case SINR reduces to SIR) [71] or by neglecting the fading component on the primary path [81][82]. These assumption are not always realistic, but are still used, since a general solution is still an open question.

Integral inequalities are an effective tool to study the bounds on system performance. For example in [21], the authors have used Jensen's inequality to derive the upper bound on achievable ergodic capacity of dual-hop transmissions in composite fading channels. The Jensen's inequality has also been used in [22] to simplify the ergodic capacity maximisation problem. This simplification is further used to develop power control and access strategies in wireless systems. Similarly, using H$\ddot{o}$lder's inequality the bounds for the moments of the received power are derived in [101], when the transmitter and receiver are uniformly distributed in a multidimensional convex space. In [102], the authors used the Cauchy-Schwarz inequality to derive the bounds on the generalised Marcum-Q function.

In general, the calculation of SINR's CDF $F_{\Upsilon}(\upsilon)$ involves the integral of product functions. This can be visualized by the derivation of the SINR's CDF given below. Let Θ_p and Θ_I denote the signal and interference power respectively, then SINR Υ

can be written [19],

$$\Upsilon = \frac{\Theta_p}{\Theta_I + N_0} = \frac{\Theta_p}{\Theta_{in}}. \tag{2.1}$$

The CDF $F_\Upsilon(\upsilon) = \Pr(\frac{\Theta_p}{\Theta_{in}} \leq \upsilon)$ becomes $F_\Upsilon(\upsilon) = \Pr(\Theta_p \leq \Theta_{in}\upsilon)$. Averaging over $\Theta_{in} \in \{N_0, b\}$ gives the CDF of Υ

$$F_\Upsilon(\upsilon) = E\left[F_{\Theta_p}(\Theta_{in}\upsilon)\right], \tag{2.2}$$

$$F_\Upsilon(\upsilon) = \int\limits_{N_0}^{b} F_{\Theta_p}\left(\upsilon\theta_{in}\right) f_{\Theta_{in}}\left(\theta_{in}\right) d\theta_{in}, \tag{2.3}$$

where, $E[.]$ is an expectation operator, $f_{\Theta_{in}}\left(\theta_{in}\right)$ is the PDF and (N_0, b) defines the support of Θ_{in}. Normally, N_0 is the minimum value of Θ_{in} and $b = \infty$.

2.4.1 Steffensen's Inequality

Steffensen's inequality among others is one of the key tools in calculating bounds on the integral of product functions. In its simplest form, the Steffensen's inequality is given in [103][20, Eqs. (2.1) & (2.2)] as

$$\int\limits_{x_1-\lambda}^{x_1} S(x)dx \leq \int\limits_{x_0}^{x_1} S(x)R(x)dx \leq \int\limits_{x_0}^{x_0+\lambda} S(x)dx \tag{2.4}$$

where $\lambda = \int\limits_{x_0}^{x_1} R(x)dx$, $S(x)$ is integrable and monotonically decreasing on (x_0, x_1), and $R(x)$ is measurable such that $0 \leq R(x) \leq 1$ for $x \in (x_0, x_1)$. From the above equation, it can be seen that the Steffensen's inequality decouples the integral of the product functions into integrals of the individual functions. The bounds are expressed as the integral of function $S(x)$ calculated over length λ from the end points (limits of actual integration problem).

Looking at equations (2.3) and (2.4), one can readily identify the resemblance between them. Various extensions of Steffensen's inequality have been proposed in

[104]-[107] and references therein. For example the extension in [104] generalizes λ by expressing it as the integral limit of an arbitrary function i.e., $\int_{x_0}^{x_0+\lambda} H(x)dx = \int_{x_0}^{x_1} R(x)dx$, where $0 \leq R(x) \leq H(x)$. The function $H(x)$ must be multiplied in the upper bound and lower bound integrals. In [105] the authors discuss the sensitivity of $H(x)$ and show that both the upper and lower bound can become loose bounds. Although all these extensions generalize the above inequality, the calculation of λ becomes complicated which is a key parameter.

One simple and notable generalisation is provided in [107, Eq. (2.4)], which states that the bounds can also be expressed in terms of any two subintervals of length λ (whereas in (5.2) subintervals are restricted to end points). However, this generalisation is useful when the coarser bounds are required or the actual integral is known in some subinterval. From an application perspective, the approximation bounds on some special functions such as the Bessel function, Beta function, Euler function and Zeta function are derived in [108] using Steffensen's inequality and the *Č*eby*š*ev functional [20]. Steffensen's inequality has also been used in [109] and in [110] to calculate the upper bound on the ergodic capacity of a maximal ratio combining system with correlated Rician fading channels and dual-hop fixed gain relay networks with Rayleigh fading respectively. In both these scenarios a negative exponential is used as $R(x)$. We make use of Steffensen's inequality in Chapter 5.

2.5 Summary

In this Chapter, we have presented a literature summary spanning various performance aspects of interweave and underlay spectrum sharing in CRN. A critical review has been performed and areas concerning this thesis have been highlighted.

Firstly, several key CRN functionalities were abstracted from the IEEE definition. Secondly, the methods and techniques to manage the forced termination probability, the blocking probability and the throughput for a single and multiple SU groups were explained. Thirdly, a generalised underlay spectrum sharing model was used to elaborate the aggregate interference and outage probability modelling in an exclusion zone method. The applicability of underlay mode to cognitive empowered FC was discussed and pros and cons of relevant techniques for interference avoidance were explained. Finally, the applicability of integral inequalities to the fundamental problems in communication theory was enumerated. In the next Chapter, we will start by analysing the fundamental QoS metric of SUs in interweave spectrum sharing.

Chapter 3

Quality of Service in Interweave Access

This Chapter aims to quantify the quality of service (QoS) parameters of SU connections in an interweave spectrum sharing scenario i.e., forced termination probability, blocking probability and throughput. These QoS parameters are of paramount significance in an interweave CRN, as they can effectively determine the feasible existence of SU group in PU channels. The work presented in this Chapter has appeared in *IEEE Transactions in Wireless Communications* [40], 3 *IEEE ComSoc Portfolio Events* (ATC, PIMRC and WCNC) [62, 63, 111], 1 international conference (*ISWPC*) [112] and 1 regional conference (*ETI-CON*) [113]. The contents of this Chapter are also set to appear in a Book titled "*Cognitive Radio System*", Intech Publishers [114]. Specifically, in this Chapter

- Simple closed form expressions for the forced termination probability, blocking probability and SU throughput are derived for both fixed and exponential payload lengths. While indicating the tradeoff between the SU access rate and its connection length (holding time [115]), the optimal mean connection length which maximizes the throughput is calculated.

- A complete and exact CTMC analyses is presented (compared to [38][41][42]). The QoS parameter are obtained for spectrally agile single SU group operating in multichannel PU network. These derivations also include SU spectrum handoff and channel reservation scenarios.
- Spectrum sharing between two SU groups is investigated in terms of probability tradeoff gains and airtime fairness. It is shown that compared to non-termination scenarios [26]-[29],[56] the access rates have very little impact on airtime fairness. A channel partitioning approach is developed to achieve airtime fairness.

The remainder of the Chapter is organised as follows. Section 3.1 presents the system model and key assumptions. Section 3.2 discusses a single channel interweave access scenario. Section 3.3 extends the discussion to include multiple PU channels and two SU groups. A single SU group is treated as a special case. The airtime fairness among the two SU groups is analyzed in Section 3.4. Section 3.5 concludes the Chapter.

3.1 System Model

In this Chapter, a widely acceptable spectrum pooling model [23, Fig. (3)] is adopted, in which a vacant wideband PU channel is divided into multiple narrowband subchannels. These narrowband subchannels are used by SU groups for their opportunistic transmissions. Fig. 3.1 shows the system model, in which there are K available PU channels $k \in \{1, 2.., K\}$. Each of the PU channels has a fixed bandwidth W_p, which is subdivided into N subchannels of bandwidth, $W_s = W_p/N$. We consider two spectrum sharing scenarios: a single SU group is interweaving the

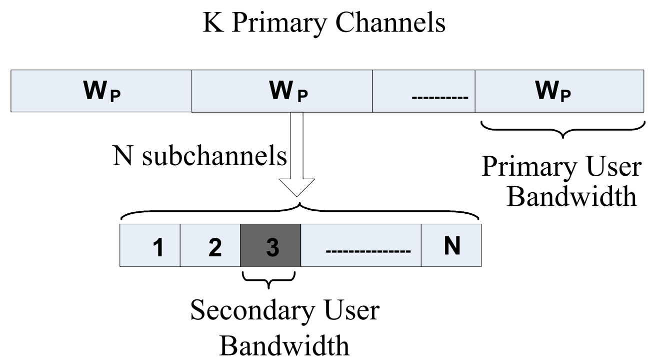

Figure 3.1: Channel arrangements of PU and SU channels, N is an integer ≥ 1

PU channels, denoted by S^1; two SU groups interweaving the PU channels, denoted by S^A and S^B.

3.1.1 Traffic Model

1. The service duration of the PU connections are assumed to be exponentially distributed with a mean $\frac{1}{\mu_p}$. The arrival of new connections from the PU group follow a Poisson process with a mean rate rate λ_p.

2. It is assumed that the PU network is an M/M/m/m loss network, where channel occupancy only depends on the mean service rate of PU group [25].

3. (a) In the case of a single PU channel and a single SU group, we consider two types of SU connections, fixed header with fixed payload and fixed header with exponentially distributed payload. The fixed header duration is denoted by $\frac{1}{\mu_h}$, the fixed payload length is denoted by $\frac{1}{\mu^1_{sf}}$, and the mean exponential payload length is denoted by $\frac{1}{\mu^1_{se}}$. The Poisson arrival rate of a single SU group is denoted by λ^1_s.

   (b) In the case of a multichannel PU network only exponential payload lengths are considered. The mean service durations of S^1, S^A and S^B are denoted by $\frac{1}{\mu_s^1}$, $\frac{1}{\mu_s^A}$ and $\frac{1}{\mu_s^B}$ respectively. Similarly, the Poisson arrival rates are λ_s^1, λ_s^A, and λ_s^B.

These models are widely adopted in the literature, see for example ([26]-[61]). The list of symbols are summarised in Table 4.1.

3.1.2 Basic Definitions and Mathematical Model

For the reader's convenience the QoS parameters are defined below.

Blocking Probability is defined as the probability that a new SU connection will be blocked due to unavailability of a vacant subchannel.

Forced Termination Probability is defined as the probability that an ongoing SU connection is terminated prematurely.

Throughput is defined as the product of the number of completed SU connections per unit time and the average duration of the completed connections.

CTMC is used to model the spectrum sharing scenario between the PU and SU groups. CTMC has been extensively used in conventional cellular systems to model the cell residence time[1], call dropping probability and handover probability [116]. In these scenarios, the birth-death process (often referred to as a loss system) is one of the commonly used CTMC models. In a CTMC model, the number of connections from the user groups are represented by states (written as $n-tuples$), such as (x_1,x_2), where x_1 and x_2 may represent the number of PU and SU connections. The transition of one state to another is based on the Markov property [25] which assumes memoryless arrivals and departures. Under stationarity assumptions, the rate of transition from and to a state is equal. This fundamental fact is used to calculate the state probabilities under the constraint that the sum of all state probabilities is

[1]The time spent by a users in a macrocell during a connected call.

Table 3.1: List of symbols-Chapter 3

Symbol	Parameter
Primary	
K	Number of PU channel
N	Number of subchannels/PU channels
λ_p	Arrival rate of PU group
μ_p	Service rate of PU group
θ_p	PU traffic intensity
Secondary	
S^1	Single SU group in PU channels
S^A and S^B	Two SU groups in PU channels
N^A (N^B)	Number of subchannels of S^A (S^B)
λ_s^1, λ_s^A and λ_s^B	Arrival rate of S^1, S^A and S^B
μ_{se}^1, μ_{se}^A and μ_{se}^B	Mean service rate of exponentially distributed payload S^1, S^A and S^B
θ_{se}^1, θ_{se}^A and θ_{se}^B	Traffic intensity of exponentially distributed payload S^1, S^A and S^B
P_{Fe}^1, P_{Fe}^A and P_{Fe}^B	Forced termination probability of exponentially distributed payload S^1, S^A and S^B
P_{Be}^1, P_{Be}^A and P_{Be}^B	Blocking probability of exponentially distributed payload S^1, S^A and S^B
ρ_{se}^1, ρ_{se}^A and ρ_{se}^B	Throughput exponentially distributed payload S^1, S^A and S^B
$\frac{1}{\mu_h}$	Header length
$P_{F(h,e)}^1$	Forced termination probability exponentially distributed payload and header S^1
$P_{B(h,e)}^1$	Blocking probability exponentially distributed payload and header S^1
$\rho_{s(h,e)}^1$	Payload throughput S^1
$\frac{1}{\mu_h}$	Header length
μ_{sf}^1	Fixed payload service rate of S^1
θ_{sf}^1	Traffic intensity of fixed payload S^1
$P_{F(h,f)}^1$	Forced termination probability with fixed payload and header S^1
$P_{B(h,f)}^1$	Blocking probability with fixed payload S^1
$\rho_{s(h,f)}^1$	Throughput fixed payload S^1

Table 3.2: List of symbols for CTMC

Symbol	**Parameter**
k	Number of PU connections
i	Number of SU connections of S^1 and S^A
y	Phase of SU connections S^1
j	Number of SU connections of S^B
l	Number of terminated SU connections S^1 and S^A
m	Number of terminated SU connections S^B

equal to 1. These state probabilities are further used to calculate the parameters of interest. Table 3.2 lists the parameters and symbols that have been used in the CTMCs throughout this Chapter.

3.2 Single PU Channel $K = 1$, with $N = 1$

The system model and assumptions are described in the previous section. We start our discussion with a simple scenario, in which a single SU group interweaves a single PU channel. Note that $N = 1$ refers to a scenario in which the bandwidths of the PU group and SU group are equal. It is assumed that each SU connection has two components, a fixed header length $\frac{1}{\mu_h}$ and a payload length. Two scenarios for payload distributions are considered. In the first scenario, the payload length is fixed $\frac{1}{\mu_{sf}^1}$, whereas in the second scenario, the payload length is exponentially distributed with a mean service rate μ_{se}^1. The payload traffic intensity [25] is defined as $\theta_{sz}^1 = \frac{\lambda_s^1}{\mu_{sz}^1}$, where $z \in \{f, e\}$ for fixed and exponentially distributed payloads.

3.2.1 Fixed Payload Length

When the payload is fixed the total connection length can be expressed by the sum of the overhead and the payload lengths, i.e.,

$$\frac{1}{\mu_{fp}} = \frac{1}{\mu_h} + \frac{1}{\mu_{sf}^1}. \tag{3.1}$$

Due to the presence of fixed length SU connections on the channel, the system is not purely Markovian and it cannot be represented by a simple birth-death process [25]. Here, an indirect approach is adopted to model this scenario by a CTMC [25]. In this approach, the connection with fixed length is replaced by a continuous group of Y exponentially distributed connections which are independent and identically distributed (i.i.d). Note that the total length of these Y i.i.d connections is Erlang distributed and the individual connection has an average length of $\frac{1}{Y\mu_{fp}}$. It is well established that as $Y \to \infty$, the total length is the same as that of the fixed length connections $\frac{1}{\mu_{fp}}$.

Since the fixed length connection is replaced by a group of Y i.i.d connections, a Y node CTMC is used to model the number of the arrivals of the connection in the group, i.e., the y^{th} node models the arrival of the y^{th} connection in the group. These states are referred to as the phases of a fixed SU connection [25]. Fig. 3.2(b) shows the complete CTMC, where the state is shown as (i, k, y), where, i and k $(\in \{0, 1\})$ represents the presence (1) and absence (0) of a SU and PU connection on the channel, $1 \leq y \leq Y$ represents the y^{th} phase of a SU connection when $i = 1$ (Fig. 3.2(a)). The total mean departure rate from each phase of the SU connection is $(Y\mu_{fp} + \lambda_p)$, where $Y\mu_{fp}$ is the completion rate of each i.i.d connection and λ_p is the termination rate due to the arrival of a PU connection. A set of balance equations for the CTMC in Fig. 3.2(b) is given as

$$\begin{cases} (\lambda_s^1 + \lambda_p)P(0,0,0) = \mu_p P(0,1,0) + Y\mu_{fp}P(1,0,Y), \\ (Y\mu_{fp} + \lambda_p)P(1,0,1) = \lambda_s^1 P(0,0,0), \\ (Y\mu_{fp} + \lambda_p)P(1,0,2) = Y\mu_{fp}P(1,0,1), \\ \vdots, \\ (Y\mu_{fp} + \lambda_p)P(1,0,Y) = Y\mu_{fp}P(1,0,Y-1), \end{cases} \tag{3.2}$$

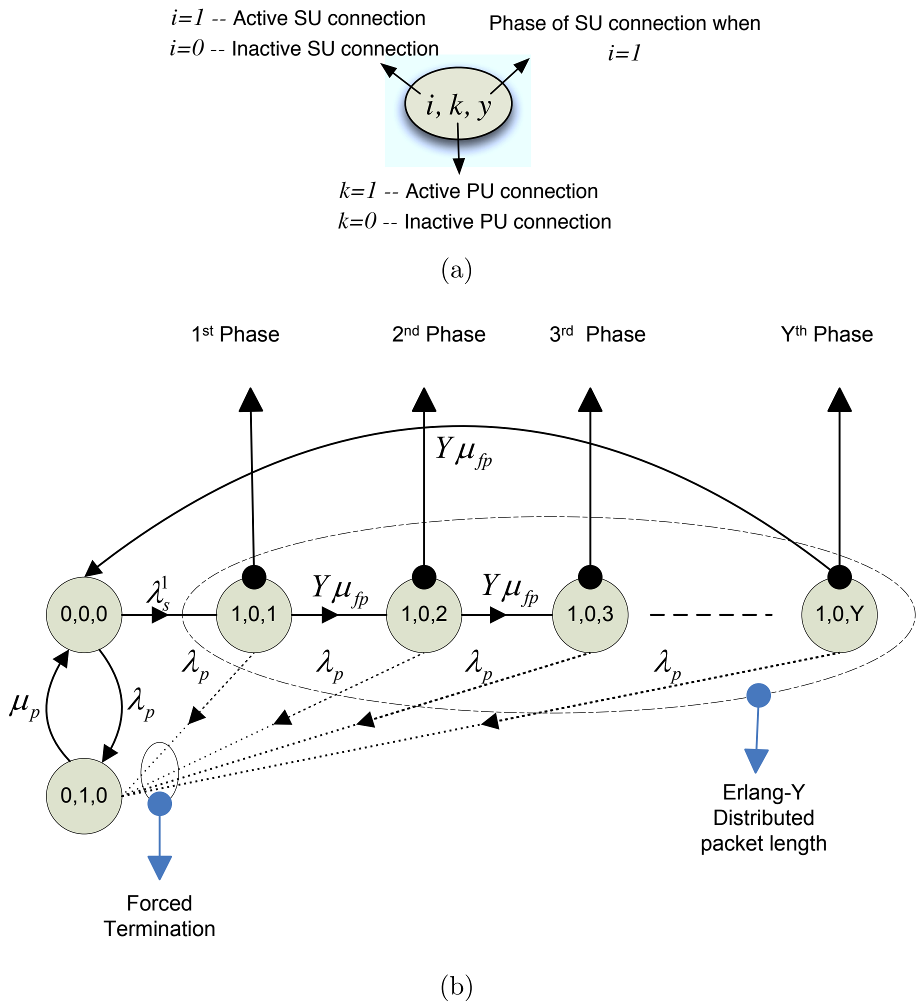

Figure 3.2: CTMC model of SU connections with fixed payload.

such that

$$P(0,0,0) + P(0,1,0) + \sum_{y=1}^{Y} P(1,0,y) = 1, \tag{3.3}$$

where, $P(i, k, y)$ represents the probability of the state (i, k, y). By simple algebraic manipulation of equations in (3.2), the probability of the y^{th} phase $P(1, 0, y)$ in terms of $P(0, 0, 0)$ can be written as

$$P(1,0,y) = \left(\frac{Y\mu_{fp}}{Y\mu_{fp} + \lambda_p}\right)^{y-1} \frac{\lambda_s^1}{(Y\mu_{fp} + \lambda_p)} P(0,0,0), \;\; y \geq 1. \tag{3.4}$$

Using $P(i, k, y)$, the expressions for the forced termination probability, blocking probability and throughput are derived.

• Blocking Probability

In Fig. 3.2(b), an incoming SU connection is blocked when the channel is occupied by a PU or SU connection. The blocking probability $P^1_{B(h,f)}(Y)$ in this scenario can be expressed as

$$P^1_{B(h,f)}(Y) = 1 - P(0,0,0). \tag{3.5}$$

Since the arrival of a PU connection is independent of a SU connection, the probability of a PU connection on the channel $P(0,1,0)$ can be written as

$$P(0,1,0) = \frac{\lambda_p}{\lambda_p + \mu_p}. \tag{3.6}$$

Using (3.2), (3.4) and (3.6), the blocking probability of a SU connection with Erlang-Y distributed connection length has the following mathematical expression

$$P^1_{B(h,f)}(Y) = 1 - \frac{\mu_p \lambda_p}{(\lambda_p + \mu_p)\left(\lambda_s^1 + \lambda_p - \left(\frac{Y\mu_{fp}}{Y\mu_{fp} + \lambda_p}\right)^Y \lambda_s^1\right)}. \tag{3.7}$$

Let $P^1_{B(h,f)} = \lim_{Y\to\infty} P^1_{B(h,f)}(Y)$ and using the following well known identity

$$e^x = \lim_{n\to\infty}\left(1 + \frac{x}{n}\right)^n, \tag{3.8}$$

the blocking probability of SU connections with fixed payload length becomes

$$P^1_{B(h,f)} = 1 - \frac{\mu_p \lambda_p}{(\lambda_p + \mu_p)\left(\lambda_s^1 + \lambda_p - e^{-\frac{\lambda_p}{\mu_{fp}}} \lambda_s^1\right)}. \tag{3.9}$$

• Forced termination Probability

Forced termination probability is defined as the probability that an ongoing SU connection is terminated prematurely. Based on the fact that the sum of forced and unforced termination rates equals to the incoming connection rate, the forced termination probability can be written as

$$P^1_{F(h,f)}(Y) = \frac{\text{SU forced termination rate}}{\text{SU Connection rate}}. \tag{3.10}$$

From Fig. 3.2.1, $\sum_{y=1}^{Y} P(1,0,y)\lambda_p$ is the total termination rate of SU connections and $(1 - P^1_{B(h,f)}(Y))\lambda^1_s$ is the incoming rate of SU connections. Using (3.10), the forced termination probability of SU with Erlang-Y distributed connection length can be written as

$$P^1_{F(h,f)}(Y) = \frac{\sum_{y=1}^{Y} P(1,0,y)\lambda_p}{(1 - P^1_{B(h,f)}(Y))\lambda^1_s}, \tag{3.11}$$

using (3.2) and (3.5), $P^1_{F(h,f)}$ can be expressed as

$$P^1_{F(h,f)}(Y) = \frac{\lambda_p}{Y\mu_{fp}} \sum_{y=1}^{Y} \left(\frac{Y\mu_{fp}}{Y\mu_{fp} + \lambda_p}\right)^y. \tag{3.12}$$

Note that the geometric series in the above equation is convergent (common ratio $\frac{Y\mu_{fp}}{Y\mu_{fp}+\lambda_p} < 1$), hence (3.12) can be simplified to

$$P^1_{F(h,f)}(Y) = \frac{Y\mu_f + \lambda_p}{Y\mu_{fp}} - \left(\frac{Y\mu_{fp}}{Y\mu_{fp} + \lambda_p}\right)^Y. \tag{3.13}$$

Let $P^1_{F(h,f)} = \lim_{Y\to\infty} P^1_{F(h,f)}(Y)$ be the forced termination probability of SU connections with fixed payload. Using (3.8), the $P^1_{F(h,f)}$ can be written as

$$P^1_{F(h,f)} = 1 - e^{(-\frac{\lambda_p}{\mu_{fp}})}. \tag{3.14}$$

- **Throughput**

Given the arrival rate λ^1_s, the SU connection completion rate is given by $(1 - P^1_{B(h,f)})(1 - P^1_{F(h,f)})\lambda^1_s$. The average payload duration of the completed SU connections is $\frac{1}{\mu^1_{sf}}$. Therefore, the aggregate payload throughput $\rho^1_{s(h,f)}$ can be written as

$$\rho^1_{s(h,f)} = (1 - P^1_{B(h,f)})(1 - P^1_{F(h,f)})\theta^1_{sf}, \tag{3.15}$$

where, $\theta^1_{sf} = \frac{\lambda^1_s}{\mu^1_{sf}}$ is the payload traffic intensity of the SU connections.

3.2.2 Exponential Payload Length

In the following, the forced termination probability, blocking probability and throughput of the SU connection with a fixed header and exponentially distributed payload length are calculated.

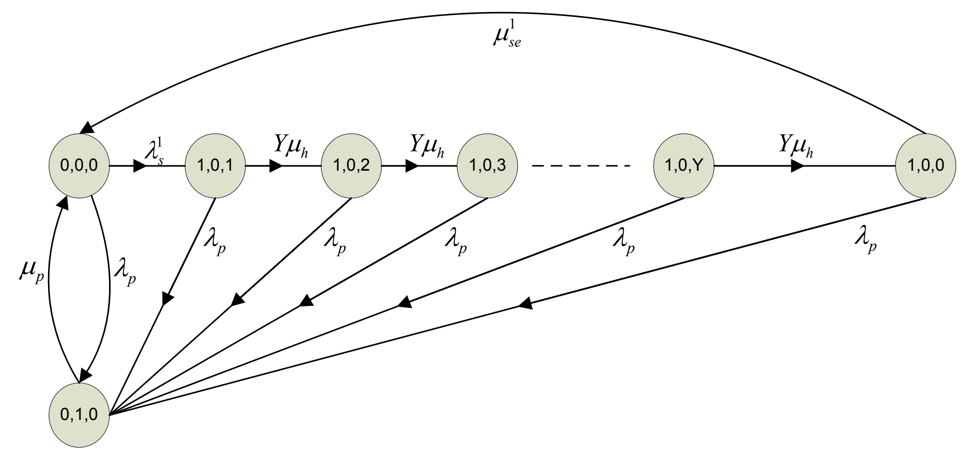

Figure 3.3: CTMC model of SU connections with fixed header and exponentially distributed payload.

Fig. 3.3 shows the CTMC of the system. In this figure the states $(1, 0, y)$, $y = \{1, \ldots Y\}$ represent the phases of fixed header portion, whereas the state $(1, 0, 0)$ represents the exponentially distributed payload portion. Similar to the previous section, the fixed header of length $\frac{1}{\mu_h}$ is modelled as a limiting case of Erlang-Y distribution, and the exponentially distributed payload length is given by $\frac{1}{\mu^1_{se}}$. The global balance equations of the above system are as follows

$$\begin{cases} (\lambda_s^1 + \lambda_p)P(0,0,0) = \mu_p P(0,1,0) + \mu_{se}^1 P(1,0,0), \\ (Y\mu_h + \lambda_p)P(1,0,1) = \lambda_s^1 P(0,0,0), \\ (Y\mu_h + \lambda_p)P(1,0,2) = Y\mu_h P(1,0,1), \\ \vdots \\ (Y\mu_h + \lambda_p)P(1,0,Y) = Y\mu_h P(1,0,Y-1), \\ (\lambda_p + \mu_{se}^1)P(1,0,0) = Y\mu_h P(1,0,Y), \end{cases} . \tag{3.16}$$

• Blocking Probability

Solving (3.16) for $P(0,0,0)$ and using (3.5), the blocking probability of the SU connections can be written as

$$P^1_{B(h,e)}(Y) = 1 - \frac{\dfrac{\mu_p \lambda_p}{(\lambda_p + \mu_p)}}{\left(\lambda_s^1 + \lambda_p - \dfrac{\lambda_s^1 \mu_{se}^1}{\mu_{se}^1 + \lambda_p}\left(\dfrac{Y\mu_h}{Y\mu_h + \lambda_p}\right)^Y\right)}. \tag{3.17}$$

In the limit let $P^1_{B(h,e)} = \lim_{Y\to\infty} P^1_{B(h,e)}(Y)$ be the blocking probability of SU connections with exponentially distributed payload length. It can be shown that

$$P^1_{B(h,e)} = 1 - \frac{\mu_p \lambda_p}{(\lambda_p + \mu_p)\left(\lambda_s^1 + \lambda_p - \dfrac{\lambda_s^1 \mu_{se}^1}{\mu_{se} + \lambda_p} e^{-\frac{\lambda_p}{\mu_h}}\right)}. \tag{3.18}$$

• Forced Termination Probability

Similar to the previous section, the forced termination probability can be calculated by using the definition in (3.11). In this scenario the forced termination probability $P^1_{F(h,e)}(Y)$ can be written as

$$P^1_{F(h,e)}(Y) = \frac{\lambda_p \sum_{y=0}^{Y} P(1,0,y)}{\lambda_s^1 P(0,0,0)}, \tag{3.19}$$

using the balance equations (3.16), the P_{FY}^{1h} can be expressed as

$$P_{F(h,e)}^{1}(Y) = \frac{\lambda_p\left(\sum_{y=1}^{Y}\left(\frac{Y\mu_h}{Y\mu_h+\lambda_p}\right)^y\right)}{Y\mu_h} + \frac{\lambda_p}{\mu_{se}^1+\lambda_p}\left(\frac{Y\mu_h}{Y\mu_h+\lambda_p}\right)^Y. \tag{3.20}$$

In the limit, let $P_{F(h,e)}^1 = \lim_{Y\to\infty} P_{F(h,e)}^1(Y)$ be the forced termination probability of SU connections with exponentially distributed payload length. Using (3.8) it can be shown that

$$\begin{aligned} P_{F(h,e)}^1 =& 1 - e^{-\frac{\lambda_p}{\mu_h}} + \frac{\lambda_p}{\mu_{se}^1+\lambda_p} e^{-\frac{\lambda_p}{\mu_h}}, \\ =& P_{F(h,0)}^1 + P_{F(0,e)}^1\left(1 - P_{F(h,0)}^1\right), \end{aligned} \tag{3.21}$$

where, $P_{F(h,0)}^1 = 1 - e^{-\frac{\lambda_p}{\mu_h}}$ and $P_{F(0,e)}^1 = \frac{\lambda_p}{\mu_{se}^1+\lambda_p}$. Note that compared to (3.14), $P_{F(h,0)}^1$ can be considered as the contribution of the fixed header to the forced termination probability, whereas $P_{F(0,e)}^1$ is the contribution of the remaining exponentially distributed part.

• Throughput

The total throughput is the product of completion rate and the average length of completed connections $\frac{1}{\mu_e}$. In this scenario, the average length of SU connections is the sum of fixed header length and the average payload length i.e.

$$\frac{1}{\mu_e} = \frac{1}{\mu_h} + \frac{1}{\hat{\mu}_{se}^1}. \tag{3.22}$$

Assume that the payload length of the completed connections is exponentially distributed. For a given forced termination probability $P_{F(0,e)}^1$, the average length of the completed connections is $\frac{1}{\hat{\mu}_{se}^1} = \frac{(1-P_{F(0,e)}^1)}{\mu_{se}^1}$ [40]. Therefore, the aggregate payload throughput $\rho_{s(h,e)}^1$ can be written as

$$\rho_{s(h,e)}^1 = (1 - P_{B(h,e)}^1)(1 - P_{F(h,e)}^1)\lambda_s^1 \frac{(1 - P_{F(0,e)}^1)}{\mu_{se}^1}. \tag{3.23}$$

3.2.3 Optimal SU PayLoad Length

In this section, the optimal payload length of SU connections which maximizes the aggregate payload throughput for a given payload traffic intensity and fixed header length is investigated. Mathematically, the optimisation problem can be expressed by

$$\begin{aligned} &\mu_{sz}^{1*} = \arg\max_{\mu_{sz}^{1}}\{\rho^{1}_{s(h,z)}\}, \\ &\text{s.t.} \qquad \frac{\lambda_s^1}{{\mu_{sz}}^1} = \theta^1_{sz}, \quad \lambda_s^1(\mu^1_{sz}) \geq 0, \quad \frac{1}{\mu_h} = c, \end{aligned} \tag{3.24}$$

where, $z \in \{f, e\}$. By substituting $\lambda_s^1 = \theta^1_{sz}\mu^1_{sz}$ and $\frac{1}{\mu_h} = c$ in (3.15) (3.23), the critical points of the above optimisation problem can be calculated from

$$\frac{d}{d\mu^1_{sz}}\rho^1_{s(h,z)} = 0 \tag{3.25}$$

- *Fixed payload length*

  From (3.15) (3.25), the optimal fixed payload length μ^{1*}_{sf} of SU connections must satisfy the following equation.

  $$\left(\frac{\lambda_p}{\mu^{1*}_{sf}\sqrt{\theta^1_{sf}}}\right)^2 + \frac{\lambda_p}{\mu^{1*}_{sf}} + e^{-\lambda_p(c+\frac{1}{\mu^{1*}_{sf}})} = 1. \tag{3.26}$$

  Although, the closed form solution of the above equation doesn't exist, μ^{1*}_{sf} can be calculated by using numerical techniques given in [117] or by using built in root finder functions in MATLAB.

- *Exponentially distributed payload length*

  Similar to the fixed payload length, the optimal mean payload length μ^{1*}_{se} must satisfy the following equation.

  $$\frac{2}{\theta^1_{se}}\left(\frac{\lambda_p}{\mu^{1*}_{se}}\right)^3 + \left(\frac{\lambda_p}{\mu^{1*}_{se}}\right)^2\left(1 + \frac{2}{\theta^1_{se}}\right) + e^{-\lambda_p c} = 1. \tag{3.27}$$

The roots of the cubic equation (3.27) can be calculated using the standard techniques described in [117].

Note that the mean optimal payload length $\frac{1}{\mu_{sf}^{1*}}$ and $\frac{1}{\mu_{se}^{1*}}$ must always be less than the mean inter-arrival length $\frac{1}{\lambda_p}$ of PU connections. This can be seen from (3.26) and (3.27), since the right hand side of both equations is equal to 1.

3.2.4 Numerical Results

In this section, we give some numerical examples of the forced termination probability, blocking probability and throughput with fixed and exponentially distributed payload length. In all the examples, $\lambda_p = 1$, $\mu_p = 4$ which gives a PU channel occupancy of 20%. In Monte Carlo simulations the following methods are used to compute the probabilities and throughput.

$$\hat{P}^1_{F(h,z)} = \lim_{T\to\infty} \frac{\text{Total No. of terminated connections in } [0,T]}{\text{Total No of } \textit{active} \text{ connections in } [0,T]},$$

$$\hat{P}^1_{B(h,z)} = \lim_{T\to\infty} \frac{\text{Total No. of blocked connections in } [0,T]}{\text{Total No. of connections in } [0,T]},$$

$$\hat{\rho}^1_{s(h,z)} = \lim_{T\to\infty} \frac{\text{Total Payload length of completed connections } [0,T]}{\text{T}}, \tag{3.28}$$

where, $z \in \{f, e\}$.

In Fig. 3.4 the blocking probability $P^1_{B(h,z)}$, forced termination probability $P^1_{F(h,z)}$ are plotted against the fixed and exponentially distributed payload length $\frac{1}{\mu^1_{sf}}$ and $\frac{1}{\mu^1_{se}}$, for a given SU payload intensity $\theta^1_{sz} = 1$. Note that $\theta^1_{sz} = \frac{\lambda^1_s}{\mu^1_{sz}}$ is the offered traffic. In the figure, $P^1_{F(h,z)}$ is an increasing function whereas $P^1_{B(h,z)}$ is a decreasing function. This is expected, because for the forced termination probability, lower

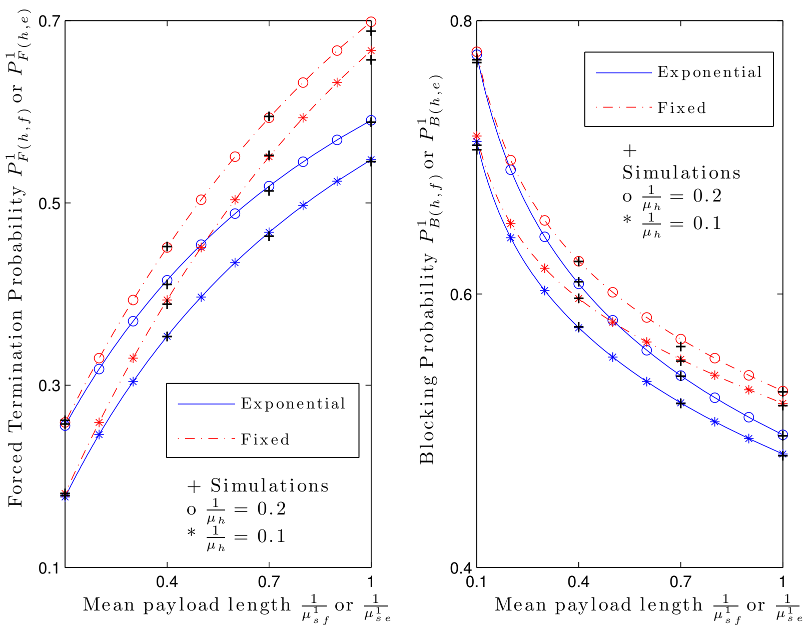

Figure 3.4: Left: Forced termination probability $P^1_{F(h,f)}$ or $P^1_{F(h,e)}$, Right: Blocking probability $P^1_{B(h,f)}$ or $P^1_{B(h,e)}$ versus SU mean payload length $\frac{1}{\mu^1_{sf}}$ or $\frac{1}{\mu^1_{se}}$ given $\{\lambda_p, \mu_p\} = \{1, 4\}$, θ^1_{se} or $\theta^1_{sf} = 1$.

connection lengths have less chance of collision with PU connections. For the blocking probability, due to the fixed payload intensity, smaller connection lengths mean faster arrival rates and more chances that SU connections are blocked. Also in Fig. 3.4 it is observed that $P^1_{F(h,e)}$ and $P^1_{B(h,e)}$ are lower than $P^1_{F(h,f)}$ and $P^1_{B(h,f)}$, respectively. This is because, for exponentially distributed connections there are more connections with smaller length than the mean connection length.

Fig. 3.5 shows the throughput curves $\rho^1_{s(h,f)}$ or $\rho^1_{s(h,e)}$ of the SU connections with fixed and exponentially distributed payload length $\frac{1}{\mu^1_{sf}}$ or $\frac{1}{\mu^1_{se}}$. In both scenarios, the figure shows that there exists an optimal payload length which maximizes the throughput. The reason is that the throughput is a function of blocking and forced termination probabilities, and the duration of the payload. For a given traffic intensity, the higher the payload length, the smaller the blocking probability. For the

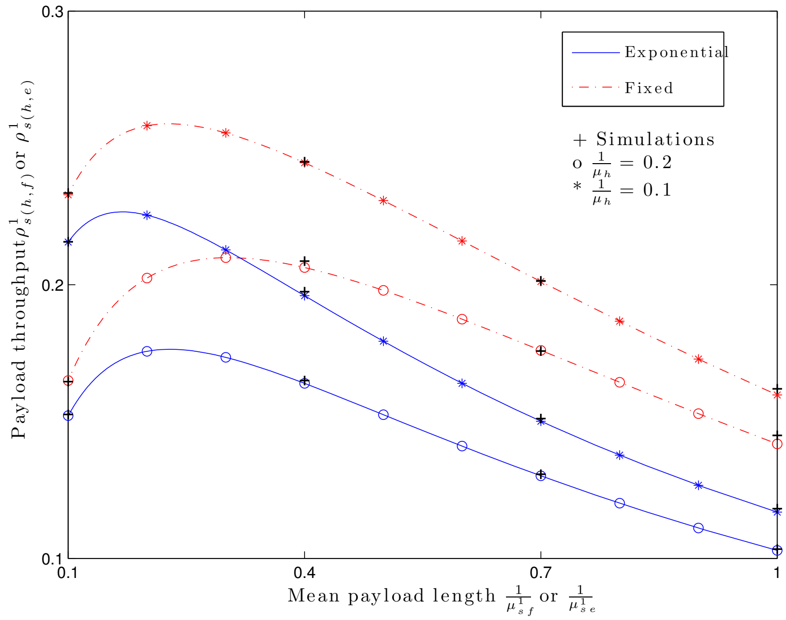

Figure 3.5: Aggregate payload throughput of SU connections $\rho^1_{s(h,f)}$ or $\rho^1_{s(h,e)}$ versus mean payload length $\frac{1}{\mu^1_{sf}}$ or $\frac{1}{\mu^1_{se}}$ given $\{\lambda_p, \mu_p\} = \{1, 4\}$, θ^1_{sf} or $\theta^1_{se} = 1$.

connection itself, since the header is fixed, the larger the payload length, the more efficient is the transmission per connection. Therefore, in terms of the blocking probability and transmission efficiency, a larger connection length is more desirable. On the other hand, larger connection size results in higher forced termination probability, hence reduced throughput.

Fig. 3.5 also shows that despite of a higher blocking probability and forced termination probability as shown in Fig. 3.4, the throughput with the fixed payload length is higher than that with the exponentially distributed payload length. This is because the average length of completed connections for the exponentially distributed payload is substantially less than that of fixed payload (3.15) (3.23). Taking into account all these factors, the fixed payload is the preferred option.

In Fig. 3.6, the optimal throughput $\rho^{1*}_{s(h,f)}$ or $\rho^{1*}_{s(h,e)}$ is plotted against the SU

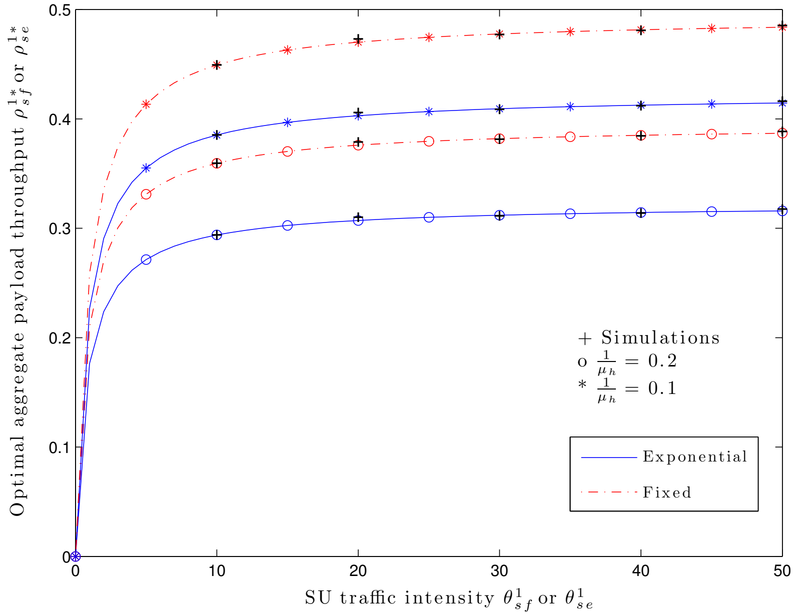

Figure 3.6: Optimal aggregate payload throughput of SU $\rho^1_{s(h,f)}$ or $\rho^1_{s(h,e)}$ versus SU traffic intensity θ^1_{sf} or θ^1_{se} given $\{\lambda_p, \mu_p\} = \{1, 4\}$.

traffic intensity θ^1_{sf} or θ^1_{se}. For each value of θ^1_{sf} or θ^1_{se}, the optimal mean payload length is calculated from (3.26) (3.27). The optimal throughput is a monotonically increasing function of SU traffic intensity. The figure also shows that there are 2 regions in terms of the rate of increase in throughput. For $0 < \theta^1_{sz} \leq 5$ the throughput increases at a relatively higher rate and there is no significant increase in throughput for $\theta^1_{sz} \geq 5$. This behaviour is expected as there is a fundamental limit in terms of achievable SU throughput for a given PU traffic intensity. In the above figure, PU occupancy is 20%, which means that a genie SU groups can reach maximum occupancy of 80%.

3.3 Multiple PU Channels ($K \geq 1$, $N \geq 1$) and Two SU groups

In this section, we first investigate the impact of spectrum sharing between two SU groups in a CRN with spectrum agility. We refer to this as the "basic system". In a basic system, the SU connection can access one of the available PU channels, however, no spectrum handoff is allowed (Fig. 3.7). Each of the two SU groups has different traffic statistics. Second, we also investigate the impact of horizontal handoff and channel reservation. The single SU group is treated as a special case, by letting θ_s tend to 0 for one of the SU groups. Such a spectrum sharing scenario has partially been considered in [56], where the effect of forced termination was neglected. This section includes the forced termination aspect, and therefore gives a more realistic result. For mathematical convenience it is assumed that the SU header length is 0.

3.3.1 Basic System

Fig. 3.8 shows the state transition diagram of a basic system. The states in the model are given by the number of active connections in the system, i.e., (i, j, k), whereas i, j are the number of active SU connections of S_A and S_B overlaying k active PU connections. The transition rate from state to state is given by the labels on the arrows. An example of a forced termination is the corner state $(i-l, j-m, k+1)$ from state (i, j, k) (shown as a dashed arrow in Fig. 3.8), where l and m represent the number of terminated active connections from S_A and S_B respectively. Following [38, Eq. (1)], the termination of $q = l + m$ out of $x = i + j$ SU connections follows a hypergeometric distribution [118], and can be written as

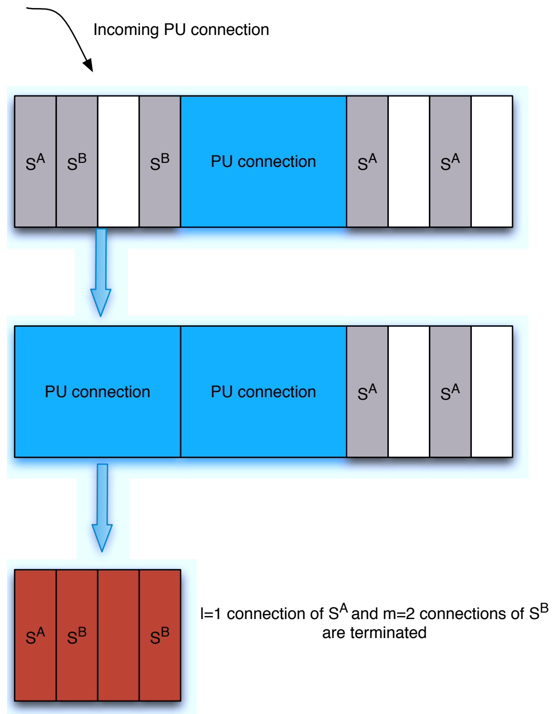

Figure 3.7: Illustration of the Basic system.

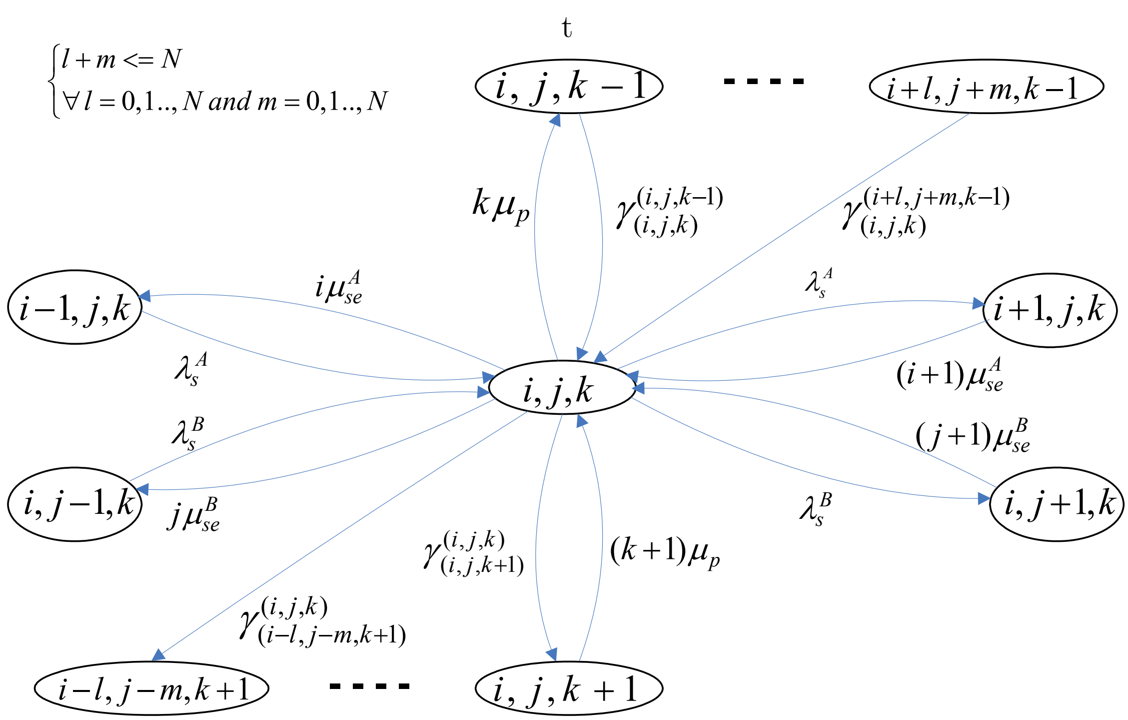

Figure 3.8: CTMC for the Basic system.

$$P^{(x,k)}_{(x-q,k+1)} = \frac{\binom{N}{q}\binom{(K-k-1)N}{x-q}}{\binom{(K-k)N}{x}}. \tag{3.29}$$

Given i and j in x, the probability of exactly l and m in q can be written as

$$P^{(i,j)}_{(i-l,j-m)} = \frac{\binom{i}{l}\binom{j}{m}}{\binom{x}{q}}. \tag{3.30}$$

Combining (3.29) and (3.30) gives the probability of having exactly l and m SU connections terminated from the state (i, j, k), and can be calculated from

$$P^{(i,j,k)}_{(i-l,j-m,k+1)} = P^{(i,j)}_{(i-l,j-m)} P^{(x,k)}_{(x-q,k+1)}. \tag{3.31}$$

The termination of l and m SU connections occurs at the arrival of each PU connection. Therefore, given the arrival rate of a PU connection λ_P, the state transition *rate* $\gamma^{(i,j,k)}_{(i-l,j-m,k+1)}$ can be written as

$$\gamma^{(i,j,k)}_{(i-l,j-m,k+1)} = P^{(i,j,k)}_{(i-l,j-m,k+1)} \lambda_p \tag{3.32}$$

By substituting (3.29) - (3.31) in (3.32), the state transition rate from (i, j, k) to $(i - l, j - m, k + 1)$ is given as

$$\gamma^{(i,j,k)}_{(i-l,j-m,k+1)} = \frac{\frac{\binom{i}{l}\binom{j}{m}}{\binom{i+j}{l+m}}\binom{N}{l+m}\binom{(K-k-1)N}{i+j-l-m}}{\binom{(K-k)N}{i+j}}\lambda_p, \tag{3.33}$$

for $0 \leq l + m \leq N$. Setting j and m to zero, (3.33) is the same as [38, Eq. (1)]. From Fig. 3.8, a set of balance equations of the CTMC model for all $0 \leq i, j \leq KN$

and $0 \le k \le K$ can be written as

$$\begin{aligned}
&\lambda_s^A P_\phi(i-1,j,k) + (i+1)\mu_{se}^A P_\phi(i+1,j,k) + \lambda_s^B P_\phi(i,j-1,k) \\
&+(j+1)\mu_{se}^B P_\phi(i,j+1,k) + (k+1)\mu_p P_\phi(i,j,k+1)+ \\
&\sum_{l=0}^{N}\sum_{m=0}^{N} \gamma_{(i,j,k)}^{(i+l,j+m,k-1)} P_\phi(i+l,j+m,k-1)\delta(l+m \le N) = \\
&\left(\lambda_s^A + i\mu_{se}^A + \lambda_s^B + j\mu_{se}^B + k\mu_P + \sum_{l=0}^{N}\sum_{m=0}^{N} \gamma_{(i-l,j-m,k+1)}^{(i,j,k)} \delta(l+m \le N)\right) P_\phi(i,j,k),
\end{aligned} \tag{3.34}$$

where, $P_\phi(i,j,k) = P(i,j,k)\phi(i,j,k)$, $\phi(i,j,k)$ is one for all valid states and zero for all non-valid states. Mathematically,

$$\phi(i,j,k) = \begin{cases} 1 & i+j \le (K-k)N, \\ 0 & \text{otherwise}, \end{cases} \tag{3.35}$$

and $P(i,j,k)$ denotes the probability that the system is in the state (i,j,k). The state probability must satisfy the following constraint

$$\sum_{i=0}^{NK}\sum_{j=0}^{NK}\sum_{k=0}^{K} P_\phi(i,j,k) = 1. \tag{3.36}$$

The set of equations expressed by (3.34) can be written as a multiplication of state transition matrix Q and state probability vector P

$$QP = 0. \tag{3.37}$$

Replacing the last row of Q, with the constraint in (3.36), the state probabilities can be solved by

$$P = Q^{-1}\epsilon, \tag{3.38}$$

where, $\epsilon^T = [0\ ,\ 0\ ,\ ..\ ,\ 1]$ and $(\cdot)^T$ is the transpose operator. For the basic system, the blocking of a new SU connection occurs when all PU channels are fully occupied. The state (i,j,k) is a blocking state if $i+j+Nk = NK$. The probabilities of all blocking states are summed to calculate the blocking probability which is given by

$$P_{Be}^{AB} = \sum_{i=0}^{NK}\sum_{j=0}^{NK}\sum_{k=0}^{K} \delta(i+j+Nk-NK)P_\phi(i,j,k). \tag{3.39}$$

For the given state (i,j,k), $\gamma_{(i-l,j-m,k+1)}^{(i,j,k)} P_\phi(i,j,k)$ is the termination rate of l and m SU connections. From the state (i,j,k), the total termination rate $F(i,j,k)$ can be written as

$$F(i,j,k) = \sum_{l=0}^{NK} \sum_{m=0}^{NK} (l+m)\gamma_{(i-l,j-m,k+1)}^{(i,j,k)} P_\phi(i,j,k)\delta_f, \tag{3.40}$$

where δ_f is given as

$$\delta_f = \begin{cases} 1 & 0 \le l+m \le N \\ 0 & \text{otherwise}, \end{cases} \tag{3.41}$$

The total connection rate is given by $(1 - P_{Be}^{AB})(\lambda_s^A + \lambda_s^B)$. Using (3.10) and (3.40) the combined forced termination probability P_{Fe}^{AB} of a SU connection can be written as

$$P_{Fe}^{AB} = \frac{\sum\limits_{i=0}^{NK}\sum\limits_{j=0}^{NK}\sum\limits_{k=0}^{K}\sum\limits_{l=0}^{N}\sum\limits_{m=0}^{N} (l+m)\gamma_{(i-l,j-m,k+1)}^{(i,j,k)} P_\phi(i,j,k)\delta_f}{(1-P_{Be}^{AB})(\lambda_s^A + \lambda_s^B)}. \tag{3.42}$$

Similarly, the individual forced termination probabilities for user groups S^A and S^B can be respectively calculated as

$$P_{Fe}^{A} = \frac{\sum\limits_{i=0}^{NK}\sum\limits_{j=0}^{NK}\sum\limits_{k=0}^{K}\sum\limits_{l=0}^{N}\sum\limits_{m=0}^{N} l\gamma_{(i-l,j-m,k+1)}^{(i,j,k)} P_\phi(i,j,k)\delta_f}{(1-P_{Be}^{AB})\lambda_s^A}, \tag{3.43}$$

and

$$P_{Fe}^{B} = \frac{\sum\limits_{i=0}^{NK}\sum\limits_{j=0}^{NK}\sum\limits_{k=0}^{K}\sum\limits_{l=0}^{N}\sum\limits_{m=0}^{N} m\gamma_{(i-l,j-m,k+1)}^{(i,j,k)} P_\phi(i,j,k)\delta_f}{(1-P_{Be}^{AB})\lambda_s^B}. \tag{3.44}$$

From (3.42),(3.43) and (3.44), it can be shown that

$$P_{Fe}^{AB} = \frac{\lambda_s^A}{\lambda_s^A + \lambda_s^B} P_{Fe}^A + \frac{\lambda_s^B}{\lambda_s^A + \lambda_s^B} P_{Fe}^B. \tag{3.45}$$

Note that P_{Fe}^{AB} is not the average of P_{Fe}^A and P_{Fe}^B except for the special case where $\lambda_s^A = \lambda_s^B$.

3.3.1.1 Special Case-Single SU Group

In this section, the forced termination and blocking probabilities for a single SU group are treated as a special case of two SU groups. Let P_{Fe}^1 and P_{Be}^1 be the forced termination and blocking probabilities of a single SU group respectively. Setting $j = 0$, $m = 0$, $\lambda_s^B = 0$, $\mu_{se}^B = 0$ in (3.33) and (3.34), we get the same equations as in [38, Eqs. (1-2)] i.e., $\gamma_{(i-l,0,k+1)}^{(i,0,k)} = \gamma_{(i-l,k+1)}^{(i,k)}$ and $P_\phi(i,0,k) = P_\phi(i,k)$. Under this condition, the expression in (3.39) for the blocking probability is identical to that of the single SU group.

Similarly, it can be shown that the forced termination probability in (3.42) can be simplified to

$$P_{Fe}^1 = \frac{\sum_{i=0}^{NK}\sum_{k=0}^{K}\sum_{l=1}^{N} l\gamma_{(i-l,k+1)}^{(i,k)} P_\phi(i,k)}{(1-P_{Be}^1)\lambda_s^1}. \tag{3.46}$$

The term $\sum_{l=1}^{NK} l\gamma_{(i-l,k+1)}^{(i,k)} P_\phi(i,k)$ in (3.46) is the termination rate of the SU connections from the state (i,k). By summing over all valid states $\phi(i,0,k)$, we get the total number of terminated connections per unit time. Note that the forced termination probability P_{Fe}^1 from [38, Eq. (4)] differs from the above, because it describes a rate rather than a probability.

3.3.2 Basic System with Spectrum Handoff and Channel Reservation

In this section, we extend the results derived in the previous section to system with spectrum handoff and channel reservation. As described previously, spectrum handoff allows an active SU connection to move to another vacant subchannel, rather being terminated by an incoming PU connection. This phenomena is illustrated in Fig. 3.9. To further ensure the continuity of existing SU connections, a small number of subchannels (marked R) are reserved exclusively for spectrum handoff purpose. These subchannels improve the forced termination probability at the expense of increased blocking probability.

In order to quantify the performance using spectrum handoff and channel reservation, the following measures are defined:

$$G_F(r) = \frac{P_{Fe}^{AB}(\text{Basic System}) - P_F(r)}{P_{Fe}^{AB}(\text{Basic System})}, r = 0 \ldots N, \tag{3.47}$$

and

$$G_B(r) = \frac{P_{Be}^{AB}(r) - P_{Be}^{AB}(\text{Basic System})}{P_{Be}^{AB}(\text{Basic System})}, r = 0 \ldots N, \tag{3.48}$$

where, $G_F(r)$ expresses the improvement (fractional reduction) in forced termination probability of the basic system when r reserved channels are used, and $G_B(r)$ describes the degradation (fractional increase) in blocking probability with r reserved channels. Since N is the maximum number of terminations per PU connection, we only consider $r \leq N$. If $r > N$ the complexity of the CTMC increases significantly as it has to cater for multiple PU arrivals rather than a single arrival. We define a measure, *tradeoff gain* $L(r)$, which relates improvement in forced termination probability to the degradation in terms of the blocking probability as

$$L(r) = \frac{G_F(r)}{G_B(r)}. \tag{3.49}$$

The condition $L(r) >> 1$ indicates that the SU network has a greater improvement in forced termination probability compared to its increase in blocking probability.

Fig. 3.10 shows the state transitions of the CTMC with r reserved channels $0 \leq r < N$. The state diagram for $r = N$ requires slight modification. In Fig. 3.10(a), spectrum handoff ensures no termination when a new PU connection is made. Fig. 3.10(b)-(e) depicts the condition when the total number of vacant

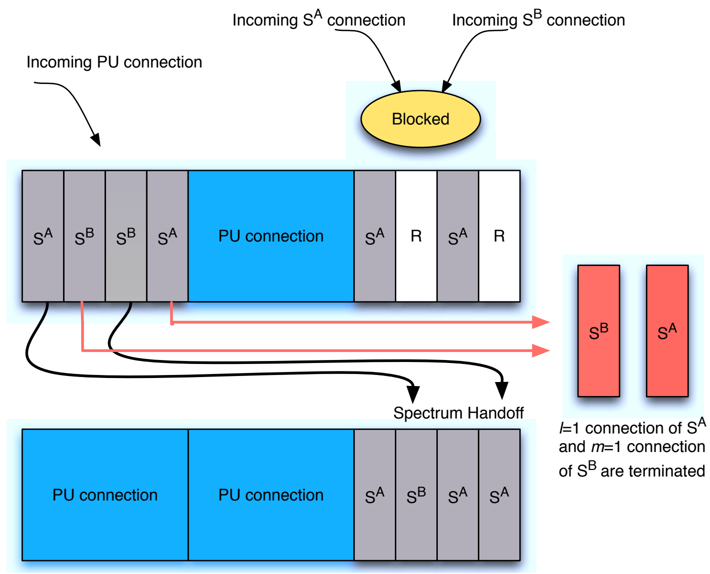

Figure 3.9: Illustration of the system with spectrum handoff and channel reservation. The number of reserved channels $r = 2$.

sub-channels is less than N. On the arrival of a new PU connection, we have $i + j + (k + 1)N > KN$, therefore forced termination occurs. Fig. 3.10(b) allows new SU connections because the number of free subchannels is greater than r. Contrary to Fig. 3.10(b), Figs. 3.10(c)-(e) will allow no new SU connections since the number of free channels are less than or equal to r. Note that there is a number of states which have a single arrow to/from state (i, j, k) . These states include the cases where either forced termination occurs, or a new SU connection is blocked because there is no vacant subchannel except the reserved subchannels. The condition Figs. 3.10(d)-(e) also signifies that the SUs are utilising the reserved channels. The state (i, j, k) in Fig. 3.10(e) can also result from other states $(i+l, j-m, k-1)$. In these transitions, forced termination occurs.

With spectrum handoff and channel reservation, the forced termination will only occur when $i+j+Nk > (K-1)N$. The arrival of a new PU connection will cause the existing SU connections to pack themselves in $(K-(k+1))N$ subchannels, i.e.,

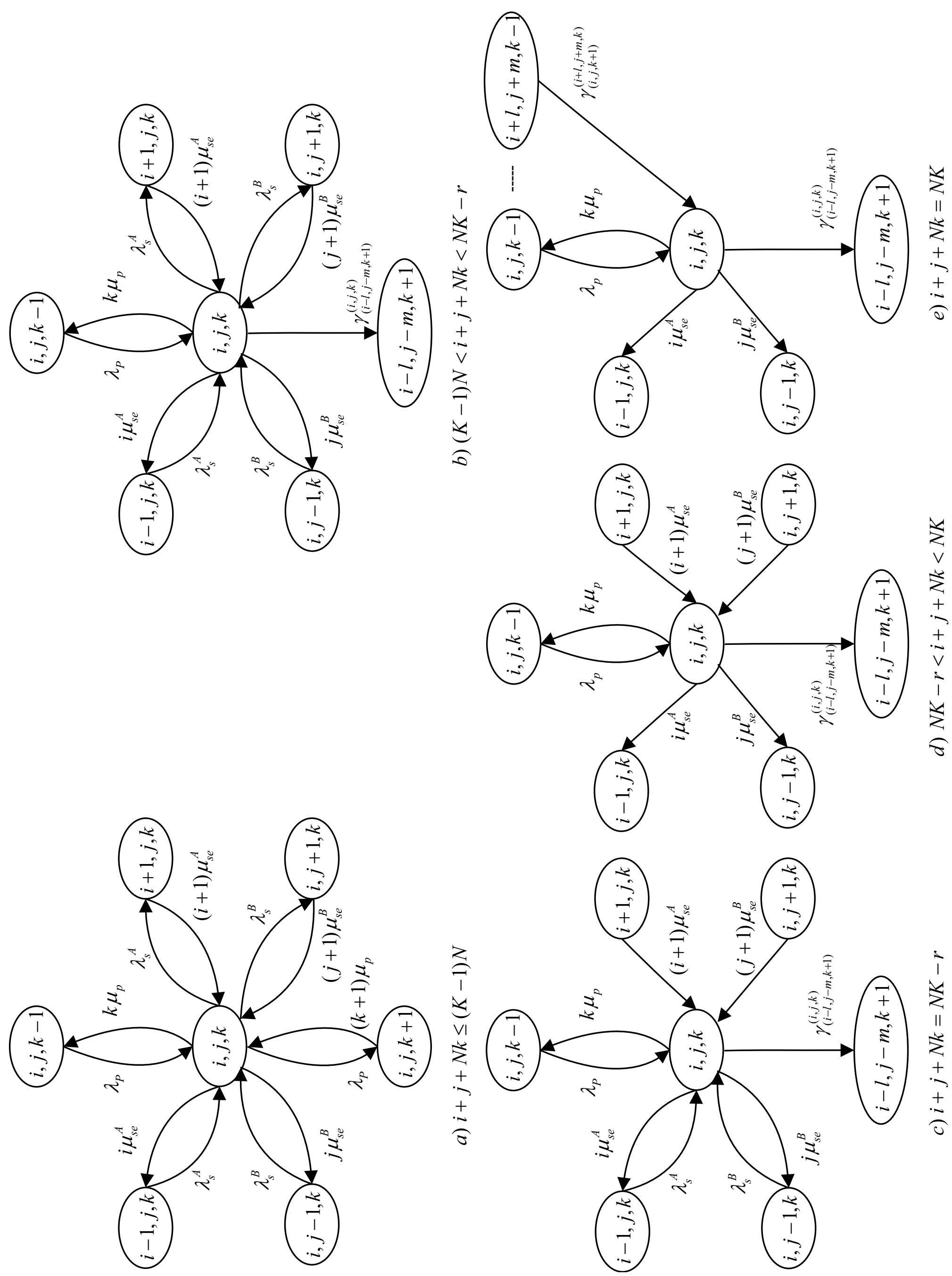

Figure 3.10: A CTMC for the system with spectrum handoff and channel reservation $r < N$. The states $(i-l, j-m, k+1)$ satisfy packing condition i.e., $(i-l)+(j-m) = (K-k-1)N$ for $0 < l+m \leq N$.

the transition of current state (i, j, k) to state $(i-l, j-m, k+1)$ with the *packing condition* $(i-l)+(j-m) = (K-k-1)N$. The rate of this transition is expressed as

$$\gamma^{(i,j,k)}_{(i-l,j-m,k+1)} = \frac{\binom{i}{l}\binom{j}{m}}{\binom{i+j}{l+m}}\lambda_p. \tag{3.50}$$

The condition of a valid state $\phi_r(i, j, k)$ for all $i, j = \{0, \ldots, KN-r\}$ and $k = \{0, \ldots K\}$ is given as

$$\phi_r(i,j,k) = \begin{cases} 1 & i+j \le (K-k)N \quad \mathrm{and i + j \le KN - r} \\ 0 & \text{otherwise.} \end{cases} \tag{3.51}$$

Similar to the basic system in the previous section, the set of balance equations for the CTMC in Fig. 3.10 are shown in Appendix A. Together with the constraint (3.36), the state probabilities $P_{\phi_r}(i, j, k) = P(i, j, k)\phi_r(i, j, k)$ can be solved using (3.37) and (3.38). With spectrum handoff and channel reservation, the blocking of a new SU connection occurs when the number of vacant subchannels is less than or equal to r. Mathematically,

$$P^{AB}_{Be}(r) = \sum_{i=0}^{NK-r}\sum_{j=0}^{NK-r}\sum_{k=0}^{K}\delta(i+j+Nk \ge KN-r)P_{\phi_r}(i,j,k). \tag{3.52}$$

Using (3.10), the combined forced termination probability with r reserved subchannels can be calculated from,

$$P^{AB}_{Fe}(r) = \frac{1}{(1-P^{AB}_{Be}(r))}\sum_{i=0}^{NK-r}\sum_{j=0}^{NK-r}\sum_{k=0}^{K}\sum_{l=0}^{N}\sum_{m=0}^{N}\frac{(l+m)}{(\lambda^A_s+\lambda^B_s)}\gamma^{(i,j,k)}_{(i-l,j-m,k+1)}P_{\phi_r}(i,j,k)\delta_{fr}. \tag{3.53}$$

The individual forced termination probabilities for user groups S^A and S^B are

$$P^{A}_{Fe}(r) = \frac{1}{(1-P^{AB}_{Be}(r))}\sum_{i=0}^{NK-r}\sum_{j=0}^{NK-r}\sum_{k=0}^{K}\sum_{l=0}^{N}\sum_{m=0}^{N}\frac{l}{\lambda^A_s}\gamma^{(i,j,k)}_{(i-l,j-m,k+1)}P_{\phi_r}(i,j,k)\delta_{fr}, \tag{3.54}$$

and

$$P_{Fe}^{B}(r) = \frac{1}{(1-P_{Be}^{AB}(r))} \sum_{i=0}^{NK-r} \sum_{j=0}^{NK-r} \sum_{k=0}^{K} \sum_{l=0}^{N} \sum_{m=0}^{N} \frac{m}{\lambda_s^B} \gamma_{(i-l,j-m,k+1)}^{(i,j,k)} P_{\phi_r}(i,j,k)\delta_{fr}, \tag{3.55}$$

where, δ_{fr} is defined as

$$\delta_{fr} = \delta((i-l)+(j-m)-(K-k-1)N)\ \delta(i+j+Nk > (K-1)N)\ \delta(0 < l+m \leq N). \tag{3.56}$$

Note that δ_{fr} consists of three conditions, i.e., the packing, termination and a valid number of dropped SU connections.

3.3.2.1 Special Case-Single SU Group

In the case of a single SU group, we set the respective parameters for S_B in Figs. 3.10(a)-(e) to 0. Note that the resulting state transition diagrams are different from [38, Fig. 4]. The latter did not include the proper state transitions for the reserved channels, which gave over optimistic result. In Figs. 3.10(a)-(e) all five state transition scenarios are included which gives a complete CTMC analysis.

The state probabilities $P_{\phi_r}(i,k)$ are calculated by following the basic system's approach(). For a single SU group, the blocking probability with r reserved subchannels can be written as

$$P_{Be}^{1}(r) = \sum_{i=0}^{NK-r} \sum_{k=0}^{K} \delta(i+Nk \geq KN-r) P_{\phi_r}(i,k). \tag{3.57}$$

The above expression states that the blocking of a new SU connection can only occur when the number of vacant subchannels are less than or equal to r. For a single SU group, the forced termination probability is given by

$$P_{Fe}^{1}(r) = \frac{\sum_{i=0}^{NK-r} \sum_{k=0}^{K} \sum_{l=1}^{N} \gamma_{(i-l,k+1)}^{(i,k)} P_{\phi_r}(i,k) \delta_f^1(r)}{(1-P_B(r)^1)\lambda_s^1}, \tag{3.58}$$

where, $\delta_f^1(r) = \delta(i + Nk > (K-1)N)\ \delta(i - (K-k-1)N - l)$. Note that $\delta_f^1(r)$ refers to two conditions. Firstly, the forced termination occurs only when $(i+Nk) > (K-1)N$. Under this condition $\gamma_{(i-l,k+1)}^{(i,k)} = \lambda_P$. Secondly, $(i-l)$ SU connections are packed into $(K-k-1)N$ available subchannels and the remaining l connections are terminated.

3.3.3 Network Throughput

The network throughput is defined as the products of the connection completion rate, the average service duration per connection and the data rate. For unit data rate, the theoretical throughput can be expressed as

$$\rho_{se}^{x_0} = (1 - P_{Be}^{x_0})(1 - P_{Fe}^{x_0})^2 \theta_{se}^{x_0} \tag{3.59}$$

where $\theta_{se}^{x_0} = (\lambda_s^{x_0}/\mu_{se}^{x_0})$ is called traffic intensity [25] and $x_0 \in \{1, A, B\}$ for single or two user groups (S_A and S_B), respectively.

For a fixed $\theta_{se}^{x_0}$, the throughput $\rho_{se}^{x_0}$ reaches a maximum when the SU service rate ($\mu_{se}^{x_0}$) approaches infinity, i.e., $\rho_{se}^{x_0 *} = \lim_{\mu_{se}^{x_0} \to \infty} \rho_{se}^{x_0}$. A simple proof is given as follows. When $\mu_{se}^{x_0} \to \infty$, we have $P_{Fe}^{x_0} \to 0$. The blocking probability in (3.59) consists of two parts i.e., $P_{Be}^{x_0} = P_{Be}^{x_0}(pri) + P_{Be}^{x_0}(sec)$, where $P_B(pri)$ is the blocking probability due to the situation in which PUs occupy all the subchannels, and $P_{Be}^{x_0}(sec)$ is the blocking probability which can be computed from the probability for a given number of vacant subchannels. It is known that $P_{Be}^{x_0}(sec)$ is constant for a fixed $\theta_{se}^{x_0}$ [25]. Therefore, the maximum achievable throughput ρ_{se}^{x} can be written as

$$\rho_{se}^{x_0 *} = \lim_{\mu_{se}^{x_0} \to \infty} (1 - P_{Be}^{x_0})(1 - P_{Fe}^{x_0}) \theta_{se}^{x_0} = (1 - P_{Be}^{x_0}(\infty)) \theta_{se}^{x_0}, \tag{3.60}$$

where, $P_{Be}^{x_0}(\infty)$ is the blocking probability when $P_{Fe}^{x_0} = 0$.

3.3.4 Numerical Results

In this section we give some numerical examples of $P_{Fe}^{x_0}$, $P_{Be}^{x_0}$, and the throughput $\rho_{se}^{x_0}$ for SUs. In all of the following simulations, we set $K = 3, N = 6$ and $P_{Fe}^{x_0}$, $P_{Be}^{x_0}$, $\rho_{se}^{x_0}$ are plotted against PU (SU) traffic intensity θ_p ($\theta_{se}^{x_0}$). In addition, service rates of the SU groups are normalised with respect to the PUs rate i.e., $\hat{\mu}_{se}^{x_0} = (\mu_{se}^{x_0}/\mu_p)$, where $x_0 \in \{1, A, B\}$. In addition, $r = 0$ indicates the spectrum handoff only condition without channel reservation.

3.3.4.1 Single SU Group

In Fig. 3.11, P_{Fe}^1 and P_{Be}^1 are plotted against $\theta_p \in [0.5, 1.5]$, for given $\theta_{se}^1 = 8$ and $\hat{\mu}_{se}^1 = 1$. It can be calculated that the range of θ_p corresponds to the PU channel occupancy from 16.43% to 43.28%. Compared to systems with spectrum handoff and channel reservation, the basic system has the lowest blocking and the highest forced termination probability. Spectrum handoff results in a significant drop in P_{Fe}^1 for a moderate increase in P_{Be}^1. The introduction of reserved channels are not particularly effective in this instance.

Fig. 3.12 shows the impact of θ_{se}^1 on P_{Fe}^1 and P_{Be}^1, for a given $\theta_p = 1$ and $\hat{\mu}_{se}^1 = 1$. The behaviour of P_{Be}^1 is similar to that in Fig. 3.11. For the basic system, P_{Fe}^1 decreases slightly as θ_{se}^1 increases. This is counter intuitive. At high θ_{se}^1, due to fixed N, the forced termination rate $\sum_{i=0}^{NK} \sum_{k=0}^{K} F(i, 0, k)$ will saturate faster than the connection rate $(1 - P_{Be}^1)\lambda_s^1$, implying an increased SU occupancy. Note that P_F is the probability of termination per occupied channel. With spectrum handoff and channel reservation P_{Fe}^1 initially decreases slightly, before increasing with θ_{se}^1. This can be explained as follows. At very low θ_{se}^1 values, the existing SU connections readily find vacant subchannels. As θ_{se}^1 increases the number of occupied channels

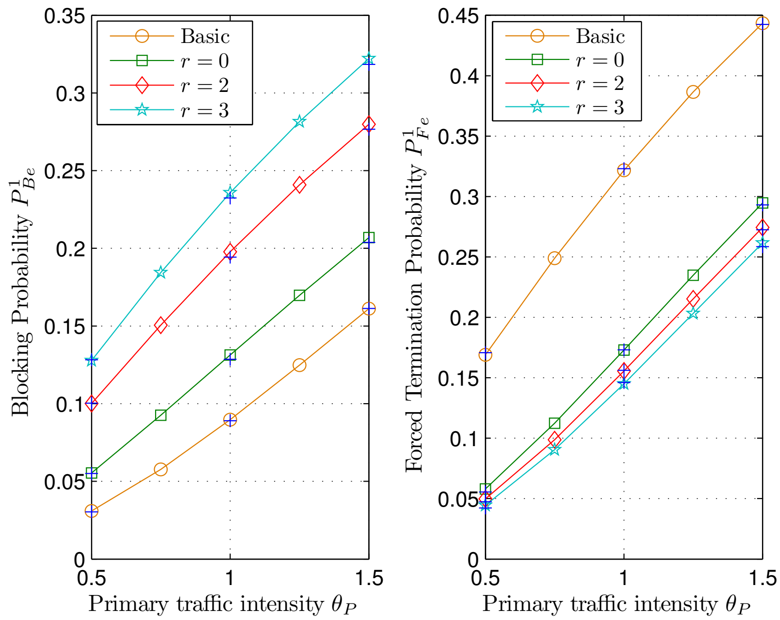

Figure 3.11: Single SU group, **Left**: Blocking probability, and **Right**: Forced termination probability versus PU traffic intensity given $\theta^1_{se} = 8$ and $\hat{\mu}^1_{se} = 1$. Simulation results are shown with "+".

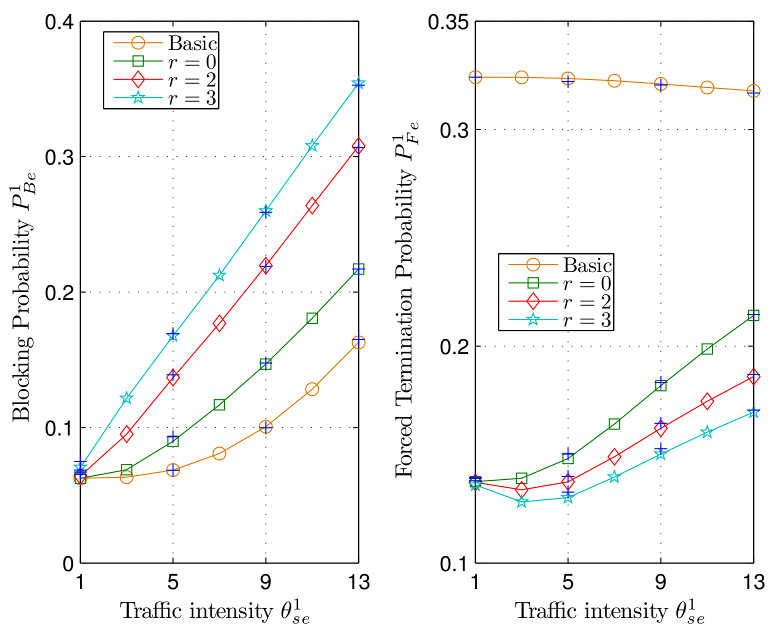

Figure 3.12: Single SU group, **Left**: Blocking probability, and **Right**: Forced termination probability versus SU traffic intensity given $\theta_p = 1$ and $\hat{\mu}^1_{se} = 1$. Simulation results are shown with "+".

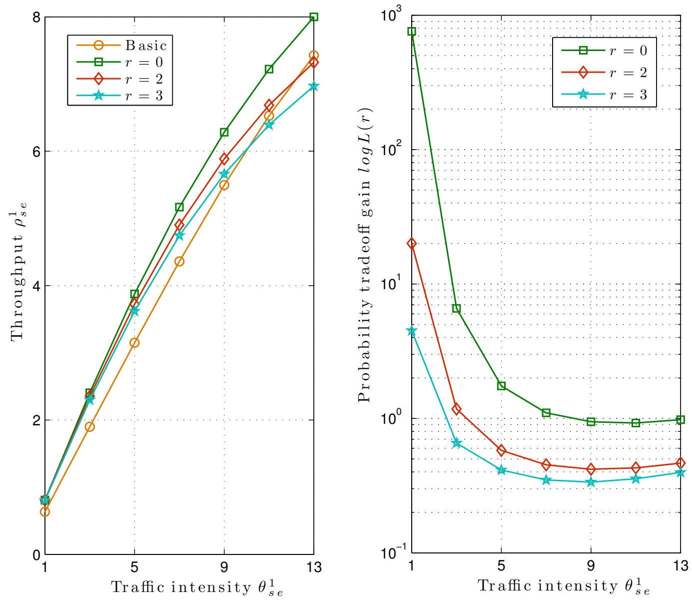

t

Figure 3.13: Single SU group, **Left**: Aggregate throughput, and **Right**: Probability tradeoff gain versus SU traffic intensity given $\theta_P = 1$ and $\hat{\mu}_{se}^1 = 1$.

increases, but there is still enough vacant subchannels to handle the arrival of a new PU connection and the probability of forced termination (for an existing connection) decreases. Eventually, at high θ_{se}^1 there are fewer vacant subchannels to accomodate the displaced subchannels and forced termination probability increases.

The throughput ρ_{se}^1 and the probability tradeoff gain $L(r)$ are shown in Fig. 3.13 for a given $\theta_p = 1$ and $\hat{\mu}_{se}^1 = 1$. At low values of θ_{se}^1, the network throughput with spectrum handoff and channel reservation is higher than the basic system. However, the same cannot be said for high values of θ_{se}^1. The curves of tradeoff gain $L(r)$ show that more reserved channel give less gain in probability tradeoff. Also, for the same r, the effectiveness of the tradeoff reduces as θ_{se}^1 increases.

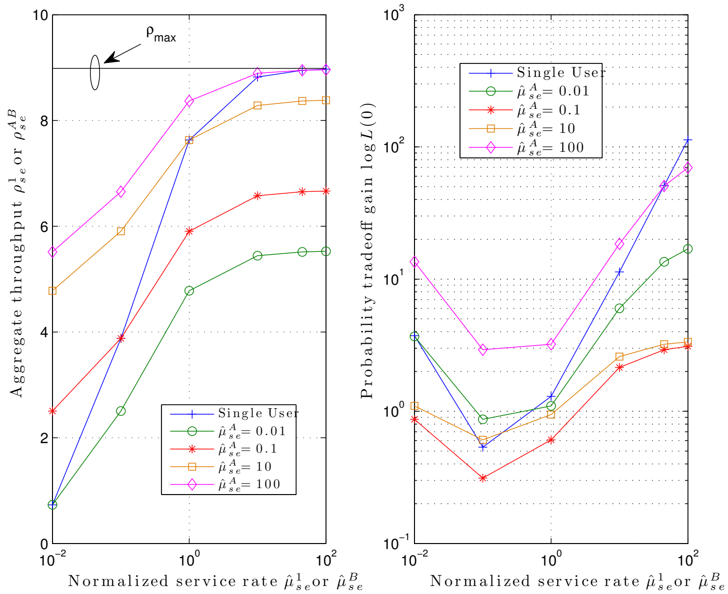

Figure 3.14: Comparison of single and two SU groups, **Left**: Aggregate Throughput, and **Right**: tradeoff gain versus normalized SU service rate given $\theta_P = 1$, $\theta^1_{se} = 12$, $\theta^A_{se} = 6$, $\theta^B_{se} = 6$ and $r = 0$.

3.3.4.2 Two SU Groups

In Fig. 3.14, we compare the throughput and probability tradeoff gain $L(r)$ of two user groups with a single SU group having the same traffic intensity i.e., $\theta^1_{se} = \theta^A_{se} + \theta^B_{se}$. In this example the abscissa is the SU service rate $\mu^B_{se}(\mu^1_{se})$ and we assume that $\theta_p = 1$, $\theta^A_{se} = \theta^B_{se} = 6$, $\theta^1_{se} = 12$, $r = 0$.

The throughput $\rho^{AB}_{se} = \rho^A_{se} + \rho^B_{se}$ and ρ^1_{se} are monotonically increasing functions of both $\hat{\mu}^A_{se}$, $\hat{\mu}^B_{se}$ and μ^1_{se} respectively. When $\hat{\mu}^1_{se} = \hat{\mu}^A_{se} = \hat{\mu}^B_{se}$ the curves ρ^{AB}_{se} intersect with single user throughput ρ^1_{se}. This is expected, since at the intersection points SUs from both S_A and S_B are arriving at the same rate which is half of that of single user group S^1. The maximum achievable throughputs for both single and two user groups are identical i.e., $\rho^{AB*}_{se} = \rho^{1*}_{se}$.

For probability tradeoff gain $L(0)$, all the curves exhibit a U-shaped behaviour.

This can be explained as follows. For relatively low service rates (long service duration), blocking probability increases at a higher rate than the rate of reduction in forced termination probability, whereas the opposite happens at high service rates (short service duration). For the given simulation parameters, service rates close to 0.1 for both groups minimise the probability trade-off gain. This example demonstrates that the SU service duration relative to the PU counterpart has significant impact on the tradeoff, and the tradeoff is much more effective when the SU service rates $\mu_{se}^{x_0}$ is much larger or smaller than the PUs.

3.4 Airtime Fairness

This section investigates the throughput fairness among two SU groups. For brevity, we limit our discussion to the spectrum handoff case only i.e., $r = 0$.

Fairness: *We define a fairness scheme in which the fractional throughput loss of both SU groups (with respect to their offered traffic θ_{se}^{z}) is equal, where $z \in \{A, B\}$*

$$\begin{aligned} G_{\rho}^{A} &= \frac{\theta_{se}^{A} - \rho_{se}^{A}}{\theta_{se}^{A}} \\ G_{\rho}^{B} &= \frac{\theta_{se}^{B} - \rho_{se}^{B}}{\theta_{se}^{B}} \end{aligned} \tag{3.61}$$

Based on the above equations, the fair metric is

$$\digamma = \frac{G_{\rho}^{A}}{G_{\rho}^{B}} \tag{3.62}$$

The scheme is optimally fair when $\digamma^{*} = 1$. In Fig. 3.15(a), the no constraint sharing gives an ideal fairness $\digamma^{*} = 1$, only for $\mu_{se}^{A} = \mu_{se}^{B}$. It applies to any values of λ_{s}^{A} and λ_{s}^{B} (Fig. 3.15 has $\lambda_{s}^{A} = 12$, $\lambda_{s}^{B} = 20$). When $\mu_{se}^{A} = \mu_{se}^{B}$, the two SU groups act as a single SU group due to the superposition of Poisson arrivals. Mathematically, $P_{Fe}^{A} = P_{Fe}^{B}$, and P_{Be}^{AB} is constant for both S^{A} and S^{B}. As the difference in the service rates between the SU groups increases, the fairness $\digamma$ deviates from its ideal value.

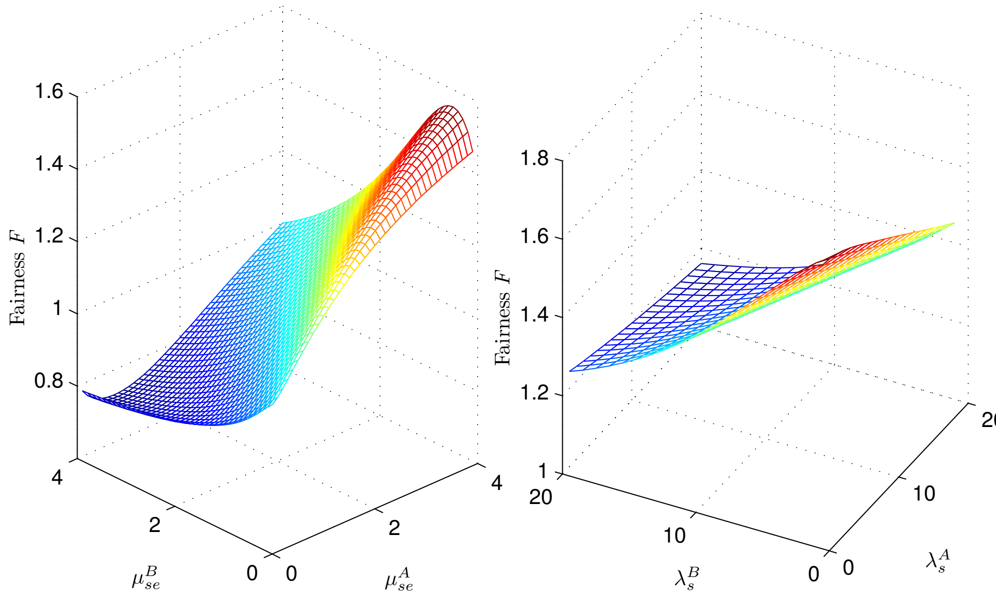

Figure 3.15: **Left**: Fairness F versus SU service rate $\mu_{se}^A(\mu_{se}^B)$ given $\lambda_s^A = 12$, $\lambda_s^B = 20$, $\mu_p = 1$ and $\lambda_p = 1$. **Right**: Fairness F, versus SU arrival rate $\lambda_s^A(\lambda_s^B)$ given $\mu_{se}^A = 0.8$, $\mu_{se}^B = 2$, $\mu_p = 1$ and $\lambda_p = 1$.

In Fig. 3.15(b), we investigate the fairness F and throughput ρ for a given $\mu_{se}^A = 0.8$ and $\mu_{se}^B = 2$. The fairness curves at low to medium values of arrival rate λ_s^A (λ_s^B) show that spectrum sharing results in an unfair distribution of channel resources among the two SU groups. The percentage loss in throughput of S^A (large connection length) is significantly higher. The arrival rate has less effect on fairness.

3.4.1 Fairness Through Channel Partitioning

In the previous section, the results show that dissimilar SU groups can lead to unfairness. In the following we investigate the potential of a channel partitioning policy to address unfairness. In essence, we restrict the maximum number of allowable active connections to N^A and N^B for S^A and S^B respectively, where $0 \leq N^A \leq NK$ and $0 \leq N^B \leq NK$. The variation of N^A and N^B gives rise to the following 3

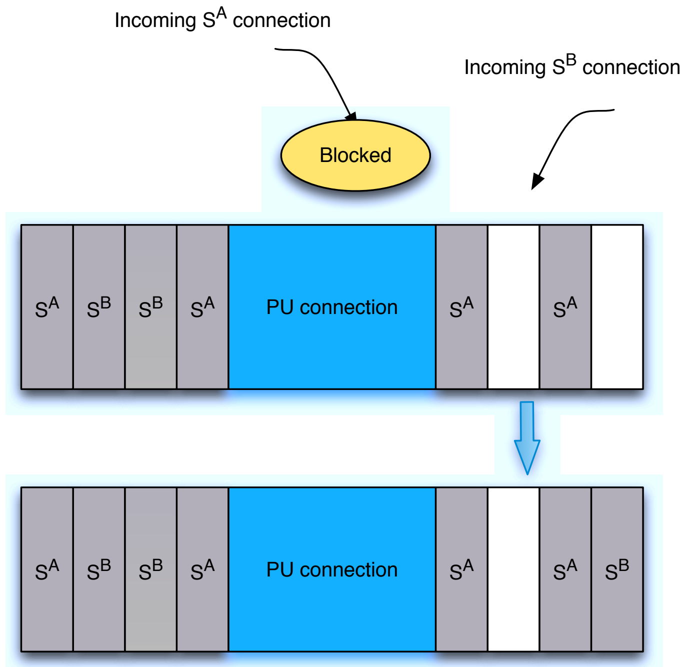

Figure 3.16: Illustration of channel partitioning scenario, $K = 3$, $N = 4$, $N^A = 4$, $N^B = 8$.

conditions. The first condition $N^A = NK - N^B$ represents a channel partitioning scenario, the second condition $N^A + N^B > NK$ is a weaker channel partitioning scenario, whereas the condition $N^A = N^B = NK$ is the no constraint scenario described in the previous subsection. Here, we only consider the channel partitioning scenario because it does not require the calculation of state probabilities in which the transmission of the SU groups overlap. A channel partitioning scenario is shown in Fig. 3.16, in which an incoming S^B connection is allowed to access the channel, while an incoming S^A connection is blocked even though there is a vacant subchannel. In the channel partitioning scenario, the objective is to find a feasible number of channels $\{N^A, N^B\}$ such that the access scheme is optimally fair i.e., $\digamma^* \approx 1$. Due to integer values of $\{N^A, N^B\}$ the optimally fair value of 1 may not always be possible. From (3.62) it is also obvious that the calculation of $\{N^A, N^B\}$ requires the knowledge of termination and blocking probabilities for both SU groups. In the following, we model this channel partitioning scenario as a simple extension of the CTMC in Section 3.3.3.

The maximum number of allowable connections of S^A and S^B are N^A and N^B i.e., $i = \{0, \ldots, N^A\}$, $j = \{0, \ldots, N^B\}$ and the state probabilities can be solved under the fundamental probability constraint (similar to the section 3.3). The blocking probabilities and forced termination probabilities are given as follows.

$$P^A_{Be} = \sum_{i=0}^{N^A-1} \sum_{j=0}^{N^B} \sum_{k=0}^{K} \delta(i + j + Nk - NK) P_{\phi_0}(i, j, k) + \sum_{j=0}^{N^B} \sum_{k=0}^{K} P_{\phi_0}(N^A, j, k), \quad (3.63)$$

$$P^B_{Be} = \sum_{i=0}^{N^A} \sum_{j=0}^{N^B-1} \sum_{k=0}^{K} \delta(i + j + Nk - NK) P_{\phi_0}(i, j, k) + \sum_{j=0}^{N^A} \sum_{k=0}^{K} P_{\phi_0}(i, N^B, k). \quad (3.64)$$

The combined blocking probability of SU groups P^{AB}_B seen by PU network is given as

$$P^{AB}_{Be} = \frac{\lambda^A_s}{\lambda^A_s + \lambda^B_s} P^A_{Be} + \frac{\lambda^B_s}{\lambda^A_s + \lambda^B_s} P^B_{Be}, \quad (3.65)$$

$$P^A_{Fe} = \frac{1}{(1 - P^A_{Be})} \sum_{i=0}^{N^A} \sum_{j=0}^{N^B} \sum_{k=0}^{K} \sum_{l=0}^{min\{N^A,N\}} \sum_{m=0}^{min\{N^B,N\}} \frac{l}{\lambda^A_s} \gamma^{(i,j,k)}_{(i-l,j-m,k+1)} P_{\phi_0}(i, j, k) \delta_{fr}, \quad (3.66)$$

and

$$P^B_{Fe} = \frac{1}{(1 - P^B_{Be})} \sum_{i=0}^{N^A} \sum_{j=0}^{N^B} \sum_{k=0}^{K} \sum_{l=0}^{min\{N^A,N\}} \sum_{m=0}^{min\{N^B,N\}} \frac{m}{\lambda^B_s} \gamma^{(i,j,k)}_{(i-l,j-m,k+1)} P_{\phi_0}(i, j, k) \delta_{fr}. \quad (3.67)$$

3.4.2 Scenario 1 $\theta^A_{se} \neq \theta^B_{se}$, $\mu^A_{se} \neq \mu^B_{se}$ and $\lambda^A_s \neq \lambda^B_s$

In Fig. 3.17 and Fig. 3.18, the fairness $\digamma$ and throughput ρ are plotted against μ^A_{se} respectively, for given $\mu^B_{se} = \mu^A_{se} + 0.3$, $\theta^A_{se} = 4$ and $\theta^B_{se} = 7$. In this condition, $P^A_{Fe} \neq$

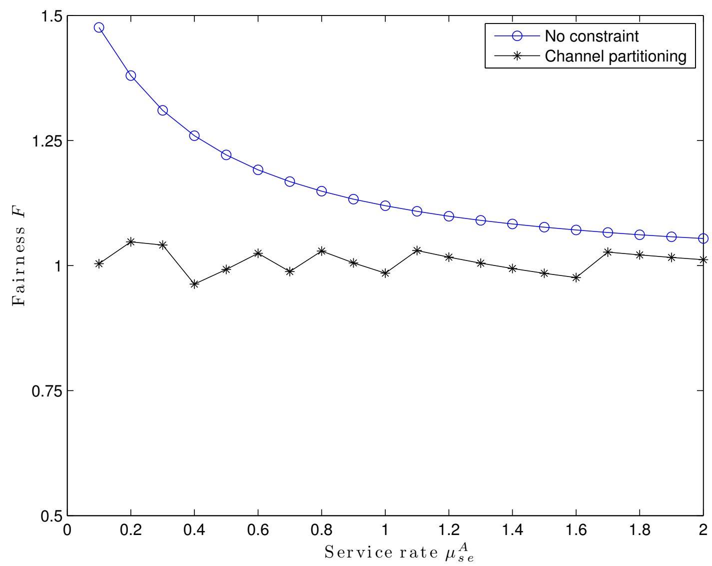

Figure 3.17: Fairness F versus SU service rate μ_{se}^A given $\theta_{se}^A = 4$, $\theta_{se}^B = 7$, $\mu_{se}^B = \mu_{se}^A + 0.3$, $\mu_p = 1$ and $\lambda_p = 1$.

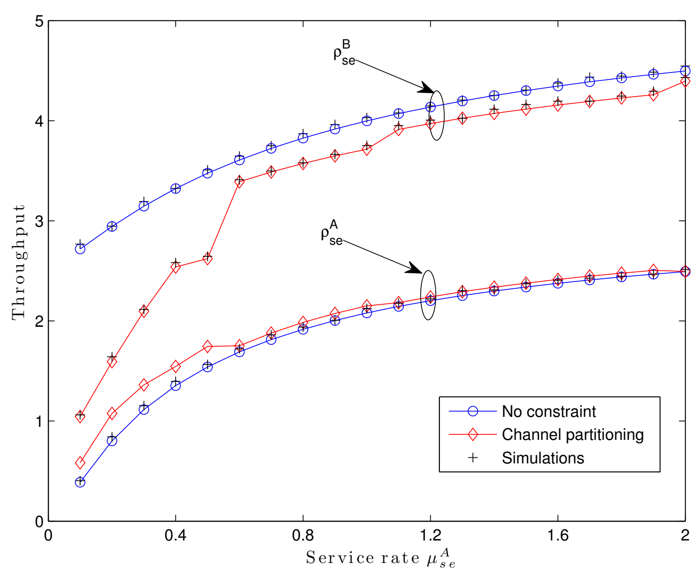

Figure 3.18: Throughput ρ versus SU service rate μ_{se}^A given $\theta_{se}^A = 4$, $\theta_{se}^B = 7$, $\mu_{se}^B = \mu_{se}^A + 0.3$, $\mu_p = 1$ and $\lambda_p = 1$.

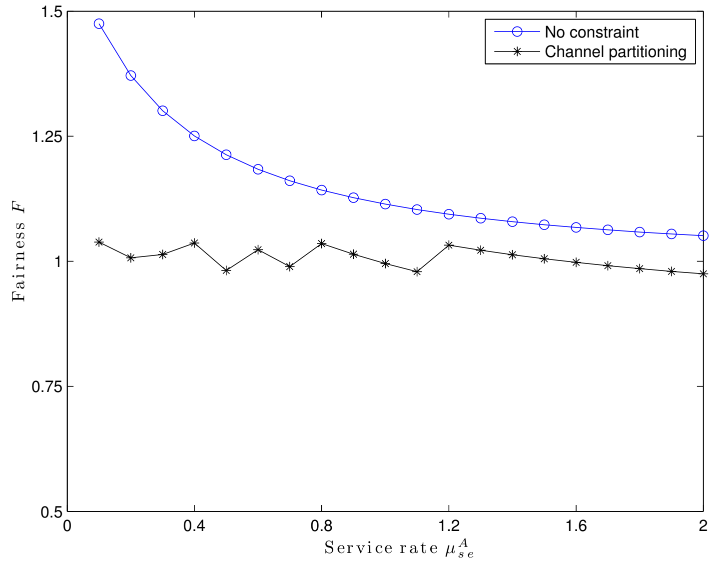

Figure 3.19: Fairness F versus SU service rate μ_{se}^A given $\theta_{se}^A(\theta_{se}^B) = 6$, $\mu_{se}^B = \mu_{se}^A + 0.3$, $\mu_p = 1$ and $\lambda_p = 1$.

P_{Fe}^B, and $P_{Be}^A \neq P_{Be}^B$. The fairness curves at low to medium values of service rate μ_s^A show that the no constraint scenario results in an unfair distribution of channels among two SU groups. The percentage loss in throughput of S^A is significantly higher (due to large P_{Fe}^A). At large values of service rate μ_{se}^A the fairness improves and throughput saturates due to the lower termination probability of both SU groups. On the other hand, the channel partitioning achieves fairness at a cost of the decrease in aggregate and individual throughput i.e., by assigning more subchannels to S^A than S^B. At higher values of μ_{se}^A (μ_{se}^B) there is almost no difference between the fairness and throughput in both strategies. The fluctuation in fairness occurs due to the integer number of subchannels.

3.4.3 Scenario 2 $\theta_{se}^A = \theta_{se}^B$, $\mu_{se}^A \neq \mu_{se}^B$ and $\lambda_s^A \neq \lambda_s^B$

Fig. 3.19 shows the fairness F curves plotted against SU service rate μ_{se}^A, given $\mu_{se}^B = \mu_{se}^A + 0.3$, $\theta_{se}^A = 6$ and $\theta_{se}^B = 6$. The arrival rate of S^A is higher than S^B

because of the offered traffic is constant for both SU groups. The curves are fairly similar to the previous figure and indicate that the smaller durations achieve better fairness.

3.5 Summary

In this Chapter, using a CTMC we have presented the exact solutions to determine the forced termination and blocking probabilities, and aggregate throughput of a SU group as well as two SU groups. Specifically,

- For a single PU channel (with only one subchannel) we have derived the optimal exponential and fixed payload lengths which maximize the SU throughput. The results show that despite higher termination and blocking probabilities, a fixed payload length provides a better throughput than an exponentially distributed payload.

- For multiple PU channels (with more than one subchannel) and two SU groups, three types of systems with were considered; without spectrum handoff (basic system): with spectrum handoff and channel reservation. For all these systems the single SU group was treated as a special case. In the former case, the results show that the blocking and forced termination probabilities increase with PU traffic intensity, as expected. However, SU traffic intensity has a different impact on the forced termination probability. The forced termination probability decreases slightly as SU traffic intensity increases for the basic system. For the systems with spectrum handoff, forced termination probability is always less than the basic system. However, there exists an optimal arrival rate that minimizes the forced termination probability. Spectrum handoff

($r = 0$) is more effective than channel reservation $r > 0$ in reducing forced termination probability for a given increase in blocking probability (tradeoff gain). The tradeoff is much more beneficial when the service rate is either very high or very low compared with the PU service rate.

- For two SU groups, we found that spectrum sharing can result in unfair channel occupancy. The problem is most prevalent when the difference between the two service rates is large. Channel partitioning (where a limit is placed on the maximum number of active connections of each S^A and S^B group) forces fairness but the throughput penalty might not be worth it.

In the next Chapter we consider underlay networks, where concurrent transmissions are allowed between the PU and the SU.

Chapter 4

Access Architecture for Secondary Femtocells in Downlink channels

In Chapter 3, the QoS parameters are calculated under the assumption of orthogonality (no interference) between the PU and SU transmissions. Generally, in wireless systems, the transmission links are bidirectional (full duplex). These bidirectional links are often identified as Uplink (UL) and Downlink (DL). In the interweave access mode, interference can be ignored at the PU and SU receivers in both the UL and DL directions. This simplifies the analysis and the QoS parameters on the UL and DL can be calculated independently. In this Chapter, the condition of orthogonality is relaxed and concurrent bidirectional PU and SU transmissions are considered. Spectrum sharing becomes an *underlay* issue. The PU transceivers are identified as PBS and PUE and SUs transceivers are identified as SBS and SUE. The transmission paths between the PUE and PBS (PUE-PBS) and the PBS-PUE is called UL and DL respectively.

A cellular network is the prime example of full duplex transmissions, in which the total coverage area is divided into cells (macrocells) to enable frequency reuse. Macrocell coverage often degrades in an indoor environment (such as the home or office) due to additional building penetration losses. Recent studies [12] [15] have shown that indoor coverage can be improved by adding a femtocell (FC) so the transmitter-receiver separation is reduced and the signal strength is improved. A FC can reuse the macrocell frequencies and, while doing so, act as a secondary network that generates UL and DL interference to the primary macrocell's PBS or PUE. To avoid and manage such interference, cognitive empowered femtocell base stations (here we identify them as SBS) have been recently proposed [89]-[100]. In these schemes, the FC works in the same mode, and shares the same spectrum as the macrocell. Transmission is not possible unless both the UL and DL spectra are essentially clear.

In general, for cellular networks the link gain is concentrated at the PBS, due to higher mounted antennas, higher gain antennas, spatial diversity, higher transmit powers and low noise figure receivers. This is evidenced by a recent spectrum analyser measurement shown in Fig. 4.1. These measurements are carried out in our laboratory (on the ground floor of a six level campus building) with an omni directional sensing antenna mounted 2 meters above the ground (similar to a FC). The DL frequencies of the GSM is clearly visible, indicating heavy activity on a number of channels but no signal is seen in the UL frequencies. UL signal splashes are rarely seen and only occur when transmission is in close proximity to our Laboratory ($<$ 50m in this environment). GSM is mainly used for voice traffic in which case spectrum usage is expected to be almost equal in both links. Clearly transmissions from the mobile units are getting to the PBS since UL and DL receiver signal levels are balanced, but the signals are not reaching our sensing antenna. Not having a 'PBS like' gain mechanisms at one end of the link (transmitter end or receiver end) has decreased the UL's signal strength. This explains the lack of UL signal activity in Fig. 4.1. PUE transmissions are generally not heard. The strong measured DL

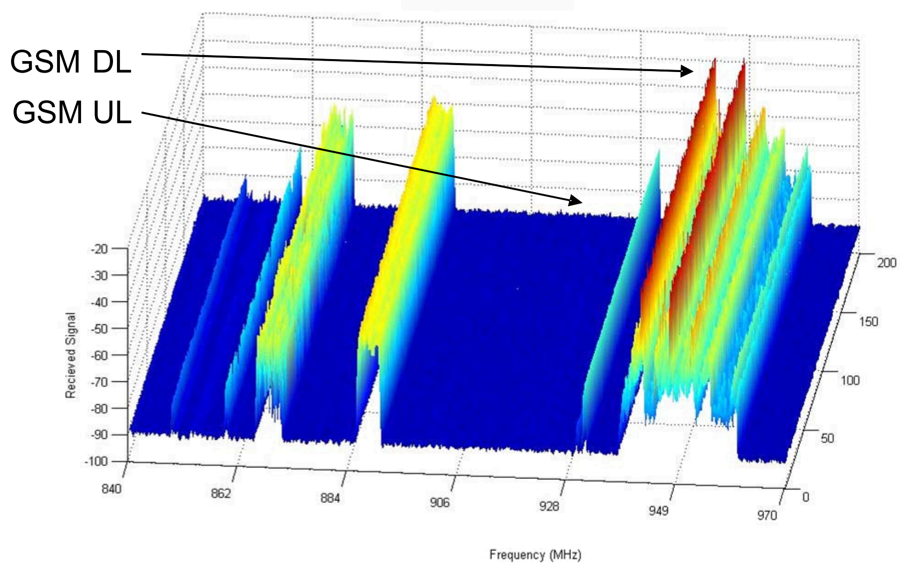

Figure 4.1: Spectrum Measurements of GSM UL and DL

spectrum indicates that any FC transmission at macro PUE power levels will interfere with the PBS, ruling out UL transmission (unless sophisticated power control methods are applied). The clear UL spectrum indicates that FC transmission in the DL spectrum will not cause interference to the PUE. However, interference to the FC from the PBS must be overcome, and this impacts the FC's coverage area. This observation is used to develop an access scheme for FCs. The contribution of this Chapter are as follows:

- We propose to operate the FC in the TDD mode using only the DL spectrum; there is therefore no interference to the PBS. To contain interference to the PUE, we exploit the duplex nature of the macrocell transmissions e.g. GSM, LTE or WiMaX. We measure the presence of the PUE by sensing its transmissions in the UL slot. If the transmissions can not be heard, we reason that the PUE is far away from the FC, in which case the FC transmissions will cause negligible interference to the PUE.

- We include the possibility of co-located sensing and access and decentralised sensing and access. The latter is applicable to low cost sensor networks, where sensing is only performed by the fusion node (the SBS in our terminology). The fusion node then schedules the sensor node transmissions. The weakness of the scheme is that the sensing and interference paths are de correlated. The sensing path (PUE to SBS) is no longer the interference path (SUE to PUE) and therefore some interference to the PUE can be expected. Reduced interference uses co-located sensing, where the sensing and interference paths are the same, for example sensing (PUE to SBS) and interfering (SBS to PUE).

- We use this model to answer the following question. What is the cross-tier interference and outage probability in the case of a uniformly distributed PUE and FC. To demystify this mathematically intractable problem, a heuristic approximation is proposed for the distance between a randomly distributed PUE and FC. It is shown that under lognormal shadowing the interference power or SNR can be accurately modelled by a Log-Skew Normal Distribution.

The remainder of the Chapter is organised as follows. In Section 4.1 and Section 4.2 we introduce the proposed scheme and system model. The distance dependent additional outage probabilities for the PUE and the SUE are derived in Section 4.3. Based on these findings the cell-wide outage probabilities are presented in Section 4.4. The approximation of the cell-wide detection probability under lognormal shadowing is shown in Section 4.5. Section 4.6 concludes the Chapter. The results in Section 4.1-4.3 have been accepted for publication in *PIMRC 2011* [119]. The findings in Section 4.1-4.5 are submitted for review in *IEEE Transactions on Vehicular Technology* [120]. The approximation presented in Section 4.6 is under review in

IET Letters [121].

4.1 Proposed Scheme

The proposed scheme in shown in Fig.4.2(a). We consider a simplified GSM network with one PBS. Underlaying this network is a SBS serving a SUE. In the GSM network, each of the UL and DL channels are divided into 8 time slots (a TDMA frame). The TDMA frames of the UL channel are transmitted with a delay of 3 time slots with respect to DL [122][Fig 4.5]. This reduces the complexity of the radio terminal front end by eliminating the need for duplexing filters. The transmission from PUE to PBS and vice versa occurs in the same slot number at both the UL and DL respectively.

In order to exploit the TDD and FDD structure of GSM, the SBS/SUE sense the DL transmission of the PBS towards the PUE at a particular time slot on frequency ω_{DL}[1]. If the time slot is active then there is a PUE on that channel in the cell. Normally this would indicate no transmission opportunity; however, for a TDD FC this need not be the case. Next the SBS/SUE switches to a corresponding time slot on the UL channel ω_{UL}. If the SBS/SUE cannot detect PUE activity, then the PUE is out of range. Here, we assume that the PUE must always transmit in its allocated time slot as would be expected in bidirectional (voice) traffic scenarios. The SBS/SUE is now free to transmit at this particular time slot on the DL frequency ω_{DL}[2]. This is based on the assumption that if the SBS/SUE cannot detect the PUE then the SBS/SUE cannot interfere with the PUE (providing its transmission

[1] This gives an indication of the interference that must be overcome by any secondary transmission (not considered in this paper). This interference may come from the PUE or other secondary FCs and can be used to determine modulation and transmission power in the secondary cell.

[2] For TDD macrocells e.g., some WiMaX and LTE networks, secondary FC transmission occurs in the section of the macrocell frame dedicated to the DL.

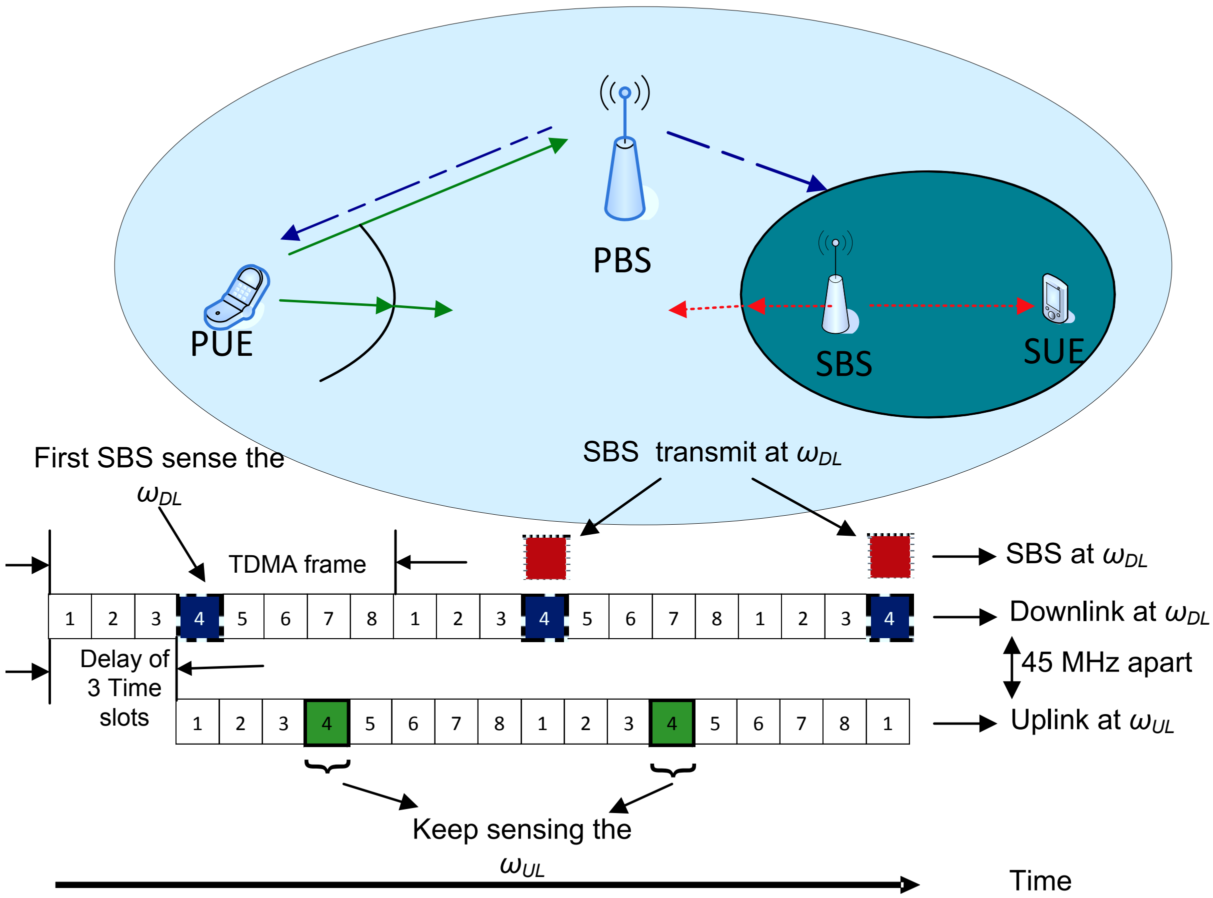

(a)

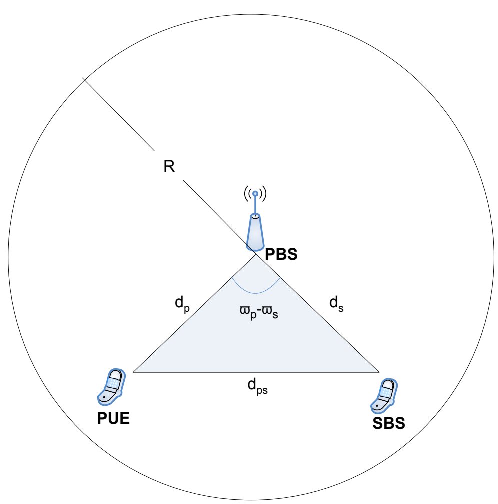

(b)

Figure 4.2: (a) Proposed scheme (b) System model geometry.

power is less than or equal to the PUE's transmission power). However, sensing imperfections and non reciprocal channels can still cause erroneous operation. This situation is shown in Fig. 4.2(a), where time slot 4 is used by the PBS to transmit to the PUE. The SBS/SUE first sense time slot 4 on ω_{DL} and than switches to time slot 4 on ω_{UL} to sense its vicinity to the PUE transmission. In Fig. 4.2(a) the SBS/SUE is not able to detect the PUE at ω_{UL} so it transmits in the time slot 4 at ω_{DL}. On the other hand, if the SBS/SUE detects the PUE to be present at ω_{UL}, it switches to another DL slot to search for available transmission opportunities.

Here we use a simplified GSM model because UL and DL slots are predefined. LTE, WiMAX would require the location/knowledge of the appropriate Resource Block, which are dynamically changing. The resource block map must therefore be decoded from the DL frame header or otherwise known to the secondary FCs [90].

4.2 System Model and Assumptions

The system model geometry is shown in Fig. 4.2. We consider a simplified GSM network with a PBS and a single PUE in a cell radius R. Underlaying this network is a FC consisting of a SBS and a SUE. Throughout this paper we assume the following.

- The PBS is located at the center of the cell with radius R. The distances between PBS-PUE, PBS-SBS, PBS-SUE, SBS-PUE and SBS-SUE are denoted by d_p, d_s, d_{pb}^{su}, d_{ps} and d_{ss} respectively.

- The COST 231 Walfisch Ikegami (WI) [123] channel model is used to quantify the propagation loss between PBS-PUE and PBS-SUE. The SISO WLAN channel model E [124] (applicable to large indoor and outdoor open spaces with no line of sight) is used to characterise the propagation loss for the PUE-SBS and SBS-SUE links.

- No fast fading is included implying some sort of local diversity measures have been applied to eliminate this effect on the receiver.

- Lognormal shadow fading is considered for all paths. The power gain between PBS-PUE, PBS-SUE, PUE-SBS, SBS-PUE and SBS-SUE are denoted by X_{pp}, X_{pb}^{su} X_{ps}, Y_{sp} and X_{ss} respectively. The standard deviation of the fades between PBS-PUE, PBS-SUE, PUE-SBS, SBS-PUE and SBS-SUE are denoted by σ_{pp}, σ_{pb}^{su}, σ_{ps}, σ_{sp} and σ_{ss} respectively.

- We assume that the shadow fading between PUE-SBS and SBS-PUE is correlated. The underlying normal distribution of the fades have a correlation coefficient ρ (in dB values).

- It is assumed that all the UL channels are fully occupied by PUE's and only the SBS is sensing and transmitting.

Table 4.1: List of symbols-Chapter 4

Parameter	**Symbol**
d_p	Distance between the PBS-PUE path
d_s	Distance between SBS-SUE
d_{ps}	Distance between PUE-SBS (SBS-PUE)
d_{pb}^{su}	Distance between PBS-SUE
d_{bp}	Breakpoint distance
$f(.)$	Probability Density Function
$F(.)$	Cumulative Distribution Function
T_{pb}	PBS transmit Power

T_{pu}	PUE transmit power
T_{sb}	SBS transmit power
G_{pb}	PBS antenna gain
G_{pb}^{D}	PBS antenna diversity gain
N_0	Noise power+Noise figure
(k_0, k_1)	Pathloss coefficients dual slope model
k	Pathloss coeff. single slope model
n	Pathloss coeff. COST 231 WI PBS-PUE, PBS-SUE
R	Cell Radius
L_0	Free space loss at 1m
ϵ_s	Sensing threshold SBS
ϵ_{out}	Outage threshold
X_{pp}	Fading gain between PBS-PUE path
X_{ps}	Fading gain between PUE-SBS path
X_{ss}	Fading gain between SBS-SUE path
X_{pb}^{su}	Fading gain between PBS-SUE path
Y_{sp}	Fading gain between SBS-PUE path
σ_{pp}	Standard deviation LN fade PBS-PUE path
σ_{ps}	Standard deviation of the LN fade PUE-SBS path
σ_{ss}	Standard deviation of the LN fade SBS-SUE path
σ_{pb}^{su}	Standard deviation of the LN fade PBS-SUE path
σ_{sp}	Standard deviation of the LN fade SBS-PUE path
ρ	Correlation coefficient of the LN fades between PUE and SBS
$w_{m_0}, w_{m_2}, w_{m_4}, w_{m_5}$	Weights of GMQ [129, Eq. (25.4.33), $(k = 1)$]
$t_{m_0}, t_{m_2}, t_{m_4}, t_{m_5}$	Abcissa of GMQ [129, Eq. (25.4.33), $(k = 1)$]
$N_{m_0}, N_{m_2}, N_{m_4}, N_{m_5}$	Number of polynomials of GHQ [129, Eq. (25.4.33), $(k = 1)$]
w_h	Weights of GHQ
t_h	Abcissa of GHQ
N_h	Number of Polynomial of GHQ
w_{m_1}, w_{m_3}	Weights of GMQ [129, Eq. (25.4.33), $(k = 0)$]
t_{m_1}, t_{m_3}	Abcissa of GMQ [129, Eq. (25.4.33), $(k = 0)$]
N_{m_1}, N_{m_3}	Number of polynomials of GHQ [129, Eq. (25.4.33),$(k = 0)$]

P_{out}^{nat}	PUE Natural outage probability
$\ddot{P}_{out}$	PUE outage probability when the SBS transmits
$\tilde{P}_{out}$	PUE outage probability when the SBS stays quiet
P_{out}^{pu}	PUE Additional outage probability
P_{out}^{su}	SUE outage probability
Φ	SNR
$\ddot{\Upsilon}_{pu}$	PUE SINR when the SBS transmits
P_{tx}^{su}	SBS Transmission probability
$\ddot{\Theta}_p$	Received signal power at PUE when the SBS transmits
$\tilde{\Theta}_p$	Received signal power at PUE when the SBS stays quiet
$\ddot{\Theta}_I$	Interference power at PUE when the SBS transmits

4.3 Distance Dependent Outage Probabilities

The total outage probability experienced by the PUE can be decomposed as

$$\begin{aligned} \text{Total Outage Probability} = {} & \text{Outage Probability when SBS transmits+} \\ & \text{Outage Probability when SBS remains quiet.} \end{aligned} \tag{4.1}$$

Let P_{out}^{tot} denote the total outage probability, P_{out}^{nat} denotes the natural outage probability of the PUE and $\ddot{P}_{out}$ is the outage probability when the SBS transmits, then the total outage probability P_{out}^{tot} can be written as

$$P_{out}^{tot} = P_{tx}^{su}\ddot{P}_{out} + (1 - P_{tx}^{su})P_{out}^{nat}, \tag{4.2}$$

where, P_{tx}^{su} is the probability that SBS transmits i.e., PUE transmissions are received below the sensing threshold. Similarly, the additional outage probability of PUE due to the SBS transmissions is:

$$P_{out}^{pu} = P_{tx}^{su}\ddot{P}_{out} - P_{tx}^{su}P_{out}^{nat}. \tag{4.3}$$

The probability $\ddot{P}_{out}$ is calculated from the SINR at the PUE i.e. $\ddot{P}_{out} = F_{\ddot{\Upsilon}_{pu}}(\epsilon_{out})$. The variable ϵ_{out} indicates the PUE outage threshold $F_{\ddot{\Upsilon}_{pu}}(\epsilon_{out})$ which must be met for a successful reception, and $\ddot{\Upsilon}_{pu}$ is given as

$$\ddot{\Upsilon}_{pu} = \frac{\ddot{\Theta}_P}{\ddot{\Theta}_I + N_0}, \tag{4.4}$$

where, $\ddot{\Theta}_p$ is the signal power from the primary path, $\ddot{\Theta}_I$ is the interference power due to SBS transmissions and N_0 is the noise power plus the noise figure of the PUE. In order to calculate P^{pu}_{out}, it is necessary to derive the distribution of P^{su}_{tx}, $\ddot{\Theta}_I$, $\ddot{\Theta}_P$ and the probability P^{nat}_{out}.

SBS Transmission Probability P^{su}_{tx}

We use signal to noise ratio (SNR) as the sensing criterion for P^{su}_{tx}. The SBS transmission is only allowed when the received SNR Φ falls below a certain threshold ϵ_s. The instantaneous received SNR is given by

$$\Phi = \frac{T_{pu} X_{ps}}{N_0 L_e(d_{ps})}, \tag{4.5}$$

where, T_{pu} is the transmit power of PUE and X_{ps} is the fading gain. The path loss $L_e(d)$ is dependent on the distance d. In the literature, single exponent models are often used to characterise $L_e(d)$, however, measurements have shown that in outdoor-indoor communication dual exponent models provide a better pathloss prediction [124], which is included in the WLAN-E model.

$$L_e(d) = \begin{cases} d^{k_0} L_0 & d \leq d_{bp} \\ d_{bp}^{k_0 - k_1} L_0 d^{k_1} & d > d_{bp} \end{cases}, \tag{4.6}$$

where, L_0 is the free space loss at 1m, d_{bp} is the break point distance after which the loss exponent increases, k_0 is the pathloss exponent before d_{bp} , and k_1 is the pathloss exponent after d_{bp}. The PDF of a lognormal fade L_F with scaling constant μ and standard deviation σ (in dB) is given as

$$f_{L_F}(l_f;\mu,\sigma) = \frac{10}{\ln(10)\sqrt{2\pi}\sigma l_f} e^{-\frac{\left(10\log_{10}\left(\frac{l_f}{\mu}\right)\right)^2}{2\sigma^2}}. \tag{4.7}$$

Given ϵ_s, the SBS transmission probability is $P_{tx}^{su} = F_\Phi(\phi \leq \epsilon_s)$. From (4.5), (4.7) and [68], the transmission probability is

$$[P_{tx}^{su} = F_\Phi(\phi \leq \epsilon_s)] = \frac{1}{2}\left(1 + \operatorname{erf}\left(\frac{10\log_{10}\left(\frac{\epsilon_s N_0 L_e(d_{ps})}{T_{pu}}\right)}{\sqrt{2}\sigma_{ps}}\right)\right), \tag{4.8}$$

where, erf(.) is Gaussian error function [68].

Interference Power $\ddot{\Theta}_I$

The SBS will only transmit and generate interference to the PUE when the sensed SNR from the PUE is $\Phi \leq \epsilon_s$. In a co-located system, the sensing and the interfering path are the same and hence the pathloss and shadow fading is identical. However, in decentralised sensing, the sensing path PUE-SBS is not the same as the interfering path SUE-PUE, because of the different locations. The pathloss is likely to be similar,[3] but depending on the separation SBS-SUE, the shadow fading (X_{ps} and Y_{sp}) could be different. Generally, X_{ps} and Y_{sp} are correlated and their correlation coefficient ρ is inversely proportional to the separation distance SBS-SUE [125]. The distribution (CDF and PDF) of the fade Y_{sp} for given fade probability of X_{ps} can be found from their joint PDF which is given in [126] as

$$f_{X_{ps},Y_{sp}}(x_{ps},y_{sp};\rho) = \frac{100}{(\ln(10))^2 2\pi x_{ps} y_{sp} \sigma_{ps}\sigma_{sp}\sqrt{1-\rho^2}} \tag{4.9}$$
$$e^{-\frac{1}{2(1-\rho^2)}\left(\left(\frac{10\log_{10}(x_{ps})}{\sigma_{ps}}\right)^2 + \left(\frac{10\log_{10}(y_{sp})}{\sigma_{sp}}\right)^2 - 2\rho\left(\frac{10\log_{10}(x_{ps})}{\sigma_{ps}}\right)\left(\frac{10\log_{10}(y_{sp})}{\sigma_{sp}}\right)\right)},$$

[3] A FC has much smaller coverage area than the macrocell

where, ρ is the correlation coefficient (between dB fade values).

The probability that fade $Y_{sp} \leq y_{sp}$ given that the SBS/SUE is transmitting $\left(X_{ps} \leq \frac{\epsilon_s N_0 L_e(d_{ps})}{G_1}\right)$ is

$$F_{X_{ps},Y_{sp}}\left(\frac{\epsilon_s N_0 L_e(d_{ps})}{G_1}, y_{sp}; \rho\right) = \int_0^{y_{sp}} \int_0^{\frac{\epsilon_s N_0 L_e(d_{ps})}{G_1}} f(x_{ps}, y_{sp}; \rho) dx_{ps} dy_{sp}. \tag{4.10}$$

The closed form of the double integral in (4.10) is unknown. By proper substitution, this integral can be transformed into a bivariate normal CDF [126]. Substituting $x_1 = \frac{10\log_{10}(\frac{\epsilon_s N_0 L_e(d_{ps})}{G_1})}{\sigma_{ps}}$, $x_2 = \frac{10\log_{10}(y_{sp})}{\sigma_{sp}}$ in (4.10) gives

$$F_{X_{ps},Y_{sp}}\left(\frac{\epsilon_s N_0 L_e(d_{ps})}{G_1}, y_{sp}; \rho\right) = \int_{-\infty}^{x_2} \int_{-\infty}^{x_1} \frac{e^{-\frac{\left(x_1^2 - 2\rho x_1 x_2 + x_2^2\right)}{2(1-\rho^2)}}}{2\pi\sqrt{1-\rho^2}} dx_1 dx_2. \tag{4.11}$$

Various approximations to solve the bivariate normal CDF have been summarised in [126] and the comparative analysis of these approximations has been performed in [127]. Note that one can also use built in MATLAB functions to numerically calculate the bivariate CDF (double integral), however, it will compromise the analytical tractability of the problem. Here, we opt for the Drezner-Wesolowsky (DW) approximation [128]. The DW method converts the above double integral to a single integral which can be efficiently solved by numerical integration techniques. The simple DW approximations is given as

$$\int_{-\infty}^{x_2} \int_{-\infty}^{x_1} \frac{e^{-\frac{\left(x_1^2 - 2\rho x_1 x_2 + x_2^2\right)}{2(1-\rho^2)}}}{2\pi\sqrt{1-\rho^2}} dx_1 dx_2 = Q(x_1)Q(x_2) + \frac{1}{2\pi}\int_0^{\rho} \frac{1}{\sqrt{1-r^2}} e^{-\frac{1}{2(1-r^2)}\left(x_1^2 - 2x_1 x_2 r + x_2^2\right)} dr, \tag{4.12}$$

where, $Q(x) = \frac{1}{2}\left(1 + \text{erf}\left(\frac{x}{\sqrt{2}}\right)\right)$. In [128], the above approximation is further modified to cater for divergence at $\rho = 1$ (integral in (4.12)). Here, this shortcoming is avoided by using the Gauss Moment Quadrature (GMQ)[4]. The above approximation is first converted into standard form by substituting $r = t\rho$ and then calculating weights w_{m_1} and abscissa t_{m_1} from [129, Eq. (25.4.33) with $k = 0$]. The final result is given below

$$F_{X_{ps},Y_{sp}}\left(\frac{\varepsilon_s N_0 L_e(d_{ps})}{G_1}, y_{sp}; \rho\right) = Q(x_1)Q(x_2) + \sum_{m_1=1}^{N_{m_1}} \frac{\rho w_{m_1} e^{-\frac{1}{2\left(1-\rho^2 t_{m_1}^2\right)}\left(x_1^2 - 2\rho t_{m_1} x_1 x_2 + x_2^2\right)}}{2\pi\sqrt{1-\rho^2 t_{m_1}^2}}. \tag{4.13}$$

As no SBS/SUE transmission occurs for $\Phi > \epsilon_s$, the above CDF becomes a truncated distribution. To calculate the distribution $\hat{F}_{X_{ps},Y_{sp}}\left(\frac{\epsilon_s N_0 L_e(d_{ps})}{G_1}, y_{sp}; \rho\right)$ (the distribution of fade from SBS-PUE when $\phi \leq \epsilon_s$), the distribution in (4.13) needs to be normalised [68] i.e.,

$$\hat{F}_{X_{ps},Y_{sp}}\left(\frac{\epsilon_s N_0 L_e(d_{ps})}{G_1}, y_{sp}; \rho\right) = \frac{F_{X_{ps},Y_{sp}}\left(\frac{\epsilon_s N_0 L_e(d_{ps})}{G_1}, y_{sp}; \rho\right)}{\int_0^{\infty} \int_0^{\frac{\epsilon_s N_0 L_e(d_{ps})}{G_1}} f(x_{ps}, y_{sp}) dx_{ps} dy_{sp}}. \tag{4.14}$$

The integral in the denominator is the marginal CDF $F_{X_{ps}}(x_{ps}) = Q(x_1)$. The interference power $\ddot{\Theta}_I$ can be calculated from the following equation

$$\ddot{\Theta}_I = T_{sb} \frac{Y_{sp}/\Phi \leq \epsilon_s}{L_e(d_{ps})}. \tag{4.15}$$

where T_{sb} is the SBS transmit power. Differentiating (4.14) and subsequently applying linear transformation, the PDF of the interference power is given as

$$f_{\ddot{\Theta}_I}\left(\ddot{\theta}_I\right) = f_{L_F}\left(\ddot{\theta}_I; \frac{T_{sb}}{L_e(d_{ps})}, \sigma_{sp}\right) + \sum_{m_1=1}^{N_m} \frac{\rho w_{m_1}\left(10\rho t_{m_1} x_1 - 10 x_2\right) e^{-\frac{1}{2\left(1-\rho^2 t_{m_1}^2\right)}\left(x_1^2 - 2\rho t_{m_1} x_1 x_2 + x_2^2\right)}}{2\pi \ln(10) Q(x_1) \ddot{\theta}_I \sigma_{\mathrm{sp}} \left(1-\rho^2 t_{m_1}^2\right)^{\frac{3}{2}}}, \tag{4.16}$$

where, $x_1 = \frac{10\log_{10}\left(\frac{\varepsilon_s N_0 L_e(d_{ps})}{G_1}\right)}{\sigma_{ps}}$ and $x_2 = \frac{10\log_{10}\left(\frac{L_e(d_{ps})\ddot{\theta}_I}{T_{sb}}\right)}{\sigma_{sp}}$.

[4]In wireless communication theory, Gaussian Quadrature methods [129] such as Gauss Hermite quadrature, Gauss moment quadrature, and Gauss-Legendre quadrature are widely acceptable to obtain solutions of complex integration problem. For example, they are recently been used in [130][131][132][133] to approximate the integrals involving gamma, lognormal and bivariate lognormal distributions.

Signal Power $\ddot{\Theta}_p$

The signal power $\ddot{\Theta}_p$ from the primary path (PBS-PUE) is given as

$$\ddot{\Theta}_P = G_2 X_{pp} L_{wi}^{-1}(d_p), \tag{4.17}$$

where, $G_2 = T_{pb}G_{pb}$, T_{pb} is the transmit power or the Effective Isotropic Radiated Power (EIRP) of the PBS, and G_{pb} is the PBS antenna gain. It is assumed that only NLOS conditions exists between PBS and PUE. The pathloss $L_{wi}(d_p)$ is calculated from the COST 231 WI model and can be written in generalised form as

$$L_{wi}(d) = L_1 \left(\frac{d}{10^3}\right)^n. \tag{4.18}$$

The value of the parameters for the calculation of L_1 are summarised in Table 4.3.

4.3.1 Additional Outage Probability of the PUE P_{out}^{pu}

The SINR $\ddot{\Upsilon}_{pu}$ in (4.4) is a ratio of random variables. The CDF of the ratio can be calculated from:

$$[\ddot{P}_{out} = F_{\ddot{\Upsilon}_{pu}}(\ddot{v}_{pu})] = \int_{N_0}^{\infty} F_{\Theta_P}\left(\ddot{v}_{pu}\theta_{in}\right) f_{\Theta_{in}}\left(\theta_{in}\right) d\theta_{in}, \tag{4.19}$$

where, $\Theta_{in} = \Theta_I + N_0$. A closed form of the integral is not known. Here, we apply the Gaussian Hermite quadrature (GHQ) [129, Eq. (25.4.46)] to approximate these integrals. The final outage probability expressions are given in (4.20), where w_h and

t_h are the weights and abscissa of GHQ.

$$\begin{aligned}
&F_{\ddot{\Upsilon}_{pu}}(\ddot{v}_{pu}) = \\
&\sum_{h=1}^{N_h} \frac{w_h}{2\sqrt{\pi}} \left(1 + \text{erf}\left(\frac{10\log_{10}\left(\ddot{v}_{pu}(e^{\frac{\ln(10)}{10}\sqrt{2}\sigma_{sp}t_h + \ln\left(\frac{T_{sb}}{L_e(d_{ps})}\right)} + N_0)\right) - 10\log_{10}\left(\frac{G_2}{L_{wi}(d_p)}\right)}{\sqrt{2}\sigma_{pp}}\right)\right) + \\
&\sum_{h=1}^{N_h} \sum_{m_1=1}^{N_m} \frac{\rho w_h w_{m_1}\left(\rho t_{m_1} x_1 - t_h\right) e^{-\frac{1}{2\left(1-\rho^2 t_{m_1}^2\right)}\left(x_1^2 - 2\rho t_{m_1} x_1 t_h\right)}}{2\pi\sqrt{2}Q(x_1)\left(1-\rho^2 t_{m_1}^2\right)} \\
&\left(1 + \text{erf}\left(\frac{10\log_{10}\left(\ddot{v}_{pu}(e^{\frac{\ln(10)}{10}\sigma_{sp}t_h\sqrt{2\left(1-\rho^2 t_{m_1}^2\right)} + \ln\left(\frac{T_{sb}}{L_e(d_{ps})}\right)} + N_0)\right) - 10\log_{10}\left(\frac{G_2}{L_{wi}(d_p)}\right)}{\sqrt{2}\sigma_{pp}}\right)\right).
\end{aligned} \tag{4.20}$$

The natural outage probability of the PUE (without interference) is given as

$$P_{out}^{nat} = \frac{1}{2}\left(1 + \text{erf}\left(\frac{10\log_{10}\left(\frac{\epsilon_{out}N_0 L_{wi}(d_p)}{G_2}\right)}{\sqrt{2}\sigma_{pp}}\right)\right). \tag{4.21}$$

Substituting (4.8), (4.20) and (4.21) in (4.3) gives the additional outage probability of the PUE caused by the SBS transmission.

4.3.2 Outage Probability of the SUE

The DL transmission from the PBS interferes with the SBS transmission to the SUE. Outage occurs at the SUE, when its SINR, Υ_{su}, is less than a certain threshold. We assume the same threshold for the primary and secondary networks (ϵ_{out}), i.e., $P_{out}^{su} = F_{\Upsilon_{su}}(\epsilon_{out})$, where

$$\Upsilon_{su} = \frac{T_{sb}X_{ss}L_e^{-1}(d_{ss})}{G_2 X_{pb}^{su} L_{wi}^{-1}(d_{pb}^{su}) + N_0} = \frac{\Theta_{ss}}{\hat{\Theta}_{in}^{s}}. \tag{4.22}$$

Given, the outage probability of the SUE, the effectiveness E_f^{sb} of the SBS transmissions (defined as the combined probability of transmission and successful reception at the SUE) can be written as:

$$E_f^{sb} = P_{tx}^{su}(1 - P_{out}^{su}). \tag{4.23}$$

The CDF of Υ_{su} can be calculated by appropriately replacing the PDF's and CDF's in (4.19). The SUE outage probability in terms of GHQ and is given as

$$F_{\Upsilon_{su}}(\upsilon_{su}) = \sum_{h=1}^{N_h} \frac{w_h}{2\sqrt{\pi}} \left(1 + \mathrm{erf}\left(\frac{10\log_{10}\left(\upsilon_{su}(e^{\frac{\log(10)}{10}\sqrt{2}\sigma_{pb}^{su}t_h + \ln\left(\frac{G_2}{L_{wi}(d_{pb}^{su})}\right)} + N_0)\right) - 10\log_{10}\left(\frac{T_{sb}}{L_e(d_s)}\right)}{\sqrt{2}\sigma_{ss}}\right)\right). \tag{4.24}$$

4.3.3 Numerical Results

In this section, we give some numerical examples that illustrate the outage probability of both the SUE and PUE. The system parameters are summarized in Table 4.2 and the parameters for the calculation of the path loss, L_1, are given in Table 4.3.3. In all the figures, the solid lines and the line markers represent analytical results and Monte Carlo simulation results, respectively. These parameters are chosen such that without any secondary interference the outage probability at the *cell edges* is approximately 0.1. In order to keep the FC coverage in line with WLAN systems, the transmit power of the SBS is T_{sb} = 16dBm which is 13dB below the PUE transmit power.

Fig. 4.3(a)-(b) shows the additional PUE outage probability, induced by the SBS, versus its distance from the SBS. This outage probability is plotted for 2 different PBS-PUE separation distances and 3 correlation factors. The additional outage curves have similar behaviour; there is no additional outage at short ranges (<100m), since the signal strength is strong and sensing is perfect. The effectiveness of the SBS is 0 in that zone. At greater separations, outage increases due to sensing errors and then reduces again as the interfering SBS signal becomes weaker. The effectiveness of the SBS transmission is at its highest for its given distance with the

Table 4.2: Simulation parameters

Notation	Value
T_{pb}	10W
T_{pu}	0.8W
T_{sb}	40mW
G_{pb}(dB)	10dB
G_{pb}^{D}(dB)	7dB
N_0 (dBm)	-112 dBm
$(\sigma_{sp}, \sigma_{ps}, \sigma_{ss})$	(6dB,6dB,6dB)
$\sigma_{pp}, \sigma_{pb}^{su}$	(12dB,12dB)
(k_0,k_1)	(2,4)
d_{bp}	10m
n	2
L_0(dB)	41dB
ϵ_s(dB)	10dB
ϵ_{out}(dB)	10dB
R	4km

Table 4.3: COST-231 parameters for calculation of L_1

Height of PBS	H_{PBS}	18m
Height of the Roof	H_{ROOF}	12m
Height of PUE	H_{PUE}	1.5m
Buildings width incl Streets	H_{B-B}	40m
Incident angle to PUE	ω	90°
DL Carrier frequency	f_d	925.2MHz
UL Carrier frequency	f_u	880.2MHz

Table 4.4: Natural outage probability of PUE P_{out}^{pu}

d_p	P_{out}^{nat}
0.5km	0.00255
3.5km	0.0819

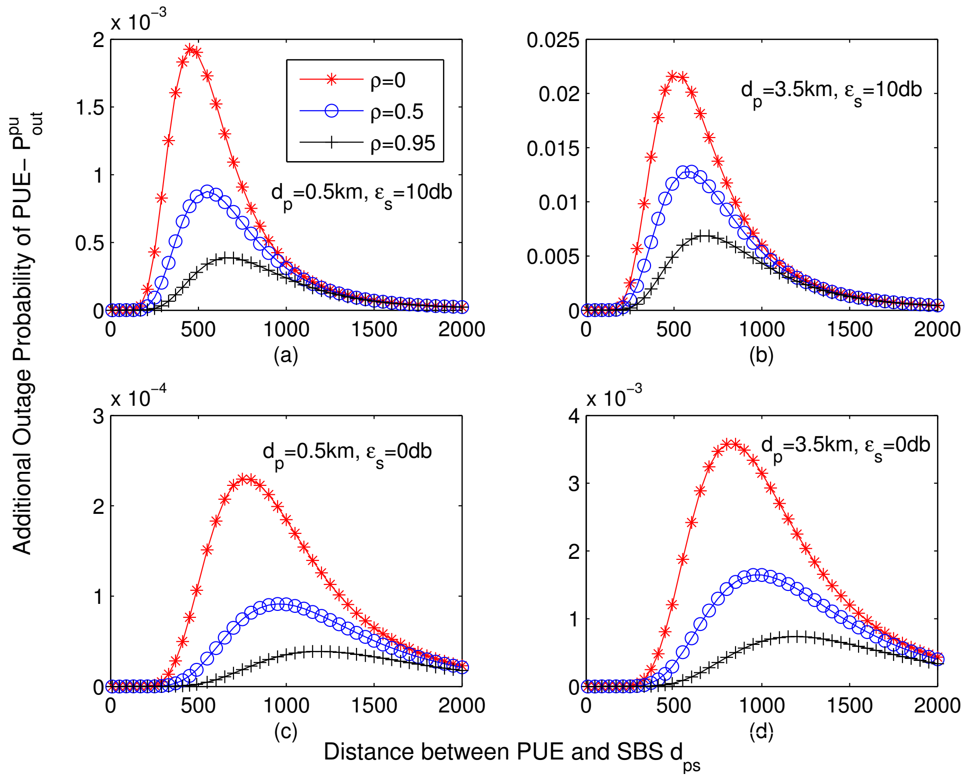

Figure 4.3: Additional outage probability of PUE induced by SBS transmission for different values of d_p and ϵ_s,given $T_{pu} = 0.8$, $T_{sb} = 40mW$. Markers on solid line represent Monte-carlo simulation results.

PBS and the SUE. As expected the plots in Fig. 4.3 indicate the greater outage susceptibility at the cell edge, $d_p = 3.5km$. However, when we compare the results to the natural outage Table 4.4 (without secondary network) we see that the SBS outage contribution is still negligible, even when the correlation between the sensing and interfering paths is zero, and a conservative sensing SNR threshold of $\epsilon_s = 10$dB. Since the sensing can be performed for a complete slot, it should be possible to detect the PUE signal well below this level [134]. Reducing ϵ_s to 0dB (Fig. 4.3(c)-(d)) suppresses the additional outage by almost an order of magnitude.

The figure also shows the impact of correlation on P^{pu}_{out}. The corresponding correlation values of lognormal shadowing for $\rho = 0.5$ and $\rho = 0.95$ (dB correlation) are

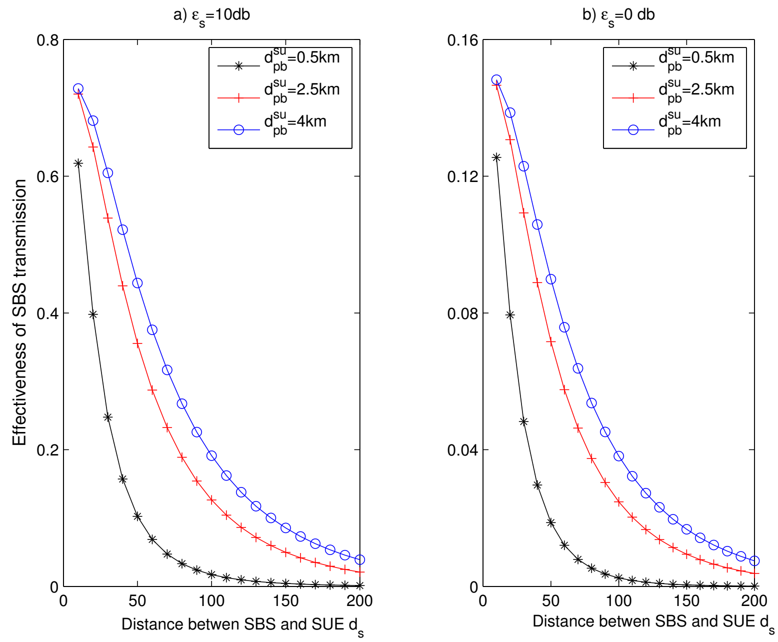

Figure 4.4: Effectiveness of SBS transmission versus SBS-SUE distance, given $d_{ps} = 700m$ $T_{pu} = 0.8$, $T_{sb} = 40mW$, Markers represent Monte Carlo simulation results.

0.2159 and 0.8684 (linear correlation) respectively. At closer distances the correlation provides a significant outage cushion to PUE. When the correlation increases from $\rho = 0$ and $\rho = 0.95$, the additional outage drops by a factor greater than 3. As correlation directly represents the separation between secondary sensing and transmit antenna [125], it is beneficial that transmit and receive antenna are as close as possible and preferably on the same node.

The effectiveness of the SBS transmission is plotted in Fig. 4.4 for the worst interference scenario of Fig. 4.3 ($d_{ps} = 700m$). Effectiveness is defined as the probability that a slot position will lead to a successful secondary transmission. It includes the probability of the slot availability and the probability of successful transmission if its available (see (4.23)). The maximum effectiveness occurs at minimal SBS-SUE distance and quickly decays with distance limiting the secondary cell size to about a 25m to 50m range. The maximum effectiveness at $d_s = 0$ is set by the transmission opportunities which is determined by the sensing threshold. Dropping sensing threshold from 10dB to 0dB reduces the transmission opportunities by a factor of 5. Clearly this is undesirable. The additional drop in the effectiveness with SBS-SUE distance is caused by outage, which is primarily due to dominant PBS interference. When the FC is close to the PBS, the interference is strong, limiting the secondary coverage zone to 20m for an effectiveness of 0.5. The coverage increases to 50m for the edge of the cell.

4.4 Cell-Wide Outage Probability

From a network design perspective, it is often desirable to know the cell-wide outage probability; the average outage probability for a fully loaded cell, when the PUE and FC are randomly distributed. These parameters are mathematically tractable in the UL spectrum [16][135]. However, in the DL spectrum these parameters are only known when the location of the PUE is fixed [81]. In this thesis, we aim to address this shortcoming and assume that both the PUE and FC are *uniformly* distributed within the PBS coverage area.

Let $\ddot{P}_{out_c}$ be the outage probability when the SBS transmits, and $\tilde{P}_{out_c}$ denote the cell-wide outage probability without SBS transmission then $P^{tot}_{out_c}$ can be written as

$$P^{tot}_{out_c} = P^{su}_{tx_c}\ddot{P}_{out_c} + (1 - P^{su}_{tx_c})\tilde{P}_{out_c}, \tag{4.25}$$

where, $P^{su}_{tx_c}$ is the probability that the SBS transmits. The additional outage probability of the PUE due to the SBS transmission is:

$$P^{pu}_{out_c} = P^{su}_{tx_c}\ddot{P}_{out_c} + (1 - P^{su}_{tx_c})\tilde{P}_{out_c} - P^{nat}_{out_c}. \tag{4.26}$$

Remark 1. Note that, unlike the distance dependent case (4.3), $\tilde{P}_{out_c}$ is not a scaled version of $P^{nat}_{out_c}$ due to randomness of the PUE and the FC.

In order to calculate $P^{pu}_{out_c}$, it is necessary to know $P^{su}_{tx_c}$, $\ddot{P}_{out_c}$, $\tilde{P}_{out_c}$ and $P^{nat}_{out_c}$. In what follows we first demystify the problem of finding $P^{su}_{tx_c}$. Secondly, we calculate the distribution of the distances between the interfering entities (SBS-PUE and PBS-SUE). Thirdly, based on the signal power statistics from the primary path, we calculate $\ddot{P}_{out_c}$ and $\tilde{P}_{out_c}$.

SBS Transmission Probability $P^{su}_{tx_c}$

Similar to the distance dependent case, we use Signal to Noise Ratio (SNR) as the sensing criterion and determine the detection probability of PUE from the CDF of the received SNR at the SBS. The instantaneous received SNR is given by

$$\Phi_c = \frac{T_{pu} X_{ps}}{N_0 L_e(D_{ps})} \tag{4.27}$$

A capital letter is used for D_{ps} to indicate that it now represents a set of values. To simplify the mathematical analysis, only single slope pathloss model is used. i.e., $L_e(D_{ps}) = L_0 D^k_{ps}$. The probability density function (PDF) of distance between uniformly scattered points in a circle radius R(m) is given in [136, Eq. (10.8)] as,

$$f_{D_{ps}}(d_{ps}, R) = \frac{2\,d_{ps}}{\pi\,R^2}\left(2\cos^{-1}\left(\frac{d_{ps}}{2\,R}\right) - \frac{d_{ps}}{R}\sqrt{1 - \frac{d^2_{ps}}{4R^2}}\right) \tag{4.28}$$

where, $0 \leq d_{ps} \leq 2R$ and the mean is $E[D_{ps}] = 0.9054R$. A similar expression for the PDF has also been derived in [137]. For a given distance d_{ps}, the probability that the SBS may not be able to hear the PUE is given in (4.8). Averaging the above probability over d_{ps} (4.28) gives $F_{\Phi_c}(\phi_c)$ i.e.,

$$F_{\Phi_c}(\phi_c) = \int_0^{(2R)} F_{X_{ps}}\left(\frac{N_0 d^k_{ps}\phi_c}{G_1}\right) f_{D_{ps}}(d_{ps}, R)\, dd_{ps} \tag{4.29}$$

where, $G_1 = \frac{T_{pu}}{L_0}$. The above integral doesn't have any closed form solution. In the last section of this Chapter, we will show that the distribution of Φ_c can be approximated by Log-Skew Normal Distribution. However, in order to maintain the continuity of the discussion we approximate this integral by the GMQ [129, Eq. (25.4.33) with $k = 1$]. The upper limit of the above integral is normalised to 1, by introducing a new variable $d_{ps} = 2Rt$. Applying GMQ gives

$$[P_{tx_c}^{su} = F_{\Phi_c}(\phi_c)] = \frac{\sum_{m_0=1}^{N_{m_0}} w_{m_0} F_{X_{ps}}\left(\frac{N_0 t_{m_0}^k (2R)^k \phi_c}{G_1}\right) A(t_{m_0})}{\sum_{m_0=1}^{N_m} w_{m_0} A(t_{m_0})}, \tag{4.30}$$

where, $A(t_{m_0}) = \frac{8}{\pi}\left(\pi - 2\sin^{-1}(t_{m_0}) - 2t_{m_0}\sqrt{1-t_{m_0}^2}\right)$, N_{m_0} is the number of polynomials used for approximation, w_{m_0} and t_{m_0} are the weights and abscissa of GMQ, their values are given in [129, Table 25.8] or can be calculated by the expressions in [129, Eq. (25.4.33)]. In the following, we will derive the distribution of the distances D_{ps} at which interference power will be generated by the SBS.

4.4.1 Distribution of Interference Generating Distances $\ddot{D}_{ps}$, and Interference Power Θ_{I_c}

It is evident from (4.8) that the fade is dependent on the mean signal power which in turn is related to the distance d_{ps}. As such the interference contributing distances $\hat{d}_{ps}$ are those for which the fade $x_{ps} \leq \frac{N_0 d_{ps}^k \epsilon_s}{G_1}$. Given $F_{X_{ps}}(x_{ps})$, the PDF of interference contributing distances is

$$f_{\ddot{D}_{ps}}(\ddot{d}_{ps}) = \frac{1}{C} F_{X_{ps}}\left(\frac{N_0 \ddot{d}_{ps}^k \epsilon_s}{G_1}\right) f_{\ddot{D}_{ps}}(\ddot{d}_{ps}), \tag{4.31}$$

where, the normalisation factor C represents the probability that the SBS cannot detect the PUE (when averaged over the whole cell), i.e., $C = F_{\Phi_c}(\epsilon_s)$. The interference power to the PUE becomes;

$$\ddot{\Theta}_{I_c} = G_3 \frac{Y_{sp}/\Phi \leq \epsilon_s}{\ddot{d}_{ps}^k}, \tag{4.32}$$

where, $G_3 = \frac{T_{sb}}{L_0}$. The CDF and PDF of Θ_I cannot be completely calculated, because combining the bivariate CDF approximation in (4.13) with (4.31) yields definite integrals for which a closed form is unknown (product of exponential and two Gauss error function with finite integral limits). Using the same procedure as in (4.29) and substituting $\ddot{d}_{ps} = 2Rt$, the CDF $F_{\Theta_I}(\theta_I)$ is given as

$$F_{\ddot{\Theta}_{I_c}}\left(\ddot{\theta}_{I_c}\right) = \int_0^1 t F_{X_{ps},Y_{sp}}\left(\frac{\epsilon_s N_0 (t2R)^k}{G_1}, \frac{\ddot{\theta}_{I_c}(t2R)^k}{G_3}; \rho\right) A(t) dt. \tag{4.33}$$

After applying GMQ and performing appropriate scaling, the final expressions of the CDF and PDF of the interference power is given below, where w_{m_2} (t_{m_2}) are the weights (abscissa) for [129, Eq. (25.4.33) with $k = 1$],

$$F_{\ddot{\Theta}_{I_c}}\left(\ddot{\theta}_{I_c}\right) = \sum_{m_2=1}^{N_{m_2}} \frac{w_{m_2} A(t_{m_2})}{F_{\Phi_c}(\varepsilon_s)} \left(Q(x_1)Q(x_2) + \sum_{m_1=1}^{N_{m_1}} \frac{\rho w_{m_1} e^{-\frac{1}{2\left(1-\rho^2 t_{m_1}^2\right)}\left(x_1^2 - 2\rho t_{m_1} x_1 x_2 + x_2^2\right)}}{2\pi\sqrt{1-\rho^2 t_{m_1}^2}} \right), \tag{4.34}$$

$$\begin{aligned} f_{\ddot{\Theta}_{I_c}}\left(\ddot{\theta}_{I_c}\right) = \sum_{m_2=1}^{N_{m_2}} \frac{w_{m_2} A(t_{m_2})}{F_{\Phi_c}(\varepsilon_s)} \Bigg(Q(x_1) f_{L_f}\left(\ddot{\theta}_{I_c}; \frac{G_3}{(t_{m_2}2R)^k}, \sigma_{sp}\right) \\ \sum_{m_1=1}^{N_{m_1}} \frac{\rho w_{m_1}\left(10\rho t_{m_1} x_1 - 10 x_2\right) e^{-\frac{1}{2\left(1-\rho^2 t_{m_1}^2\right)}\left(x_1^2 - 2\rho t_{m_1} x_1 x_2 + x_2^2\right)}}{2\pi \ln(10) \ddot{\theta}_I \sigma_{\mathrm{sp}} \left(1-\rho^2 t_{m_1}^2\right)^{\frac{3}{2}}} \Bigg), \end{aligned} \tag{4.35}$$

where, $x_1 = \frac{10\log_{10}\left(\frac{\varepsilon_s N_0 (t_{m_2}2R)^k}{G_1}\right)}{\sigma_{ps}}$, $x_2 = \frac{10\log_{10}\left(\frac{(t_{m_2}2R)^k \ddot{\theta}_{I_c}}{G_3}\right)}{\sigma_{sp}}$.

4.4.2 Distribution of $\ddot{D}_p$

Since the distances d_{ps}, d_p and d_s are correlated, a change in the PDF distribution of d_{ps} (4.31) also changes the distributions of both d_p and d_s. In the following, we derive the distribution of the distances $f_{\ddot{D}_p}(\ddot{d}_p)$, for which the SBS *cannot* detect the PUE (the SBS transmits), and the distances $f_{\tilde{D}_p}(\tilde{d}_p)$, for which the SBS *can* detect the PUE (the SBS does not transmit).

Remark 2. The distribution of $\tilde{D}_s$, $f_{\tilde{D}_s}(\tilde{d}_s)$ is same as $f_{\tilde{D}_p}(\tilde{d}_p)$.

The separation d_{ps} between PUE and SBS is given by the cosine rule. The location of the PUE is given by $d_p\angle\varpi_p$ (polar representation), and the location of the SBS is given by $d_s\angle\varpi_s$ i.e.

$$d_{ps} = \sqrt{d_p^2 + d_s^2 - 2d_pd_s\cos(\varpi_p - \varpi_s)}, \tag{4.36}$$

where, $\varpi_p - \varpi_s$ is an angle between the SBS and the PUE (Fig. 4.2(b)).

4.4.2.1 $f_{\ddot{D}_p}(\ddot{d}_p)$, for which the SBS *cannot* detect the PUE

Here, the probability that the SBS is going to transmit from distance d_{ps} is given by $F_{X_{ps}}\left(\frac{N_0 d_{ps}^k \epsilon_s}{G_1}\right)$. Due to circular symmetry of the problem the angle distributions do not change. Since the SBS is uniformly(independently) placed, the change in distance distribution of the PBS-PUE $f_{\ddot{D}_p}(\ddot{d}_p)$, is same as the change in distance distribution of the PUE-SBS path, $f_{\ddot{D}_{ps}}(\ddot{d}_{ps})$. This change is the scaling factor $\frac{1}{C}F_{X_{ps}}\left(\frac{N_0 \ddot{d}_{ps}^k \epsilon_s}{G_1}\right)$ from (4.31), and gives after substituting for d_{ps}

$$f_{\ddot{D}_p}(\ddot{d}_p, d_s, \varpi) = \frac{1}{F_{\Phi_c}(\epsilon_s)} F_{X_{ps}}\left(\frac{\epsilon_s N_0\left(\ddot{d}_p^2 + d_s^2 - 2\ddot{d}_p d_s\cos(\varpi_p - \varpi_s)\right)^{\frac{k}{2}}}{G_1}\right) f_{D_p}(\ddot{d}_p). \tag{4.37}$$

The above equation is a joint function of $\ddot{d}_p$ and d_s and $\varpi = \varpi_p - \varpi_s$. To find the distribution of $f_{\ddot{D}_p}(\ddot{d}_p)$ over a whole cell, the variables d_s and ϖ need to be marginalised. The angles ϖ_p and ϖ_s are uniformly distributed ans so the distribution of ϖ can be calculated from the convolving the PDF R.Vs [68]. The PDF of d_s and ϖ is given as

$$f_{D_s}(d_s) = \frac{2d_s}{R^2}, f_{\Pi}(\varpi) = \begin{cases} \frac{2\pi - |\varpi|}{4\pi^2}, -2\pi \leq \varpi \leq 2\pi \end{cases}. \tag{4.38}$$

The PDF $f_{\ddot{D}_p}(\ddot{d}_p)$ can be calculated by solving the following integrals.

$$f_{\ddot{D}_p}(\ddot{d}_p) = \frac{\int\limits_0^R \int\limits_{-2\pi}^{2\pi} f_{\ddot{D}_p}(\ddot{d}_p, d_s, \varpi) f_{\varpi}(\varpi) f_{D_s}(d_s) d\varpi \; dd_s}{\int\limits_0^R \int\limits_0^R \int\limits_{-2\pi}^{2\pi} f_{\ddot{D}_p}(\ddot{d}_p, d_s, \varpi) f_{\Pi}(\varpi) f_{D_s}(d_s) d\varpi \; dd_s \; d\ddot{d}_p}. \tag{4.39}$$

The denominator is a scaling factor which represents the average probability of distance d_p over which the SBS cannot detect the PUE. The solution of the above integrals do not exist. Applying GMQ's and simplifying the notation, $\sum\limits_{m_3}^{N_{m_3}} \sum\limits_{m_4}^{N_{m_4}} = \sum\limits_{m_3,m_4}^{N_{m_3},N_{m_4}}$, the final expression is given below,

$$f_{\ddot{D}_p}(\ddot{d}_p) = \tag{4.40}$$
$$\frac{\sum\limits_{m_3,m_4}^{N_{m_3},N_{m_4}} 4w_{m_3}w_{m_4}(1-t_{m3})F_{X_{ps}}\left(\frac{\varepsilon_s N_0\left(\ddot{d}_p^2+\left(Rt_{m_4}\right)^2-2\ddot{d}_pRt_{m_4}\cos(2\pi t_{m_3})\right)^{\frac{k}{2}}}{G_1}\right)f_{D_p}(d_p)}{\sum\limits_{(m_3,m_4,m5)}^{N_m} 8w_{m_3}w_{m_4}w_{m_5}(1-t_{m3})F_{X_{ps}}\left(\frac{\varepsilon_s N_0\left(\left(Rt_{m_5}\right)^2+\left(Rt_{m_4}\right)^2-2R^2t_{m_4}t_{m_5}\cos(2\pi t_{m_3})\right)^{\frac{k}{2}}}{G_1}\right)},$$

where, w_{m_3} (t_{m_3}) are the weights (abscissa) for [129, Eq. (25.4.33) with $k = 0$], w_{m_4} (t_{m_4}) and w_{m_5} (t_{m_5}) are the weights (abscissa) for [129, Eq. (25.4.33) with $k = 1$].

4.4.2.2 $f_{\tilde{D}_p}(\tilde{d}_p)$, for which the SBS *can* detect the PUE

The distribution of $f_{\tilde{D}_p}(\tilde{d}_p)$ can be calculated by replacing $F_{X_{ps}}\left(\frac{N_0 d_{ps}^k \epsilon_s}{G_1}\right)$ by $1 - F_{X_{ps}}\left(\frac{N_0 d_{ps}^k \epsilon_s}{G_1}\right)$ in (4.37).

4.4.3 Outage Probability of the PUE When the SBS Transmits $\ddot{P}_{out}$

Denoting $\ddot{\Theta}_{p_c}$ as the PUE's received signal power from the PBS when the SBS transmits, the SINR $\ddot{\Upsilon}_{pu_c}$ and $\ddot{P}_{out_c}$ is given as

$$\ddot{\Upsilon}_{pu_c} = \frac{\ddot{\Theta}_{p_c}}{\ddot{\Theta}_{I_c} + N_0} = \frac{G_2 X_{pp}\left(10^{-3}\ddot{D}_p\right)^{-n}}{\ddot{\Theta}_{in_c}}, \quad \ddot{P}_{out_c} = F_{\ddot{\Upsilon}_{pu_c}}(\epsilon_{out}). \tag{4.41}$$

Applying the similar procedure as in (4.29) and using GMQ, the CDF of $\ddot{\Theta}_{p_c}$ is:

$$F_{\ddot{\Theta}_{p_c}}(\ddot{\theta}_{p_c}) = \sum_{m_5}^{N_{m_5}} \frac{Rw_{m_5}}{2}\left(1 + \text{erf}\left(\frac{10\log_{10}\left(\frac{\ddot{\theta}_{p_c}\left(Rt_{m_5}\right)^n}{G_2 10^{3n}}\right)}{\sqrt{2}\sigma_p}\right)\right) f_{\ddot{D}_p}(Rt_{m_5}). \tag{4.42}$$

Assuming $\ddot{\Theta}_{p_c}$ and $\ddot{\Theta}_{I_c}$ to be independent because they include independent shadow fading gains[5]. A procedure similar to (4.19) is adopted to express the integral in terms of GHQ. Using (4.35), the CDF of $\ddot{\Upsilon}_{pu_c}$ is given as

$$F_{\ddot{\Upsilon}_{pu_c}}(\ddot{\upsilon}_{pu_c}) = \sum_{m_2=1}^{N_{m_2}} \sum_{h=1}^{N_h} \frac{w_{m_2} w_h A(t_{m_2})}{F_{\Phi_c}(\varepsilon_s)} \left(\frac{Q(x_1)}{\sqrt{\pi}} F_{\ddot{\Theta}_{p_c}}\left(\ddot{\upsilon}_{pu_c}\left(e^{\frac{\ln(10)}{10}\left(\sqrt{2}\sigma_{sp}t_h + \mu_{m_2}\right)} + N_0\right)\right) + \right.$$
$$\sum_{m_1=1}^{N_{m_1}} \frac{2\rho w_{m_1}\left(\rho t_{m_1} x_1 - t_h \mu_{m_1}\right) e^{-\frac{1}{\mu_{m_1}^2}\left(x_1^2 - 2\rho x_1 t_{m_1} t_h \mu_{m_1}\right)}}{\sqrt{2}\pi \mu_{m_1}^2}$$
$$\left. F_{\ddot{\Theta}_{p_c}}\left(\ddot{\upsilon}_{pu_c}\left(e^{\frac{\ln(10)}{10}\left(\sigma_{sp}t_h\mu_{m_1} + \mu_{m_2}\right)} + N_0\right)\right)\right), \tag{4.43}$$

where, $\mu_{m_1} = \sqrt{2(1-\rho^2 t_{m_1}^2)}$, $\mu_{m_2} = 10\log_{10}\left(\frac{G_3}{(t_{m_2}2R)^k}\right)$.

[5]This has been verified based on simulation analysis which was carried out over all the relevant range of system parameters. The results indicated that the correlations between $\ddot{\Theta}_{p_c}$ and $\ddot{\Theta}_{I_c}$ is in the order of 10^{-3} and thus can be neglected.

4.4.4 Outage Probability of the PUE When the SBS Stays Quiet $\tilde{P}_{out_c}$

When the SBS does not transmit, the outage probability $\tilde{P}_{out_c}$ can be calculated from the SNR $\tilde{\Upsilon}_{pu_c}$.

$$\tilde{\Upsilon}_{pu_c} = \frac{\tilde{\Theta}_{p_c}}{N_0} = \frac{G_2 X_{pp}\left(10^{-3}\tilde{D}_p\right)^{-n}}{N_0}, \tilde{P}_{out_c} = F_{\tilde{\Upsilon}_{pu_c}}(\epsilon_d), \tag{4.44}$$

where, $\tilde{\Theta}_{p_c}$ is the received power at the PUE from the PBS, and $\tilde{D}_p$ is the set of distances when the SBS is not transmitting. The distribution of $f_{\tilde{D}_p}(\tilde{d}_p)$ is obtained by changing $F_{X_{ps}}(.)$ in (4.40) to $1 - F_{X_{ps}}(.)$ in $f_{\ddot{D}_p}(\ddot{d}_p)$. The probability $\tilde{P}_{out_c}$ is calculated by replacing G_2 with $\frac{G_2}{N_0}$ in the error function (4.42).

4.4.5 Natural Outage Probability of the PUE, P_{out}^{nat}

Similar to the previous scenario, the natural outage can be calculated from the SNR at the PUE. The natural outage is

$$[P_{out_c}^{nat} = F_{\Upsilon_{pu_c}^{nat}}\left(\upsilon_{pu_c}^{nat}\right)] = \frac{e^{(l_p + \frac{10\log_{10}(10^6 G_4)}{\sqrt{2}\sigma_{pp}})2\beta_{pp}}\left(1 + \text{erf}\left(\frac{10\log_{10}\upsilon_{pu_c}^{nat}}{\sqrt{2}\sigma_{pp}} + l_p\right)\right)}{2R^2} - \tag{4.45}$$
$$\frac{e^{-2\left(\frac{10\log_{10}\upsilon_{pu_c}^{nat} - 10\log_{10}(10^6 G_4)}{\sqrt{2}\sigma_{pp}}\right)\beta_{pp} + \beta_{pp}^2}\left(1 + \text{erf}\left(\frac{10\log_{10}\upsilon_{pu_c}^{nat}}{\sqrt{2}\sigma_{pp}} + l_p - \beta_{pp}\right)\right)}{2R^2},$$

where, $G_4 = \frac{G_2}{N_0}$, $l_p = \frac{10n\log_{10}R - 10\log_{10}(10^6 G_4)}{\sqrt{2}\sigma_{pp}}$, $\beta_{pp} = \frac{\ln(10)\sqrt{2}\sigma_{pp}}{10n}$.

The additional outage probability is calculated based on equations (4.26) (4.45) and the outage probability derivations in the previous sections.

4.4.6 Numerical Results

In this section, we give some numerical examples of detection probability P_d, Interference power Θ_{I_c}, and the additional outage probability $P_{out_c}^{pu}$ of the PUE. In

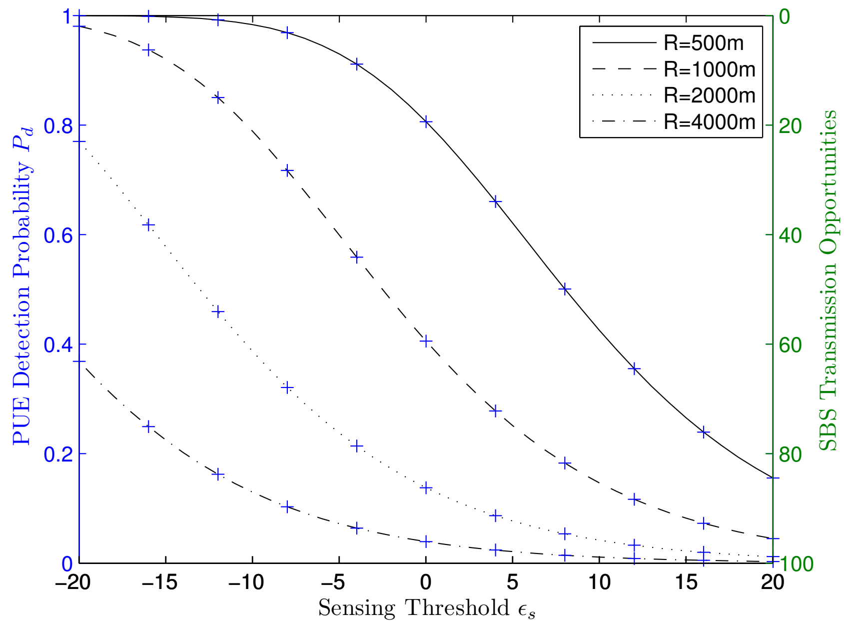

Figure 4.5: Detection probability P_d of PUE for different values of R and sensing threshold ϵ_s, given $T_{pu} = 0.8$W, and $k = 3.5$. The SBS transmission probability on the right hand axis.

simulations the antenna gains of the PUE and SBS are assumed to be 1 and the factors G_1, G_3 are calculated as follows

$$G_1 = \frac{T_{pu}}{L_0}, (G_3) = \frac{T_{sb}}{L_0}. \tag{4.46}$$

The values of the quadrature variables are taken as $\{N_{m_0}, N_{m_1}, N_{m_2}, N_{m_3}, N_{m_4}, N_{m_5}\} =$ 20 and $N_h = 16$. The values of the system parameters are summarised in Table 4.2 and Table 4.3.3 unless mentioned otherwise. Although some of the values in Table 4.2 are mentioned in dB, they are transformed to linear scale prior to numerical evaluation. Fig. 4.5 shows the detection probability of the PUE versus the sensing threshold, as calculated from (4.29). The marker '+' represent the simulation values which clearly agree with the derived results. The detection probability reduces as the cell size R is increased, indicating a higher probability that the SBS is outside the transmission range of the PUE. For a normal macrocell radius of $1000 - 2000$m

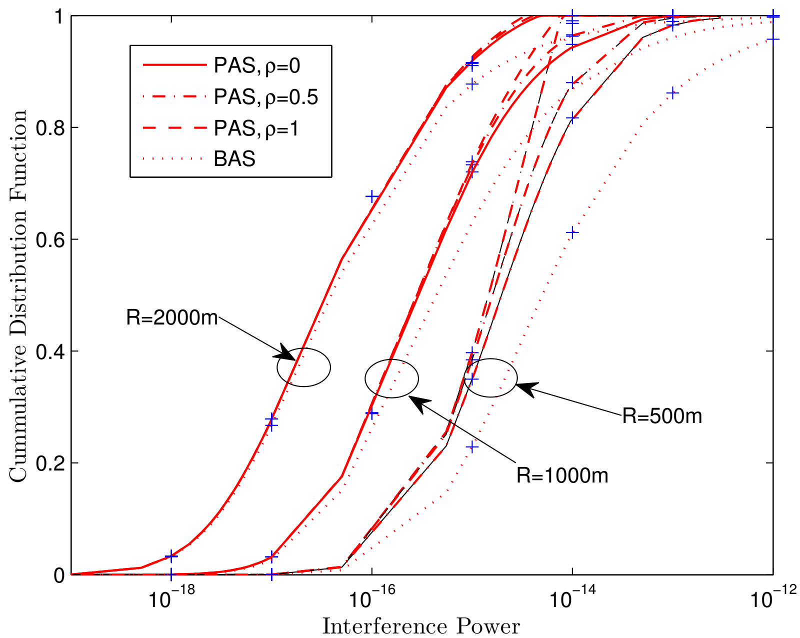

Figure 4.6: CDF of interference power for different values of R and ρ, given $k = 3.5$, $T_{sb} = 100mW$, and $\epsilon_s = 10$dB.

and $\epsilon_s = 10$dB, the SBS can only detect $5 - 17\%$ of the PUE transmissions. When the PUE is not detected the SBS has a transmission opportunity and its probability is shown on the right hand axis. The curve shows the trade off between the sensing threshold and the transmission opportunity. Lower sensing thresholds treat interference in a more conservative way, reducing the transmission opportunities. It is particularly so for small cells, the effectiveness of the secondary FC reduces to 20% for a sensing threshold of $\epsilon_s = 0$dB in a cell of radius $R = 500$m.

Note. In order to investigate the impact of UL sensing, we include the scenario $\epsilon_s = \infty$ termed as **Basic Access Scheme (BAS)**. In BAS, the SBS is always transmitting in the DL channel. The scheme with a finite sensing threshold is referred as **Probabilistic Access Scheme (PAS)**.

Fig. 4.6 shows the CDF of the interference power to the PUE, given $T_{sb} =$

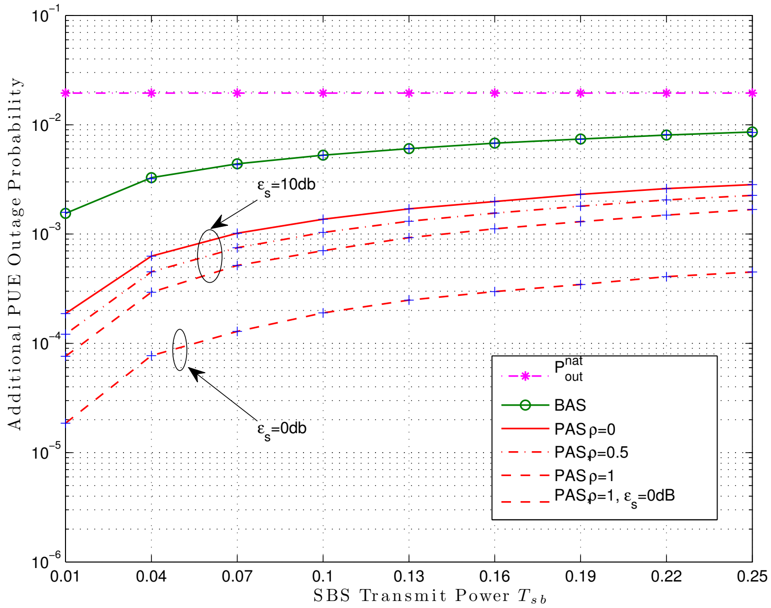

Figure 4.7: Additional outage probability of PUE as a function of SBS transmit power given $R = 2000m$, $k = 3.5$, and $\epsilon_{out} = 10$dB.

$100mW$. The effect of correlation between the sensing and interference paths is shown by the dashed lines. The effect of correlation is more dominant in small cells, where higher interference powers occur. A 100% correlation between the paths places a hard limit on the interference power; in this case $0.86e-15$W (approximately -110dBm), which is 2dB above the noise floor (N_0 in Table 4.2). 20% of transmissions would exceed this power level if there was no correlation between the paths for a cell size of $R = 500$m. This drops to 5% for a 1000m cell and is negligible for cell sizes of 2000m or greater.

Fig. 4.7 plots the additional outage probability caused by the presence of a secondary cell. The top line shows the natural outage probability $P^{nat}_{out_c}$ without SBS transmission is 2%, averaged over the cell. It is primarily caused by shadow fading on the PBS-PUE path, The second line shows the additional outage caused by the

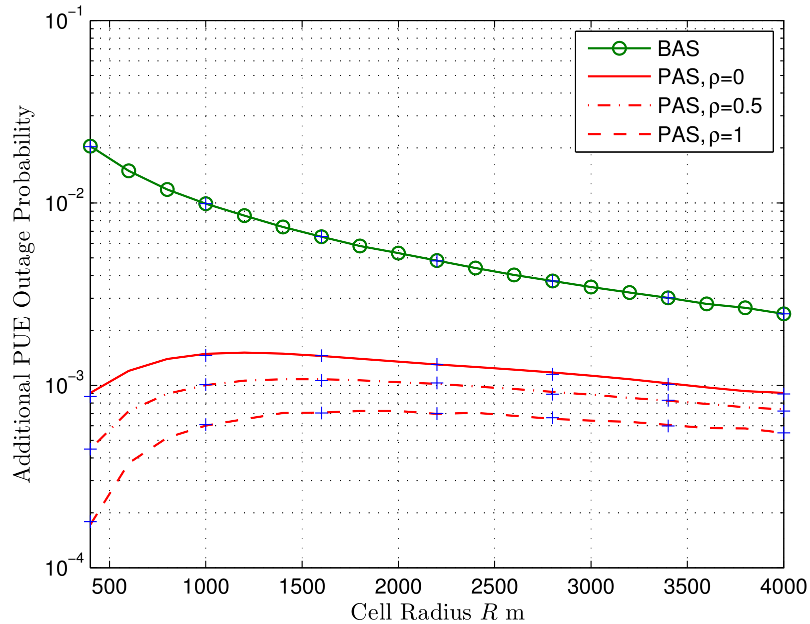

Figure 4.8: Additional outage probability of PUE for different cell radius, given $k = 3.5$, $T_{sb} = 100mW$, $\epsilon_s = 10$dB, and $\epsilon_{out} = 10$dB.

SBS without using any sensing mechanism. The additional outage is minimal, 0.5%, at the normal operating wireless LAN power of $20dbm$ (0.1W). Sensing drops this to 0.14% even when the sensing and interference paths are uncorrelated. Correlation almost halves this figure to 0.07% outage increase. Lower sensing thresholds ($\epsilon_s =$ 0dB) give even lower outage increases, but are not recommended because of the lower transmission opportunities for the SBS (Fig. 4.5). In all the above cases the additional outage is negligible compared to the natural outage and would not be noticed. But we must emphasise that it is only for one secondary cell. Multiple secondary FCs would be expected in a macrocell. We can expect the additional outage to increase by the number of such secondary cells (first order approximation). As an example, if it was deemed acceptable to allow the natural outage to increase by a factor of 2 (to 4% in this example), then 4 FCs can be accommodated without any sensing $T_{sb} = 20$dBm, and with sensing this would increase to 14 for $\rho = 0$, and 28 for $\rho = 1$. Any further increase in FC numbers would require a reduction in their transmission powers. At $T_{sb} = 10$dBm, ($\epsilon_s = 10dB$) the number of FCs without sensing can be increased to 13 and with sensing to 100 for $\rho = 0$ or 250 for $\rho = 1$.

Fig. 4.8 shows the PUE outage probability with respect to cell radius R. The PUE additional outage caused by the BAS scheme is significantly high, emphasising the need of sensing for cell radii < 1500m. In the case of PAS, we notice that the peak of the additional outage occurs when the macrocell radius is between $1000 - 2000$m. Smaller cells are more likely to sense the PUE (because of strong signal levels) while in larger cells, the PUE is more likely to be out of range, resulting in lower outages in both cases. Again we see that correlation approximately halves the additional outage. Note that the curve for a correlation of $\rho = 0.5$ is almost midway between $rho = 0$ and $\rho = 1$, indicating an approximate linear relationship between ρ and $P^{pu}_{out_c}$.

4.5 An Approximate Distribution of Distance Between Uniformly Distributed Points

The calculation of the PDF $f_{\Phi_c}(\phi_c)$ and the CDF $F_{\Phi_c}(\Phi_c)$ lacks mathematical tractability due to the presence of inverse trigonometric and circular symmetric functions in $f_{D_{ps}}(d_{ps})$. For example, when the fading power is lognormal, the closed form solution cannot be obtained. The problem also exists for rectangular spatial distribution in [139], though it is not a very good model for the single cell geometry. In the following, we present an approximate distribution of $f_{D_{ps}}(d_{ps})$ so that the ratio distribution in (4.27) can be quantified. Although the resulting distribution

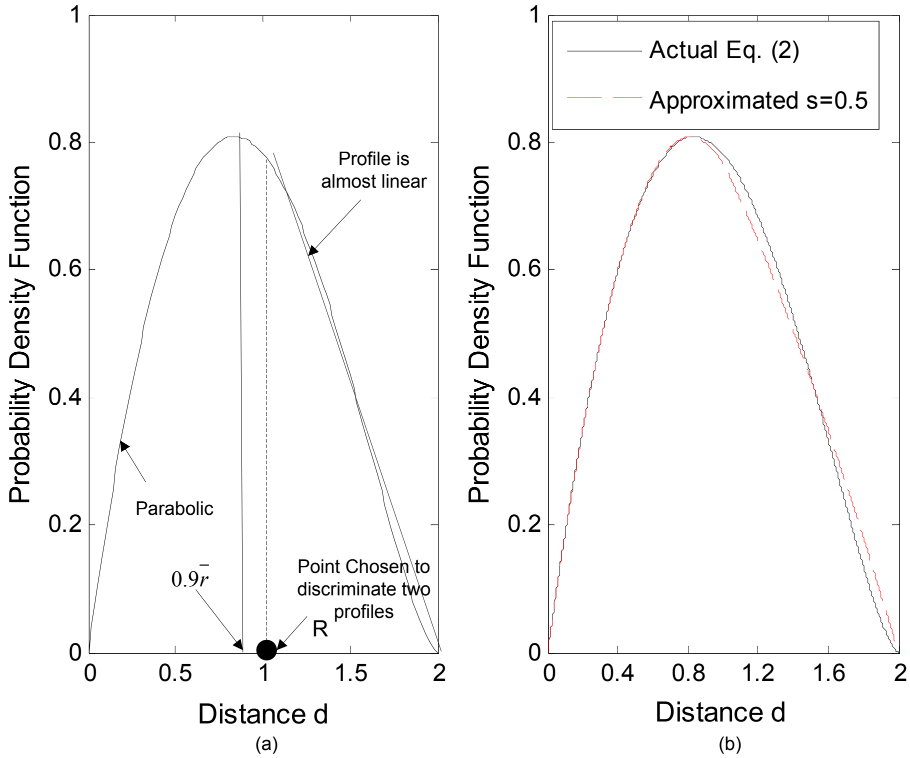

Figure 4.9: Ideal and approximated probability density function of the distance between uniformly distributed points in a circle with unit radius

has a closed form it is still mathematically inconvenient. We apply further simplifications and show that the Skew Normal Distribution can approximate $f_{\Phi_c}(\phi_c)$ where the cell SNR is measured in dB (i.e. $f_{\Phi_c^{dB}}(\phi_c^{dB})$). To the best of our knowledge such an approximation has not been presented before.

4.5.1 Heuristic Approximation (HA).

Fig. 4.9(a) shows the plot of $f_{D_{ps}}(d_{ps})$ for $R = 1$. It can be seen that the profile (slope) of the distribution changes around R. The left portion of the distribution follows a parabolic (quarter circle) curve, whereas the right portion nearly follows a straight line with a negative slope. Using these observations, the PDF is approximated as parabolic in the left portion, whereas in the right portion instead of employing a straight line approximation, we opted for a form $md + bd^s$,

$$\hat{f}_{D_{ps}}(d_{ps}) = \begin{cases} a\left(2\bar{r}d_{ps} - d_{ps}^2\right) & 0 \leq d_{ps} \leq R, \\ a\left(md_{ps} + bd_{ps}^s\right) & R < d_{ps} \leq 2R, \end{cases} \tag{4.47}$$

where, $\bar{r}$ ($\approx 0.9E[D]$) is the mode of the $f_{D_{ps}}(d_{ps})$ and a is a normalisation constant such that the integral of the PDF is equal to 1. The values of m and b are calculated such that the transition from the left portion to the right portion is continuous at R and the PDF reaches zero at 2R ($f_{D_{ps}}(2R) = 0$). The values of these variables are: $m = \frac{-b(2R)^s}{(2R)}$, $b = \frac{(2R)(2R\bar{r}-R^2)}{(2R)R^s - R(2R)^s}$, $a = \frac{1}{\bar{r}R^2 - \frac{R^3}{3} + m\frac{3R^2}{2} + b\frac{(2R)^{s+1}-(R)^{s+1}}{s+1}}$. The value of s is calculated such that the mean absolute difference between the curves ($E[|f_D(d) - f_{\hat{D}}(d)|]$) is minimized. We found the minimum error to be 0.0171 (2.1% of the PDF maximum) for $s = 0.5$. The values of m, b and a for $s = 0.5$ are: $b = 2.1501R^{1.5}$, $m = -1.5203R$, $a = 1.2167R^{-3}$. The approximated PDF curve for $s = 0.5$ is shown in Fig. 4.9(b). The transmission probability over the cell is $P_{tx_c}^{su} = F_{\Phi_c}(\epsilon_s)$. Similar to (4.19), the CDF can be calculated by solving the integral in (4.29),

$$F_{\Phi_c}(\phi_c) = \int_0^{2R} F_X\left(\frac{\phi_c D_{ps}^k L_0 N_0}{T_{pu}}\right) \hat{f}_{D_{ps}}(d_{ps})\, dd_{ps}. \tag{4.48}$$

If we use the Heuristic Approximation (HA) in (4.47), the above integral can be split into two sub integrals with limits 0 to R and R to $2R$ respectively. Using a similar procedure, the CDF or the PDF can be obtained for other fading distributions e.g., gamma distribution. The following closed form CDF $F_{\Phi_c}(\phi_c)$ is calculated by algebraic manipulation and using the integral identity [149, Eq. (1.5.2.3)]

$$
\begin{aligned}
&F_{\Phi_c}(\phi_c) = \\
&\frac{a\,\bar{r}e^{\beta_1^2}g^{\frac{2}{k}}}{2}\left(e^{-\beta_1(\beta_1+2l_0)}J\left(\frac{10\log_{10}\phi_c}{\sqrt{2}\sigma_{ps}}-l_0\right)-e^{\frac{-20\beta_1\log_{10}\phi_c}{\sqrt{2}\sigma_{ps}}}J\left(\frac{10\log_{10}\phi_c}{\sqrt{2}\sigma_{ps}}-\beta_1-l_0\right)\right)- \\
&\frac{ae^{\frac{9\beta_1^2}{4}}g^{\frac{3}{k}}}{6}\left(e^{-\frac{3}{4}\beta_1(4l_0+3\beta_1)}J\left(\frac{10\log_{10}\phi_c}{\sqrt{2}\sigma_{ps}}-l_0\right)-e^{-\frac{30\beta_1\log_{10}\phi_c}{\sqrt{2}\sigma_{ps}}}J\left(\frac{10\log_{10}\phi_c}{\sqrt{2}\sigma_{ps}}-\frac{3\beta_1}{2}-l_0\right)\right)+ \\
&\frac{ame^{\beta_1^2}g^{\frac{2}{k}}}{4}\left(\begin{array}{l}-e^{-\beta_1(2l_0+\beta_1)}J\left(\frac{10\log_{10}\phi_c}{\sqrt{2}\sigma_{ps}}-l_0\right)+e^{(2l_1-\beta_1)\beta_1}J\left(\frac{10\log_{10}\phi_c}{\sqrt{2}\sigma_{ps}}+l_1\right)+ \\ e^{-\frac{20\beta_1\log_{10}\phi_c}{\sqrt{2}\sigma_{ps}}}\left(J\left(\frac{10\log_{10}\phi_c}{\sqrt{2}\sigma_{sp}}-l_0-\beta_1\right)-J\left(\frac{10\log_{10}\phi_c}{\sqrt{2}\sigma_{ps}}+l_1-\beta_1\right)\right)\end{array}\right)+ \\
&\frac{abe^{\frac{9\beta_1^2}{16}}g^{\frac{3}{2k}}}{3}\left(\begin{array}{l}-e^{-\frac{3}{8}\beta_1(4l_0+\frac{3\beta_1}{2})}J\left(\frac{10\log_{10}\phi_c}{\sqrt{2}\sigma_{ps}}-l_0\right)+e^{\frac{3}{8}\beta_1(4l_1-\frac{3\beta_1}{2})}J\left(\frac{10\log_{10}\phi_c}{\sqrt{2}\sigma_{ps}}+l_1\right)+ \\ e^{-\frac{30\beta_1\log_{10}\phi_c}{2\sqrt{2}\sigma_{ps}}}\left(J\left(\frac{10\log_{10}\phi_c}{\sqrt{2}\sigma_{ps}}-l_0-\frac{3\beta_1}{4}\right)-J\left(\frac{10\log_{10}\phi_c}{\sqrt{2}\sigma_{ps}}+l_1-\frac{3\beta_1}{4}\right)\right)\end{array}\right).
\end{aligned}
\tag{4.49}
$$

The PDF in dB ϕ_c^{dB} scale is shown below

$$
\begin{aligned}
&f_{\Phi_c^{dB}}(\phi_c^{dB}) = \\
&a\beta_0\,\bar{r}g^{\frac{2}{k}}e^{{\beta_1}^2-2\beta_0\phi_c^{dB}}J\left(\frac{\phi_c^{dB}}{\sqrt{2}\sigma_{ps}}-\beta_1-l_0\right)-0.5a\beta_0g^{\frac{3}{k}}e^{\frac{9{\beta_1}^2}{4}-3\beta_0\phi_c^{dB}}J\left(\frac{\phi_c^{dB}}{\sqrt{2}\sigma_{ps}}-\frac{3\beta_1}{2}-l_0\right) \\
&0.5a\beta_0\mathrm{m}g^{\frac{2}{k}}e^{{\beta_1}^2-2\beta_0\phi_c^{dB}}\left(J\left(\frac{\phi_c^{dB}}{\sqrt{2}\sigma_{ps}}-\beta_1+l_1\right)-J\left(\frac{\phi_c^{dB}}{\sqrt{2}\sigma_{ps}}-\beta_1-l_0\right)\right)+ \\
&0.5a\beta_0bg^{\frac{3}{2k}}e^{\frac{9{\beta_1}^2}{16}-\frac{3\beta_0\phi_c^{dB}}{2}}\left(J\left(\frac{\phi_c^{dB}}{\sqrt{2}\sigma_{ps}}-\frac{3\beta_1}{4}+l_1\right)-J\left(\frac{\phi_c^{dB}}{\sqrt{2}\sigma_{ps}}-\frac{3\beta_1}{4}-l_0\right)\right),
\end{aligned}
\tag{4.50}
$$

where, $J(.) = 1 + \mathrm{erf}(.)$, $\beta_0 = \frac{\ln(10)}{10k}$, $l_0 = \frac{10\log_{10}\left(g/R^k\right)}{\sqrt{2}\sigma}$, $l_1 = \frac{10\log_{10}\left((2R)^k/g\right)}{\sqrt{2}\sigma}$, $\beta_1 = \frac{\ln(10)\sqrt{2}\sigma}{10k}$, and $g = \frac{T_{pu}}{L_0 N_0}$.

4.5.2 Central Moment Matching- Skew Normal Distribution

Although, the above equation represents a fairly accurate closed form solution, it is still inconvenient for further analysis. In the following, we first derive 2 key properties of $f_{\Phi_c^{dB}}(\phi_c^{dB})$ and use them as a basis for moment matching to obtain a mathematically tractable PDF.

Remark 3. The following properties can also be derived from the original distribution (4.28). Here, we use HA due to the ease of analysis and demonstration.

Property 1. The PDF $f_{\Phi_{dB}}(\phi_{dB})$ is always unimodal.

From (4.27), $\Phi_c^{dB} = X_{dB} + D_{dB}$, where $X_{dB} = 10\log_{10} X_{ps}$ and $D_{dB} = -10k\log_{10} D_{ps}$. An alternate method of calculating $f_{\Phi_{dB}}(\phi_{dB})$ requires the convolution of the PDF $f_{X_{dB}}(x_{dB})$ and $\hat{f}_{D_{dB}}(d_{dB})$ [68]. From [141], it is well known that the convolution of log-concave unimodal functions is also unimodal. Since $f_{X_{dB}}(x_{dB})$ (Gaussian distribution) is unimodal and log-concave [68], the unimodality can be established by proving the log-concavity of $\hat{f}_{D_{dB}}(d_{dB})$, i.e., $\frac{d^2\log(f_{D_{dB}}(d_{dB}))}{dd_{dB}^2} \leq 0$, where

$$\frac{d^2\log(f_{D_{dB}}(d_{dB}))}{dd_{dB}^2} = \begin{cases} -\frac{0.4330R^{2.5}e^{\frac{0.115d_{dB}}{k}}}{k^2\left(2.15R^{1.5}-1.52\mathrm{R}e^{\frac{0.115d_{dB}}{k}}\right)^2} & \begin{array}{l}-10k\log_{10}2R < d_{dB} \leq \\ -10k\log_{10}(R)\end{array} \\ -\frac{0.0865Re^{\frac{0.23d_{dB}}{k}}}{k^2\left(1-1.6298Re^{\frac{0.23d_{dB}}{k}}\right)^2} & -10k\log_{10}R < d_{dB} \leq +\infty \end{cases} \tag{4.51}$$

Since the second derivative is negative on both the intervals, the Property 1 is proved.

Property 2. The PDF $f_{\Phi_c^{dB}}(\phi_c^{dB})$ is skewed.

This can be visualised by the fact that the third central moments of the sum of two independent random variables $(X_{dB} + D_{dB})$ follow the superposition law [68]. Since the third central moment of $X_{dB} = 0$, the skewness, ξ_{dB}, of $f_{\Phi_c^{dB}}(\phi_c^{dB})$ can be simplified as

$$\xi_{dB} = \frac{(332126 + 107.454(\ln R) + 79.1966(\ln R)^2 - 108.098(\ln R)^3)}{(3911.05 + \beta^2\sigma^2 \times 10^{-4} + 0.527864(\ln R) - 1.08075(\ln R)^2)^{1.5}}, \tag{4.52}$$

where $\beta = \frac{\ln(10)}{10k}$. Traditionally, the gamma distribution is widely used in approximating distributions with Moment matching such as composite fading and lognormal fading [142][143]. However, the problem of using gamma distribution is that it does not strictly follow unimodality [144]. To account for both unimodality and skewness we choose the Skew Normal distribution (SND). From [145, Eq. (3)], the PDF and the CDF of SND S_{nd} is given as

$$f_{\mathrm{S_{nd}}}(\mathrm{s_{nd}};\alpha_{\mathrm{snd}},\zeta_{\mathrm{snd}},\chi_{\mathrm{snd}}) = \frac{1}{\sqrt{2\pi}\chi} e^{-\frac{(\mathrm{s_{nd}}-\zeta_{\mathrm{snd}})^2}{2\chi_{\mathrm{snd}}^2}} \left(1+\mathrm{erf}\left(\frac{\mathrm{s_{nd}}\alpha_{\mathrm{snd}}-\alpha_{\mathrm{snd}}\zeta_{\mathrm{snd}}}{\sqrt{2}\chi_{\mathrm{snd}}}\right)\right), \tag{4.53}$$

$$F_{\mathrm{S_{nd}}}(\mathrm{s_{nd}};\alpha_{\mathrm{snd}},\zeta_{\mathrm{snd}},\chi_{\mathrm{snd}}) = Q\left(\frac{\mathrm{s_{snd}}-\zeta_{\mathrm{snd}}}{\chi_{\mathrm{snd}}}\right) - 2\mathbb{T}\left(\frac{\mathrm{s_{nd}}-\zeta_{\mathrm{snd}}}{\chi_{\mathrm{snd}}},\alpha_{\mathrm{snd}}\right),$$

where, $\mathbb{T}(.,.)$ is the Owen's T function [145], ζ_{snd} is the location parameter, χ_{snd} is the scale parameter, and α_{snd} indicates the right(>0) or left skewness (<0). The mean μ_{snd}, variance σ_{snd}, and skewness ξ_{snd} of the SND is given as

$$\mu_{\mathrm{snd}} = \zeta_{\mathrm{snd}} + \chi_{\mathrm{snd}}\delta_{\mathrm{snd}}\sqrt{\frac{2}{\pi}}, \text{ where } \delta_{\mathrm{snd}} = \frac{\alpha_{\mathrm{snd}}}{\sqrt{1+\alpha_{\mathrm{snd}}^2}}, \tag{4.54}$$

$$\sigma_{\mathrm{snd}}^2 = \chi_{\mathrm{snd}}^2\left(1-\frac{2\delta_{\mathrm{snd}}^2}{\pi}\right), \quad \xi_{\mathrm{snd}} = \left(\frac{4-\pi}{2}\right)\frac{\left(\delta_{\mathrm{snd}}\sqrt{\frac{2}{\pi}}\right)^3}{\left(1-\frac{2\delta_{\mathrm{snd}}^2}{\pi}\right)^{3/2}},$$

whereas, the mean and the variance of Φ_c^{dB} are:

$$\mu_{dB} = 10\log_{10}\left(\frac{T_p}{L_0N_0}\right) + \frac{0.244238-1.00011\ln(R)}{\beta}, \tag{4.55}$$

$$\sigma_{dB}^2 = \sigma^2 + \frac{0.391105}{\beta^2} + \frac{5.27864\times10^{-5}(\ln R)}{\beta^2} - \frac{1.08075\times10^{-4}(\ln R)^2}{\beta^2}$$

Note that the maximum allowable value of skewness ξ_{snd} is 0.995 [145], with slight abuse of notation we write $\xi_{dB} = \min\{0.995, \xi_{dB}\}$. For small R, the terms containing $\ln(R)$ in σ_{dB} and ξ_{dB} can be ignored. Equating the above with (4.54) gives,

$$\delta_{\mathrm{snd}} = \sqrt{\frac{\xi_{dB}^2}{0.3622+0.6366\xi_{dB}^2}}, \quad \alpha_{\mathrm{snd}} = \frac{\xi_{dB}}{\sqrt{0.3622-0.3634\xi_{dB}^2}}, \tag{4.56}$$

$$\chi_{\mathrm{snd}} = \sqrt{\sigma_{dB}^2 + 1.75759\sigma_{dB}^2\xi_{dB}^2}, \quad \zeta_{\mathrm{snd}} = \mu_{dB} - 0.7979\chi_{\mathrm{snd}}\delta_{\mathrm{snd}}.$$

If $\alpha_{\mathrm{snd}} = 0$ and only μ_{dB} and σ_{dB} are matched, the SND distribution in (4.53) becomes the normal distribution (ND). The PDF and the CDF $f_{\Phi_c}(\phi_c)$ and $F_{\Phi_c}(\phi_c)$

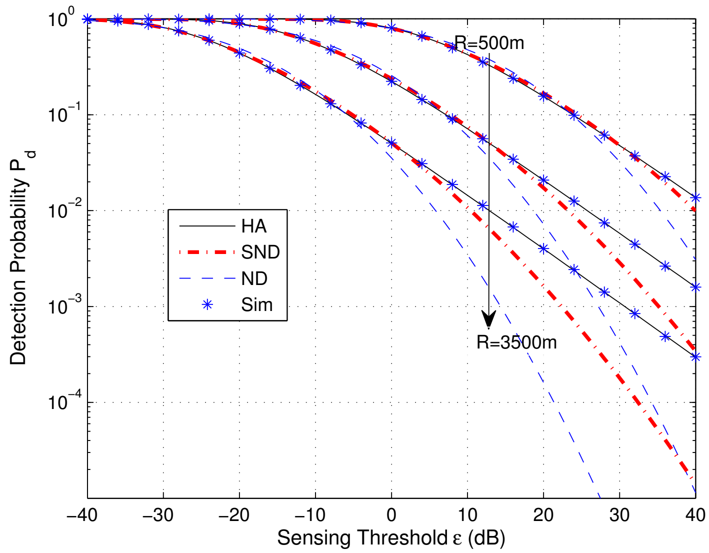

Figure 4.10: Detection probability $P_{d_c} = 1 - P^{su}_{tx_c} = 1 - F_{\Phi_c}(\phi_c)$ versus sensing threshold for different cell radii R. Monte Carlo simulations are shown by the marker '*'.

can be calculated from $f_{\Phi_c^{dB}}(\phi_c^{dB})$ by simple random variable transformation (Log-Skew Normal Distribution).

Numerical Results

Fig. 4.10 shows the detection probability $P_{d_c} = 1 - P^{su}_{tx_c} = 1 - F_{\Phi_c}(\phi_c)$, of the PUE for different values of sensing threshold, ϵ_s and cell radius, R. The simulation parameters are $T_{pu} = 0.8$, $L_0 = 10^{\frac{41}{10}}$, $\sigma = 6$dB, $k = 3.5$ and $N_0 = 10^{\frac{-142}{10}}$W. For these parameter values and $R = 1000m$, the PDF curves are shown in Fig. 4.11(a). Both the PDF and the CDF curves highlight that the difference between the Monte Ccarlo and heuristic approximation based result is very small. The Skew Normal Distribution (SND) provides a better fit than Normal Distribution (ND). To test the goodness of fit, we apply the Kolmogorov-Smirnov (KS) method [68, Eq. (9.71)] to the three distributions. Similar to [146], the sole purpose here is to establish convergence (rather than the hypothesis (hyp) acceptance or rejection). For the

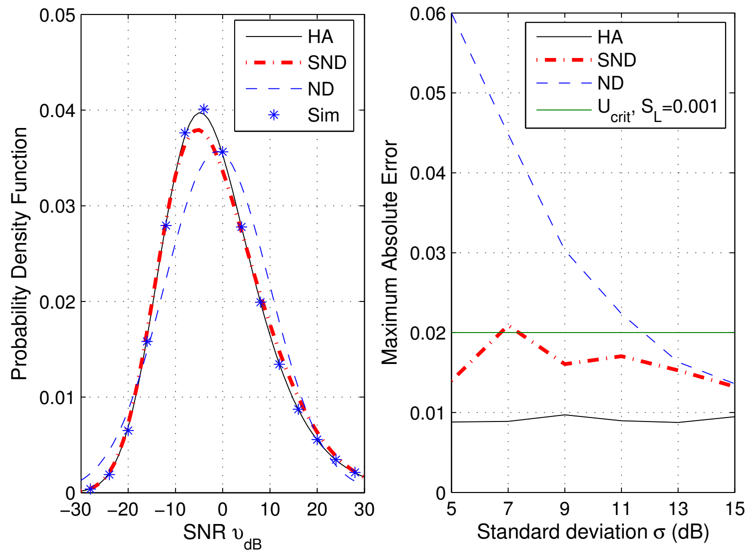

Figure 4.11: Left: PDF of SNR, Right: Absolute maximum error for KS method. Monte Carlo simulations are shown by the marker '*'.

sample size S_Z, the KS measures the maximum absolute error $\mathbb{U}_{max}$ between the hypothesised distribution F_{hyp} ($hyp \in \{\text{HA}, \text{SND}, \text{ND}\}$) and the Monte Carlo (sim) distribution F_{sim}. This error is compared to a critical error $\mathbb{U}_{crit}$ for the given significance level S_L [68, Eq. (9.73)]. If $\mathbb{U}_{max} \leq \mathbb{U}_{crit}$, the term $1 - S_L$ gives the probability that the simulation results are within the tolerance region on both side of the hypothetical curve i.e. $F_{sim} - \mathbb{U}_{max} \leq F_{sim} \leq F_{hyp} + \mathbb{U}_{max}$ [68], where the tolerance is $\pm\mathbb{U}_{crit}$. For example, for the significance level of $S_L = 0.001$, the critical error is $\mathbb{U}_{crit} = 0.02$. If the maximum absolute error is $\mathbb{U}_{max} = 0.019$, then 99.99% of the Montecarlo CDF values are within the hypothesised distribution's range of ± 0.02 (since $0.019 < 0.02$).

Fig. 4.11(b) shows $\mathbb{U}_{max}$ and $\mathbb{U}_{crit}$ for the three hypothesised distribution where $\mathbb{U}_{crit} = 0.02$ is calculated for a sample size $S_Z = 10,000$ and the significance level $S_L = 0.001$. The simulations are averaged over 10 runs. The heuristic approximation gives the lowest maximum error, well below the critical level $\mathbb{U}_{crit}$. The Skew Normal

Distribution (SND) remains under the $\mathbb{U}_{crit} = 0.02$ in the measurement range of the fading standard deviation. The ND stays above the critical error $\mathbb{U}_{crit}$, for $\sigma < 12$dB, however as σ increases the ND improves and converges to the SND approximation. The maximum absolute error of 0.02 represents a 2% of full scale difference between the CDFs, $F_{\Phi_c}(\phi_c)$. Note this is consistent with the curves in (Fig. 4.10) where the discrepancies between Monte Carlo simulations and the SND generally occur below 2×10^{-2} on the log scale of detection probability.

4.6 Summary

In this Chapter, we have presented a sensing and access scheme which exploits the duplexing structure of the cellular networks. In essence, it enables secondary FCs (SBS and SUE) to use sensing information from the UL channel to transmit in the corresponding DL channel. This is hypothesised by the spectrum measurement carried out in our lab, indicating strong DL signals and very weak (non-existent) UL signals. We have presented an example of a GSM network which provides this sensing and access flexibility. This scheme can be generalised to next generation networks like LTE, provided the resource block map is known or can be decoded.

In a location aware scenario, we have derived expressions for interference power and outage probability of the PUE that considers distance dependent path loss, shadow fading and correlation between the sensing and the interfering paths. We use correlation to examine the scenarios in which the sensing and transmissions are not necessarily confined to the same node. The PUE is most susceptible to interference at a distance of between $0.5 - 1$km from the FC. Correlation can halve the additional PUE outage caused by the SBS. As the PUE-SBS distance increases ($>$ 1.5km) pathloss becomes dominant and the correlation gain fades away. We found that this DL access scheme is more suitable for home/office or other indoor applications, where the intended range of FC is less than $\leq$ 50m. The FC range drops to 20m when operated close to the PBS ($<$ 0.5km) because of DL interference from the macrocell. Therefore, to increase the FC range, the SBS needs to transmit with more power which is possible considering the low interference susceptibility of the PUE near the PBS.

In a cell-wide scenario, we quantified the expected interference and outage probability for a randomly placed PUE and SBS. The additional PUE outage is low compared to the natural outage of the macrocell, indicating the potential for multiple FC activity. The results indicate that the sensing requirement can be relaxed in the case of a single FC with cell radii $>$ 1500m. Conservative setting of the sensing threshold (0dB) reduces SBS transmission opportunities and in the case of small cells makes the FC as good as useless (always off). To quantify the SBS transmission opportunities in a shadow fading environment, a heuristic approximation is presented for the distance distribution between two uniformly scattered points. The resulting unwieldily expression for the transmission opportunity is simplified to a Skew Normal Distribution using central moment matching. This hypothesis is verified through the Kolmogorov- Smirnov goodness of fit test with an error of less than 2%.

Fast fading is not considered in the above analysis, its affect can be marginalised by diversity measures such as: sensing in multiple TDMA frames (time diversity); using multiple antennas (space diversity); transmitting (coding) over multiple frames; aggregating channels (wide band transmission) or frequency hopping (hopping pattern must be known).

Chapter 5

On Generalised SINR Bounds: A Steffensen's Inequality Approach

In the previous Chapter, we learned that the integral leading up to the CDF or the PDF of the SINR is mathematically intractable. This shortcoming was addressed by using Gaussian quadratures (Section 4.1-Section 4.5). However, their application depends on the integral form [129] and their accuracy is a function of the number of polynomials. A different approach that removes these dependencies relies on integral inequalities. Although not as accurate as quadratures, integral inequalities establish a bounding region by exploiting the properties of the integrand functions. This region establishes the variation in the actual outcome and can be further used to study system performance.

In general, the CDF (or the PDF) calculation of arithmetically involved random variables requires a solution to an integral of product functions. Integral inequalities decouple the integral of product functions to the integrals of individual functions, by exploiting the convexity, monotonicity etc. of the integrands. Specifically, the SINR is a ratio of random variables (2.1) and its CDF involves the integral calculated over the product of numerator CDF and denominator PDF (2.3). For reader's convenience, the CDF expressions is given below

$$F_{\Upsilon}(\upsilon) = \int_{N_0}^{b} F_{\Theta_p}(\upsilon\theta_{in})\, f_{\Theta_{in}}(\theta_{in})\, d\theta_{in}, \tag{5.1}$$

where, Υ represents SINR, $F_{\Upsilon}(\upsilon)$ is the SINR's CDF [1], Θ_p denote the received power from the primary path, Θ_{in} is the interference plus noise power (Θ_i $+N_0$), $F_{\Theta_p}(.)$ is the CDF of Θ_p, and $f_{\Theta_{in}}(\theta_{in})$ is the PDF of θ_{in}. Generally, the solution of the above integral is unknown for commonly used fading models such as gamma and lognormal distributions. One may be tempted to solve this problem by integral inequalities such as Cauchy-Schwarz-Buniakowsky inequality, *Č*eby*š*ev inequality, Minkowski inequality, and H*ö*lder's inequality etc., due to inherent similarities in the functional form. However, these inequalities express both the individual integrals (numerator CDF $F_{\Theta_p}(\upsilon\theta_{in})$ and the denominator PDF $f_{\Theta_{in}}(\theta_{in})$) over the same integration limits as the original integral(5.1). Since, one of the individual integrals involves a CDF, the end results are often intractable.

Fortunately, Steffensen's inequality provides us with a form in which the integral of one individual function defines the integral limit of the other integral. By careful selection of the individual function, the problem described in the previous paragraph can be averted. In particular, the contributions of this Chapter are as follows.

- We apply Steffensen's inequality to derive generalised bounds for the SINR's CDF by assuming that the fading on the signal path (PBS-PUE) and the interfering path (SBS-PUE) are independent, and the mode[2] of their PDF's

[1] The first and second order statistics of the SINR using negative moments of random variables are provided in [148].

[2] The mode is the defined as the value of a random variable at which its PDF attains a maximum value [68]. In practice, it is equivalent to finding a maximum of a function. Mode is a key property of any probability density function. It is well known for commonly used distribution, such as Lognormal, Gamma, and Gaussian distributions. For the cases in which the mode is not known, one can approximate it using series expansion.

are known.

- We show that if the interfering path's PDF is unimodal (the majority of fading distribution are unimodal [150]), then the possibility of trivial bounds can be avoided.

- We apply these derivations to gamma-gamma fading channels and present previously unknown bounds. Furthermore, the effects of the interfering path's scale and shape parameters on these bounds are investigated.

5.1 Steffensen's Inequality

In its simplest form, the Steffensen's inequality is given as [20, Eqs. (2.1) & (2.2)]

$$\int_{x_1-\lambda}^{x_1} S(x)dx \leq \int_{x_0}^{x_1} S(x)R(x)dx \leq \int_{x_0}^{x_0+\lambda} S(x)dx \tag{5.2}$$

where $\lambda = \int_{x_0}^{x_1} R(x)dx$, $S(x)$ is integrable and monotonically decreasing in (x_0, x_1), and $R(x)$ is measurable such that $0 \leq R(x) \leq 1$ for $x \in (x_0, x_1)$. From the above equation, it can be seen that Steffensen's inequality decouples the integral of the product functions into integrals of the individual functions. The bounds are expressed as the integral of function $S(x)$ calculated over length λ from the end points (limits of the actual integration problem).

Notation

We use the following notation to identify the bounds, $\Omega_b^z(y)$, where $y \in \{L, U\}$ refers to the lower and upper bound respectively. Since this paper investigates multiple lower and upper bounds, we use $z \in \{1, 2, 3, 4\}$ to identify the particular bound. The variable b is the upper integration limit.

The remainder of the Chapter is organised as follows. In Section 5.2 we derive the bounds over the support of the interfering path's PDF. Section 5.3 is dedicated to unimodal distributions. Based on these derivations, the bounds on gamma-gamma fading are given in Section 5.4. The results showing the tightness of the bounds are given in Section 5.5. Section 5.6 outlines the conclusion. The findings of this Chapter will be submitted for review in *IEEE Transactions on Wireless Communications* [147].

5.2 Lower and Upper bounds of CDF, When Θ_{in} has Bounded Support $[N_0, b)$

Applying the Steffensen inequality to (5.1) such that, $x_0 = N_0$, $x_1 = b$, $x = \theta_{in}$, $S(x) = 1 - F_{\Theta_p}(\upsilon\theta_{in})$, $R(x) = \frac{f_{\Theta_{in}}(\theta_{in})}{f^*_{\Theta_{in}}}$, where $f^*_{\Theta_{in}} = \max\{f_{\Theta_{in}}(\theta_{in})\}$. By simple algebraic manipulation, the following bounds on CDF are obtained.

$$\Omega_b^1 : f^*_{\Theta_{in}} \int\limits_{N_0}^{N_0 + \left(f^*_{\Theta_{in}}\right)^{-1}} F_{\Theta_p}(\upsilon\theta_{in})\, d\theta_{in} \leq F_\Upsilon(\upsilon) \leq f^*_{\Theta_{in}} \int\limits_{b - \left(f^*_{\Theta_{in}}\right)^{-1}}^{b} F_{\Theta_p}(\upsilon\theta_{in})\, d\theta_{in} \tag{5.3}$$

5.2.1 Lower and Upper bounds of CDF, When Θ_{in} has Semi-Infinite Support $[N_0, \infty)$

In (5.3), if b approaches ∞, the CDF has following bounds.

$$\Omega_\infty^1 : f^*_{\Theta_{in}} \int\limits_{N_0}^{N_0 + \left(f^*_{\Theta_{in}}\right)^{-1}} F_{\Theta_p}(\upsilon\theta_{in})\, d\theta_{in} \leq F_\Upsilon(\upsilon) \leq f^*_{\Theta_{in}} \lim_{b\to\infty} \int\limits_{b - \left(f^*_{\Theta_{in}}\right)^{-1}}^{b} F_{\Theta_p}(\upsilon\theta_{in})\, d\theta_{in} \tag{5.4}$$

The upper bound in the above equation can be simplified using the identities; $F_{\Theta_p}(\infty) = 1$ and $f^*_{\Theta_{in}} > 0$, which gives

$$F_\Upsilon(\upsilon) \leq 1 \tag{5.5}$$

In the above equation, we note that the upper bound on the CDF is too trivial. To overcome this shortcoming, equation (5.1) is integrated by parts. Denoting [3]

$$C(\theta_{in}) = \int f_{\Theta_{in}}(\theta_{in}) d\theta_{in}, \quad \text{and} \quad D(\upsilon\theta_{in}) = \frac{dF_{\Theta_p}(\upsilon\theta_{in})}{d\theta_{in}}, \tag{5.6}$$

the CDF can be written as

$$F_\Upsilon(\upsilon) = C(b)\, F_{\Theta_p}(\upsilon b) - F_{\Theta_p}(\upsilon N_0)\, C(N_0) - \underline{\int_{N_0}^{b} D(\upsilon\theta_{in})\, C(\theta_{in}) d\theta_{in}} \tag{5.7}$$

Applying Steffensen's principle such that $S(x) = C(b) - C(\theta_{in})$, $R(x) = \frac{D(\upsilon\theta_{in})}{q_c(\upsilon)}$, where $q_c(\upsilon) = \max(D(\upsilon\theta_{in}))$ (for notational convenience we drop υ in $q_c(\upsilon)$) the limits on the underlined term are

$$-q_c \int_{b-\lambda}^{b} C(\theta_{in}) d\theta_{in} \leq - \int_{N_0}^{b} C(\theta_{in})\, D(\upsilon\theta_{in}) d\theta_{in} \leq -q_c \int_{N_0}^{N_0+\lambda} C(\theta_{in}) d\theta_{in} \tag{5.8}$$

where $\lambda_0 = \int_{N_0}^{b} \frac{D(\upsilon\theta_{in})}{q_c} d\theta_{in} = \frac{F_{\Theta_p}(\upsilon b)}{q_c} - \frac{F_{\Theta_p}(\upsilon N_0)}{q_c}$. Combining the above equation with (5.7) gives:

$$\Omega_b^2 : C(b)\, F_{\Theta_p}(b) - F_{\Theta_p}(\upsilon N_0)\, C(N_0) - q_c \int_{b-\lambda_0}^{b} C(\theta_{in}) d\theta_{in} \leq F_\Upsilon(\upsilon) \leq C(b)\, F_{\Theta_p}(\upsilon b)$$
$$-F_{\Theta_p}(\upsilon N_0)\, C(N_0) - q_c \int_{N_0}^{N_0+\lambda_0} C(\theta_{in}) d\theta_{in} \tag{5.9}$$

As b approaches infinity, the above bounds simplifies to

$$\Omega_\infty^2 : F_{\Theta_p}(\upsilon N_0) \leq F_\Upsilon(\upsilon) \leq C(\infty) - F_{\Theta_p}(\upsilon N_0)\, C(N_0) - q_c \int_{N_0}^{N_0+\lambda_0} C(\theta_{in}) d\theta_{in}, \tag{5.10}$$

[3]The indefinite integral of PDF $f_{\Theta_{in}}(\theta_{in})$ may not be equal to the CDF $F_{\Theta_{in}}(\theta_{in})$, e.g., lognormal distribution. The equality condition only hold when $C(\theta_{in}) = 0$.

after applying the following:

$$\lim_{b\to\infty} -q_c \int_{b-\lambda_0}^{b} C\left(\theta_{in}\right) d\theta_{in} = -C(\infty) + C(\infty) F_{\Theta_p}\left(\upsilon N_0\right), \text{ and} \tag{5.11}$$

$$C(\infty) F_{\Theta_p}\left(\upsilon N_0\right) - F_{\Theta_p}\left(\upsilon N_0\right) C\left(N_0\right) = F_{\Theta_p}\left(\upsilon N_0.\right)$$

Following the definition of SINR (4.41), the lower bound in Ω^2_∞ is a fairly trivial bound as it represents SNR.

5.3 CDF bounds- When $f_{\Theta_{in}}(\theta_{in})$ is Unimodal

An alternate to the above that generally leads to a tighter upper bound involves splitting the PDF $f_{\Theta_{in}}(\theta_{in})$ (in (5.1)) into multiple subintervals. Since the majority of fading distributions are unimodal, we choose 2 subintervals separated at the distribution mode. This leads to monotonically increasing and monotonically decreasing profiles of $f_{\Theta_{in}}(\theta_{in})$. In the following, we derive the CDF bounds. The PDF bounds are given in Appendix B.

5.3.1 Lower and Upper bounds of CDF, When Θ_{in} has Bounded Support $[N_0, b)$

We split the integral in (5.1) to sub integrals such

$$F_\Upsilon(\upsilon) = \overbrace{\int_{N_0}^{\theta^*_{in}} F_{\Theta_p}\left(\upsilon\theta_{in}\right) f_{\Theta_{in}}\left(\theta_{in}\right) d\theta_{in}}^{I_1} + \underbrace{\int_{\theta^*_{in}}^{b} F_{\Theta_p}\left(\upsilon\theta_{in}\right) f_{\Theta_{in}}\left(\theta_{in}\right) d\theta_{in}}_{I_2} \tag{5.12}$$

Applying Steffensen inequality such that $R(x) = F_{\Theta_p}\left(\upsilon\theta_{in}\right)$ is same in both I_1 and I_2, and $S(x) = f^*_{\Theta_{in}} - f_{\Theta_{in}}(\theta_{in})$ in I_1 and $S(x) = f_{\Theta_{in}}(\theta_{in})$ in I_2, the following bounds are obtained on I_1 and I_2.

$$F_{\Theta_{in}}\left(N_0 + \lambda_1\right) - F_{\Theta_{in}}\left(N_0\right) \leq I_1 \leq F_{\Theta_{in}}\left(\theta^*_{in}\right) - F_{\Theta_{in}}\left(\theta^*_{in} - \lambda_1\right) \tag{5.13}$$

$$\int_{b-\lambda_2}^{b} f_{\Theta_{in}}\left(\theta_{in}\right) d\theta_{in} \leq I_2 \leq F_{\Theta_{in}}\left(\theta_{in}^* + \lambda_2\right) - F_{\Theta_{in}}\left(\theta_{in}^*\right) \tag{5.14}$$

where, $\lambda_1 = \int\limits_{N_0}^{\theta_{in}^*} F_{\Theta_p}\left(\upsilon\theta_{in}\right) d\theta_{in}$, $\lambda_2 = \int\limits_{\theta_{in}^*}^{b} F_{\Theta_p}\left(\upsilon\theta_{in}\right) d\theta_{in}$. Combining I_1 and I_2 gives

$$\Omega_b^3 : F_{\Theta_{in}}\left(N_0 + \lambda_1\right) - F_{\Theta_{in}}\left(N_0\right) + \int\limits_{b-\lambda_2}^{b} f_{\Theta_{in}}\left(\theta_{in}\right) d\theta_{in} \leq I_2 \leq F_{\Theta_{in}}\left(\theta_{in}^* + \lambda_2\right) - F_{\Theta_{in}}\left(\theta_{in}^* - \lambda_1\right) \tag{5.15}$$

Alternatively, the bounds on I_2 can be obtained from (5.9) by replacing N_0 with θ_{in}^*, and than combining with (5.13). The bound on (5.1) now becomes:

$$\begin{aligned} &\Omega_b^4 : F_{\Theta_{in}}\left(N_0 + \lambda_1\right) - F_{\Theta_{in}}\left(N_0\right) + C\left(b\right) F_{\Theta_p}(b) - F_{\Theta_p}\left(\upsilon\theta_{in}^*\right) C\left(\theta_{in}^*\right) - \\ &q_c \int\limits_{b-\lambda_3}^{b} C\left(\theta_{in}\right) d\theta_{in} \leq I_2 \leq F_{\Theta_{in}}\left(\theta_{in}^*\right) - F_{\Theta_{in}}\left(\theta_{in}^* - \lambda_1\right) + C\left(b\right) F_{\Theta_p}(b) - \\ &F_{\Theta_p}\left(\upsilon\theta_{in}^*\right) C\left(\theta_{in}^*\right) - q_c \int\limits_{\theta_{in}^*}^{\theta_{in}^*+\lambda_3} C\left(\theta_{in}\right) d\theta_{in} \end{aligned} \tag{5.16}$$

where $\lambda_3 = \int\limits_{\theta_{in}^*}^{b} \frac{D(\upsilon\theta_{in})}{q_c} d\theta_{in} = \frac{F_{\Theta_p}(\upsilon b)}{q_c} - \frac{F_{\Theta_p}\left(\upsilon\theta_{in}^*\right)}{q_c}$

5.3.2 Lower and Upper bounds of CDF, When Θ_{in} has Semi-Infinite Support $[N_0, \infty)$

As b approaches infinity in Ω_b^3 (5.15), the bounds reduce to

$$\Omega_\infty^3 : F_{\Theta_{in}}\left(N_0 + \lambda_1\right) - F_{\Theta_{in}}\left(N_0\right) \leq F_\Upsilon(\upsilon) \leq 1 - F_{\Theta_{in}}\left(\theta_{in}^* - \lambda_1\right) \tag{5.17}$$

This is because for $\upsilon > 0$, the factor λ_2 will approach ∞ (since $F_{\Theta_p}\left(\upsilon\theta_{in}\right)$ is an increasing function of θ_{in}) and the integral in the lower bound of I_2 approaches 0.

$$\lim_{\{b,\lambda_2\}\to\infty} \int_{b-\lambda_2}^{b} f_{\Theta_{in}}\left(\theta_{in}\right) d\theta_{in} = 0 \tag{5.18}$$

Similarly, applying the limit Ω_b^4 (5.16) and using the result in (5.11) gives:

$$\Omega_\infty^4 : F_{\Theta_{in}}(N_0+\lambda_1) - F_{\Theta_{in}}(N_0) - F_{\Theta_p}(\upsilon\theta_{in}^*)\,C(\theta_{in}^*) + C(\infty)F_{\Theta_p}(\upsilon\theta_{in}^*) \leq F_\Upsilon(\upsilon)$$
$$\leq F_{\Theta_{in}}(\theta_{in}^*) - F_{\Theta_{in}}(\theta_{in}^*-\lambda_1) + C(\infty) - F_{\Theta_p}(\upsilon\theta_{in}^*)\,C(\theta_{in}^*) - q_c \int\limits_{\theta_{in}^*}^{\theta_{in}^*+\lambda_3} C(\theta_{in})d\theta_{in} \tag{5.19}$$

5.4 Gamma-Gamma fading

In this section, we derive SINR's CDF bound when the signal powers on both the primary and the interfering paths are gamma distributed i.e., gamma-gamma fading. The gamma distribution is a Pearson-III type distribution, often used in modelling composite fading channels [131][143] and is given by

$$f_{\Theta_x}(\theta_x; m_x, \beta_x) = \theta_x^{m_x-1}\frac{e^{-\theta_x/\beta_x}}{\beta^{m_x}\,\Gamma(m_x)} \text{ for } \theta_x \geq 0 \tag{5.20}$$

$$F_{\Theta_x}(\theta_x; m_x, \beta_x) = \frac{\gamma\left(m_x, \frac{\theta_x}{\beta_x}\right)}{\Gamma(m_x)} \tag{5.21}$$

where $x \in \{i, p\}$, i represents the interference path and p represents the primary path, m_x is the shape parameters and β_x is the scale parameter, $\gamma(m_x, y)$ and $\Gamma(m_x)$ are lower incomplete and complete gamma functions respectively [129]. Both functions are a special form of the generalised incomplete gamma function and are defined in [151]

$$\Gamma(m_x, y_0, y_1) = \int_{y_0}^{y_1} t^{m_x-1}\,e^{-t}\,\mathrm{d}t \tag{5.22}$$

$$\gamma(m_x, y_1) = \Gamma(m_x, 0, y_1), \quad \Gamma(m_x, y_0) = \Gamma(m_x, y_0, \infty), \quad \Gamma(m_x) = \Gamma(m_x, 0, \infty)$$

The SINR's PDF can be calculated by differentiating (5.1) with respect to υ i.e.,

$$f_\Upsilon(\upsilon) = \int\limits_{N_0}^{b} \frac{dF_{\Theta_p}(\upsilon\theta_{in})}{d\upsilon} f_{\Theta_{in}}(\theta_{in})\,d\theta_{in} \tag{5.23}$$

Substituting (5.20) in (B.1) and subsequently applying integral identity in [149, Eq. (3.383.4)], the SINR's PDF becomes[4]

$$\begin{aligned} f_{\Upsilon}(\upsilon) =& \frac{\upsilon^{m_p-1} e^{\frac{N_0}{m_i}}}{\beta_p^{m_p}\Gamma(m_p)\beta_i^{m_i}} \left(\frac{\beta_p+\beta_i\upsilon}{\beta_p\beta_i}\right)^{-\frac{m_p+m_i+1}{2}} N_0^{\frac{m_p+m_i-1}{2}} e^{\frac{(\beta_p+\beta_i\upsilon)N_0}{2\beta_p\beta_i}} \\ & W_{\frac{m_p-m_i+1}{2},-\frac{m_p+m_i}{2}}\left(\frac{(\beta_p+\beta_i\upsilon)\,N_0}{\beta_p\beta_i}\right) \end{aligned} \tag{5.24}$$

where, $W_{(.,.)}(.)$ is Whittaker function [149]. The gamma-gamma SINR's CDF can be obtained by integrating the above expression, however, to the authors' knowledge the integral is not known except for some special case $m_p = 1$ [140, Eq. (1.13.2.1)]. In what follows we apply the bounds of the previous section directly to the CDF of gamma-gamma SINR. The mode and the maximum value of the gamma distribution is given in [150].

$$\theta_{in}^* = N_0 + (m_i-1)\beta_i;\ f_{\theta_{in}}^* = (m_i-1)^{m_i-1}\beta_i\frac{e^{-(m_i-1)}}{\Gamma(m_i)},\quad m_i \geq 1 \tag{5.25}$$

Applying (5.4), the bounds Ω_∞^1 are

$$\frac{f_{\theta_{in}}^{*-1}\gamma\left(m_p,\frac{\left(\upsilon f_{\theta_{in}}^{*-1}+\upsilon N_0\right)}{\beta_p}\right)+N_0\Gamma\left(m_p,\frac{N_0\upsilon}{\beta_p},\frac{\left(\upsilon f_{\theta_{in}}^{*-1}+\upsilon N_0\right)}{\beta_p}\right)}{\Gamma(m_p)} - \frac{\beta_p\Gamma\left(1+m_p,\frac{N_0\upsilon}{\beta_p},\frac{\left(\upsilon f_{\theta_{in}}^{*-1}+\upsilon N_0\right)}{\beta_p}\right)}{\upsilon\Gamma(m_p)} \leq F_{\Upsilon}(\upsilon) \leq 1 \tag{5.26}$$

Similarly, the bound Ω_∞^2 can be calculated by using the following equations,

$$q_c = \frac{\upsilon e^{-(m_p-1)}(m_p-1)^{m_p-1}}{\beta_p\Gamma(m_p)},\quad \lambda_0 = \frac{\beta_p\Gamma(m_p)(1-\gamma(m_p,N_0\upsilon/\beta_p))}{\upsilon e^{-(m_p-1)}(m_p-1)^{m_p-1}} \tag{5.27}$$

$$\begin{aligned} \Omega_\infty^2 : \frac{\gamma(m_p,\frac{\upsilon N_0}{\beta_p})}{\Gamma(m_p)} \leq F_{\Upsilon}(\upsilon) \leq & \frac{(1-\gamma(m_p,N_0\upsilon/\beta_p))\gamma\left(m_i,\frac{\beta_p\Gamma(m_p)(1-\gamma(m_p,N_0\upsilon/\beta_p))}{\upsilon\beta_i e^{-(m_p-1)}(m_p-1)^{m_p-1}}\right)}{\Gamma\left(m_i\right)} - \\ & \frac{\upsilon e^{-(m_p-1)}(m_p-1)^{m_p-1}\beta_i\gamma\left(1+m_i,\frac{\beta_p\Gamma(m_p)(1-\gamma(m_p,N_0\upsilon/\beta_p))}{\upsilon\beta_i e^{-(m_p-1)}(m_p-1)^{m_p-1}}\right)}{\beta_p\Gamma(m_p)\Gamma\left(m_i\right)} \end{aligned} \tag{5.28}$$

[4]The distribution in (5.24) can also be calculated using Jacobian transformation ([11] see Appendix) or Mellin Transformation [152].

The lower bound in (5.26) and upper bound in (5.28) can be combined to calculate the complete bound on the CDF of SINR.

5.4.1 Unimodal

It is well known that gamma distribution is unimodal [150] for $m_i > 1$. Since the mode of the gamma distribution is known, the bounds are given as follows.

$$\Omega_\infty^3 : \frac{1}{\Gamma(m_i)}\gamma\left(m_i, \frac{\theta_{in}^*\gamma\left(m_p,\frac{\upsilon\theta_{in}^*}{\beta_p}\right)-N_0\gamma\left(m_p,\frac{\upsilon N_0}{\beta_p}\right)}{\beta_i\Gamma(m_p)} - \frac{\beta_p\Gamma\left(1+m_p,\frac{\upsilon N_0}{\beta_p},\frac{\upsilon\theta_{in}^*}{\beta_p}\right)}{\upsilon\beta_i\Gamma(m_p)}\right) \leq F_\Upsilon(\upsilon) \leq$$
$$1 - \frac{1}{\Gamma(m_i)}\gamma\left(m_i, \theta_{in}^* - N_0 - \frac{\theta_{in}^*\gamma\left(m_p,\frac{\upsilon\theta_{in}^*}{\beta_p}\right)+N_0\gamma\left(m_p,\frac{\upsilon N_0}{\beta_p}\right)}{\beta_i\Gamma(m_p)} + \frac{\beta_p\Gamma\left(1+m_p,\frac{\upsilon N_0}{\beta_p},\frac{\upsilon\theta_{in}^*}{\beta_p}\right)}{\upsilon\beta_i\Gamma(m_p)}\right) \tag{5.29}$$

$$\Omega_\infty^4 : +\frac{1}{\Gamma(m_i)}\gamma\left(m_i, \frac{\theta_{in}^*\gamma\left(m_p,\frac{\upsilon\theta_{in}^*}{\beta_p}\right)-N_0\gamma\left(m_p,\frac{\upsilon N_0}{\beta_p}\right)}{\beta_i\Gamma(m_p)} - \frac{\beta_p\Gamma\left(1+m_p,\frac{\upsilon N_0}{\beta_p},\frac{\upsilon\theta_{in}^*}{\beta_p}\right)}{\upsilon\beta_i\Gamma(m_p)}\right) +$$
$$\frac{\gamma\left(m_p,\frac{\upsilon\theta_{in}^*}{\beta_p}\right)\left(1-\frac{\gamma(m_i,m_i-1)}{\Gamma(m_i)}\right)}{\Gamma(m_p)} \leq F_\Upsilon(\upsilon) \leq \frac{\gamma(m_i,m_i-1)}{\Gamma(m_i)}\left(1 - \frac{\gamma\left(m_p,\frac{\upsilon\theta_{in}^*}{\beta_p}\right)}{\Gamma(m_p)}\right) -$$
$$\frac{1}{\Gamma(m_i)}\gamma\left(m_i, \theta_{in}^* - N_0 - \frac{\theta_{in}^*\gamma\left(m_p,\frac{\upsilon\theta_{in}^*}{\beta_p}\right)+N_0\gamma\left(m_p,\frac{\upsilon N_0}{\beta_p}\right)}{\beta_i\Gamma(m_p)} \frac{\beta_p\Gamma\left(1+m_p,\frac{\upsilon N_0}{\beta_p},\frac{\upsilon\theta_{in}^*}{\beta_p}\right)}{\upsilon\beta_i\Gamma(m_p)}\right) -$$
$$\frac{ve^{-(m_p-1)}(m_p-1)^{m_p-1}}{\beta_p\Gamma(m_p)\Gamma(m_i)}\left(\lambda_3\,\gamma\left(m_i, m_i-1+\frac{\lambda_3}{\beta_i}\right) - \beta_i\Gamma\left(m_i+1, m_i-1, m_i-1+\frac{\lambda_3}{\beta_i}\right)\right.$$
$$\left. + (N_0-\theta_{in}^*)\Gamma\left(m_i, m_i-1, m_i-1+\frac{\lambda_3}{\beta_i}\right)\right) \tag{5.30}$$

where, $\lambda_3 = \frac{\beta_p\Gamma(m_p)}{ve^{-(m_p-1)}(m_p-1)^{m_p-1}}\left(1 - \frac{\gamma\left(m_p,\upsilon\theta_{in}^*/\beta_p\right)}{\Gamma(m_p)}\right)$.

5.5 Numerical Results

In this section we present some numerical results using the bounds derived in the previous Sections. The actual CDF curves in these examples are verified by Monte Carlo simulation and numerical integration of (5.1) using Gaussian quadratures [129]. For brevity only Monte Carlo results are shown. Without loss of generality,

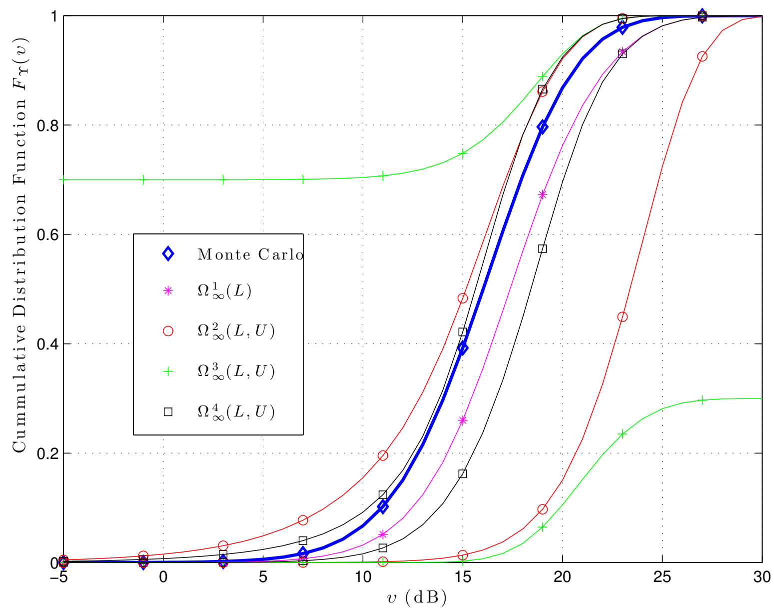

Figure 5.1: Bounds in symmetrical fading conditions $\beta_i = 2$, $\beta_p = 100$, $m_p = m_i = 2.5$, $N_0 = 1$.

we can write $\Upsilon = \frac{\frac{\Theta_p}{N_0}}{\frac{\Theta_i}{N_0}+1}$, in which case the scale parameters, β_i and β_p are normalised by N_0.

Fig. 5.1 plots the CDF bounds under symmetrical fading conditions i.e., when the shape parameters of fading on the primary path and interfering path are equal $m_p = m_i = 2.5$ (corresponding to Rician fading with a $K_p = K_i = 3.4365$ [153]). In this scenario $E[\Theta_i] = 5$ and $E[\Theta_p] = 250$, thus representing a weak interference channel. In general, the lower bounds $\Omega^1_\infty(L)$ and $\Omega^4_\infty(L)$ are strongest at small CDF values, whereas for the CDF values greater than 0.1 the upper bounds are strongest. The best lower bound is $\Omega^1_\infty(L)$, though its upper bound $\Omega^1_\infty(U)$ is trivial.

Considering the upper bounds, at these signal strengths, $\Omega^4_\infty(U)$ provides tightest upper bound ($\Omega^2_\infty(U)$, $\Omega^3_\infty(U)$ which is only matched by $\Omega^4_\infty(U)$ at large (0.98) CDF values). This can be explained as follows. At small to medium v values, λ_1 will

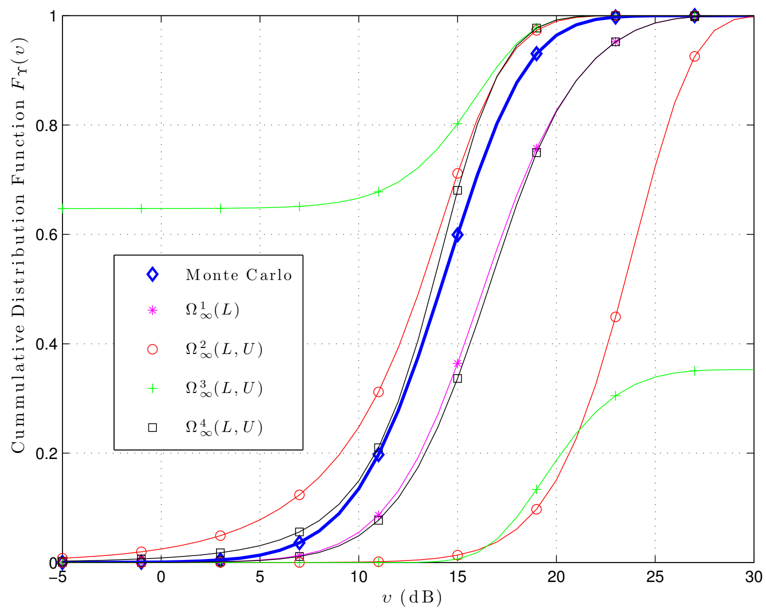

Figure 5.2: Bounds in asymmetrical fading conditions $\beta_i = 2$, $\beta_p = 100$, $m_p = 2.5$, $m_i = 4$, $N_0 = 1$.

be insignificant (as the channel on the primary path is strong). Although $\lambda_0 > \lambda_3$, $C(\theta_{in})$ is an increasing function and the integral $\int_{\theta^*_{in}}^{\theta^*_{in}+\lambda_3} C(\theta_{in})$ in $\Omega^4_\infty(U)$ yields a larger area compared to $\int_{N_0}^{N_0+\lambda_0} C(\theta_{in})$ in $\Omega^2_\infty(U)$, and thus a tighter bound. However, at large υ values, λ_3 approaches 0 and the effect of $\int_{N_0}^{N_0+\lambda_0} C(\theta_{in})$ is comparable to that of $F_{\Theta_{in}}(\theta^*_{in} - \lambda_1)$. This behaviour is also obvious from the $\Omega^3_\infty(U)$ (which is a subset of $\Omega^4_\infty(U)$). The comparable behaviour doesn't hold if the interfering channel is too weak, where $\Omega^4_\infty(U)$ crosses $\Omega^2_\infty(U)$. at large values of SINR. However, the difference between the two is very small.

Fig. 5.2 plots the CDF bounds in asymmetrical fading conditions i.e., $m_p = 2.5$, $m_i = 4$ (corresponding to Rician K factor $K_p = 3.4365$, $K_i = 6.5$). The profile of the curves are fairly similar to the previous figure. However, it is interesting to note that the difference between $\Omega^1_\infty(L)$ and $\Omega^4_\infty(L)$ is decreased to an extent they are almost equal. The change in Ω_∞^3 is insignificant. Unlike the upper bounds there is no comparable correspondence between the expressions for $\Omega_\infty^1(L)$ and $\Omega_\infty^4(L)$, however, the variation is established by considering the impact of m_i on their individual behaviour. The decrease in $\Omega_\infty^1(L)$ value can be understood by the fact that maximum of the interfering PDF $f_{\theta_{in}}^*$ (5.25) is a monotonically decreasing function of m_i ($m_i > 1$). Although the integration limit in (5.4) increases with m_i($N_0 + 1/f_{\theta_{in}}^*$), the multiplication of $f_{\theta_{in}}^*$ with this integral compensates this increase. The increase in $\Omega_\infty^4(L)$ can be visualized by substituting $F_{\Theta_{in}}(\theta_{in}) = C(\theta_{in})$ in (5.19)

$$\begin{aligned}\Omega_\infty^4(L) &= \overbrace{F_{\Theta_{in}}\left(N_0+\lambda_1\right)}^{T_1=\Omega_\infty^3(L)} + \overbrace{F_{\Theta_p}\left(\upsilon\theta_{in}^*\right)\left(1-F_{\Theta_{in}}(\theta_{in}^*)\right)}^{T_2} \\ &= \tfrac{1}{\Gamma(m_i)}\gamma\left(m_i, \int\limits_{N_0}^{N_0+(m_i-1)\beta_i} \tfrac{F_{\Theta_p}(\upsilon\theta_{in})d\theta_{in}}{\beta_i}\right) + F_{\Theta_p}\left(\upsilon(N_0+(m_i-1)\beta_i)\right)\left(1-\tfrac{\gamma(m_i,m_i-1)}{\Gamma(m_i)}\right)\end{aligned} \tag{5.31}$$

For a given primary path parameters and β_i, it is obvious that T_1 is increasing function of m_i, whereas T_2 represents a trade off at large values of m_i (as $\gamma(m, m-1)$ is an increasing function of m). In this scenario, since β_i has not changed and m_i is considerably small, $\Omega_\infty^4(L)$ increases. This is also indicated by $T_1 = \Omega_\infty^3$ in Fig. 5.2 and Fig. 5.3. In Fig. 5.3, the bounds $\Omega_\infty^4(L)$ and $\Omega_\infty^1(L)$ cross over validating the above hypothesis.

The bounds $\Omega_\infty^3(L,U)$ and $\Omega_\infty^2(L)$ are the worst bounds in all scenarios. This is because, contrary to other bounds, $\Omega_\infty^3(L,U)$ variation is only determined by the area spanned by $F_{\Theta_p}(\upsilon\theta_{in})$ from 0 to θ_{in}^*, whereas the bound $\Omega_\infty^2(L)$ completely ignores the interferer.

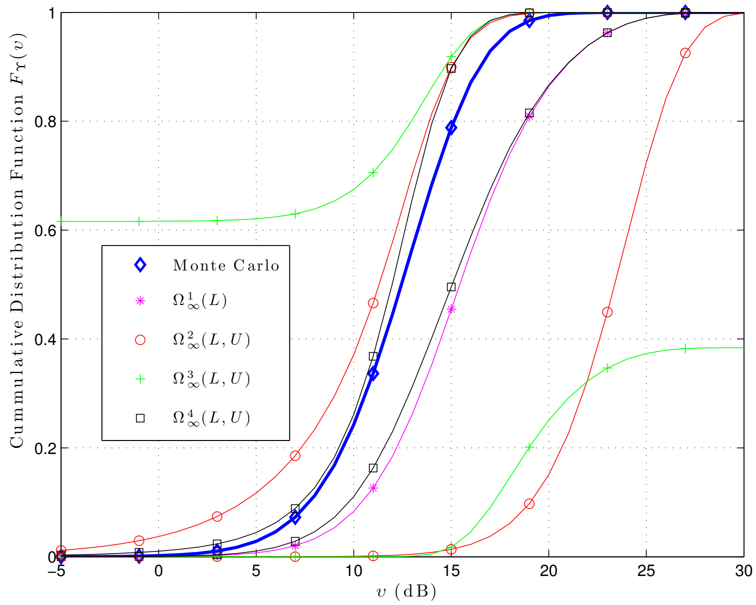

Figure 5.3: Bounds in asymmetrical fading conditions- Impact of Interfering path's shape parameter, $\beta_i = 2$, $\beta_p = 100$, $m_p = 2.5$, $m_i = 6$, $N_0 = 1$.

5.6 Summary

In this Chapter, assuming the knowledge of the mode of the primary and interfering PDFs we have presented 4 generalised bounds on the SINR's CDF using Steffensen's inequality. Specifically, 2 bounds are obtained by applying Steffensen's inequality directly, while the remaining 2 bounds are obtained by segregating the unimodal PDF. The bounds derived in this paper are not only applicable to SINR but they also lend themselves to the calculation of other product/ratio distribution. In the case of gamma-gamma fading, we found that these bounds are sensitive to the shape parameters of the interfering path's PDF. The lower bounds at small SINR values are tighter than their corresponding upper bounds, however, at medium-large SINR values the upper bounds are fairly accurate. Exploiting the unimodal property of the interfering PDF results in a tighter upper bound, though its lower bound counterpart is only suitable for large values of m_i ($m_i > 5$). $\Omega^1_\infty(L)$ and $\Omega^4_\infty(U)$ are the best lower and upper bound on SINR respectively for practical values of m_i. Importantly all the bounds obtained in this paper honor the fundamental probability axioms.

Chapter 6

Conclusion and Further Research

In this thesis, we focused on two spectrum sharing techniques for cognitive radio networks; namely interweave access and underlay access. In the interweave approach, the widely acknowledged spectrum pooling model was adopted and the secondary user QoS parameters were derived. These parameters included, forced termination probability, blocking probability and throughput. In the underlay approach, a sensing and access architecture was proposed. The scheme is suitable for femtocell deployment in the downlink spectrum of cellular networks. The femto - macro coexistence was analyzed using SINR as a performance metric. The mathematical intractability of deriving the victim receiver's SINR probability distribution in a fading channel environment was addressed using Gaussian quadratures and Steffensen's inequality.

Chapter 3, used a continuous time Markov chain model to calculate the QoS of a secondary network operating in both a single channel and a multichannel primary network. The Montecarlo simulations vindicate the theoretical results which showed that for a single channel the throughput can be increased by employing fixed connection lengths (slot times) rather than exponentially distributed connection lengths.

In a multichannel primary network it is possible to avoid forced termination by using spectrum handoff, where active secondary users can switch channels upon the arrival of a primary connection. Additional connection continuity can be assured by incorporating reserved channels. However as the number of reserved channels, r, increases, the tradeoff gain (the ratio of the reduction in forced termination to the increase in blocking probability) reduces rapidly. In general, $r = 0$ gives the best compromise. Two groups of secondary users with different traffic statistics was also considered. It was shown that the airtime fairness between the groups was governed by the difference between their average connection length. Limiting the active connections from the dominant user group can result in fairness, however, it is not recommended for large connection lengths.

Chapter 4 considered the underlay problem, which allows concurrent transmission in both the primary (macrocell) and secondary (femtocell) network. Laboratory measurements indicated that secondary operation in the downlink spectrum is less likely to cause interference to the primary network. Therefore, a TDD secondary network operating in downlink spectrum was considered. Transmissions in the secondary network are inhibited if the primary user is detected in the uplink. The outage probability of both the primary and secondary networks were derived. It was shown that correlation between the sensing and interfering paths reduces the additional primary outage by a factor of 2, emphasising the benefit of co-located sensing and access nodes. Sensing from the secondary base station and transmitting from the secondary terminal is therefore not recommended; each should sense prior to its transmission. Although, sensing is necessary for the existence of multiple femtocells within a macrocell, a conservative sensing threshold can debilitate the effectiveness of the femtocell transmissions. On average, the sensing can be relaxed in the case of a single femtocell opperating in a large Macro cell. For WLAN like transmit powers, the results indicate that this scheme is applicable to applications in which the intended femtocell range is less than 50m and this reduces further in close proximity of the macrocell base station.

The equations for SINR distribution derived in the previous Chapter require numerical solutions. In Chapter 5, we use bounding technique to avoid the numerical solutions. A Steffensen's inequality approach is devised to calculate the generalized bound on SINR's CDF. These bounds are also applicable to various open problems in wireless communication theory. It has been shown that the upper bounds can be significantly improved by applying Steffensen's inequality separately on the increasing and the decreasing profile of the interfering path's PDF. A similar procedure removes the triviality on the lower bounds. For the gamma-gamma fading scenario, the bounds are more sensitive to the shape of interfering path's PDF. The results show that the upper bounds are more accurate than their corresponding lower bounds. The accuracy of the upper bounds is between $1\% - 15\%$ for medium to high SINR values.

6.1 Future Work

Interweave access

In this thesis, the QoS parameters were calculated under a fixed bandwidth requirement using Markovian assumptions. Various applications, such as Internet browsing and video chat also exhibit non-Markovian behaviour due to self similarity.

- In future work, it is possible to analyze the impact of self similarity on the QoS parameters.

- We can extend the results to include many PU groups and SU groups with variable bandwidth requirements. In these scenarios it will be interesting to investigate the optimal packing order.

Underlay access

- For an underlay system, the results can be easily extended to study the cell-wide FC user performance, for which the majority of the derivations are already given in this thesis. Fast fading can also be incorporated into the analysis. This is still an open research problem.

- Since it is expected that multiple FCs will exist in a macrocell coverage area, the modelling of aggregate interference distribution in cross-tier and inner-tier will be a key research area. The cooperation among FCs and adaptive sensing threshold policies can also be considered to improve FC effectiveness.

Appendix A

Global balance equations

This Appendix presents the global balance equations for state transition diagrams in Figs. 3.10(a)-(e).

- **Fig. 3.10(a):** $i + j + Nk \leq (K-1)N$

$$\begin{aligned}&\lambda_s^A P_{\phi_r}(i-1,j,k) + (i+1)\mu_{se}^A P_{\phi_r}(i+1,j,k) + \lambda_s^B P_{\phi_r}(i,j-1,k) + \\ &(j+1)\mu_{se}^B P_{\phi}(i,j+1,k) + \lambda_p P_{\phi_r}(i,j,k-1) + (k+1)\mu_p P_{\phi_r}(i,j,k+1) = \\ &\left(\lambda_s^A + i\mu_{se}^A + \lambda_s^B + j\mu_{se}^B + k\mu_p + \lambda_P\right) P_{\phi_r}(i,j,k)\end{aligned} \tag{A.1}$$

- **Fig. 3.10(b):** $(K-1)N < i + j + Nk < NK - r$

$$\begin{aligned}&\lambda_s^A P_{\phi_r}(i-1,j,k) + (i+1)\mu_{se}^A P_{\phi_r}(i+1,j,k) + \lambda_s^B P_{\phi_r}(i,j-1,k) + \\ &(j+1)\mu_{se}^B P_{\phi_r}(i,j+1,k) + \lambda_P P_{\phi_R}(i,j,k-1) = \\ &\left(\lambda_s^A + i\mu_{se}^A + \lambda_s^B + j\mu_{se}^B + k\mu_P + \sum_{l=0}^{N}\sum_{m=0}^{N} \gamma_{(i-l,j-m,k+1)}^{(i,j,k)} \delta_{fr}\right) P_{\phi_r}(i,j,k)\end{aligned} \tag{A.2}$$

- **Fig.3.10(c):** $i + j + Nk = NK - r$

$$\begin{aligned}&\lambda_s^A P_{\phi_r}(i-1,j,k) + (i+1)\mu_{se}^A P_{\phi_r}(i+1,j,k) + \lambda_s^B P_{\phi_r}(i,j-1,k) + \\ &(j+1)\mu_{se}^B P_{\phi_r}(i,j+1,k) + (k+1)\mu_p P_{\phi_r}(i,j,k+1) + \lambda_p P_{\phi_r}(i,j,k-1) = \\ &\left(i\mu_{se}^A + j\mu_{se}^B + k\mu_p + \sum_{l=0}^{N}\sum_{m=0}^{N} \gamma_{(i-l,j-m,k+1)}^{(i,j,k)} \delta_{fr}\right) P_{\phi_r}(i,j,k)\end{aligned} \tag{A.3}$$

- **Fig. 3.10(d):** $NK - r \leq i + j + Nk < NK$

$$\begin{aligned}&(i+1)\mu_{se}^A P_{\phi_r}(i+1,j,k) + (j+1)\mu_{se}^B P_{\phi_r}(i,j+1,k) + \lambda_p P_{\phi_r}(i,j,k-1) = \\ &\left(i\mu_{se}^A + j\mu_{se}^B + k\mu_p + \sum_{l=0}^{N}\sum_{m=0}^{N} \gamma_{(i-l,j-m,k+1)}^{(i,j,k)} \delta_{fr}\right) P_{\phi_r}(i,j,k)\end{aligned} \tag{A.4}$$

- **Fig. 3.10(e):** $i + j + Nk = NK$

$$
\begin{aligned}
&(i+1)\mu_{se}^{A} P_{\phi_r}(i+1, j, k) + (j+1)\mu_{se}^{B} P_{\phi_r}(i, j+1, k) + \lambda_p P_{\phi_r}(i, j, k-1) + \\
&\sum_{l=0}^{N} \sum_{m=0}^{N} \gamma_{(i,j,k)}^{(i+l,j+m,k-1)} P_{\phi_r}(i+l, j+m, k-1)\ \delta_f = \\
&\left(i\mu_{se}^{A} + j\mu_{se}^{B} + k\mu_p + \sum_{l=0}^{N} \sum_{m=0}^{N} \gamma_{(i-l,j-m,k+1)}^{(i,j,k)} \delta_{fr} \right) P_{\phi_r}(i, j, k)
\end{aligned}
\tag{A.5}
$$

Appendix B

Bounds of $f_\Upsilon(\upsilon)$

Differentiating the equation (5.1) with respect of υ, the PDF problem of SINR is given as

$$f_\Upsilon(\upsilon) = \int_{N_0}^{b} \frac{dF_{\Theta_p}(\upsilon\theta_{in})}{d\upsilon} f_{\Theta_{in}}(\theta_{in})\, d\theta_{in} \tag{B.1}$$

Similar to Section 5.4, we split the integral in two subintegrals as in (5.12).

$$f_\Upsilon(\upsilon) = \overbrace{\int_{N_0}^{\theta^*_{in}} \frac{dF_{\Theta_p}(\upsilon\theta_{in})}{d\upsilon} f_{\Theta_{in}}(\theta_{in})\, d\theta_{in}}^{I'_1} + \underbrace{\int_{\theta^*_{in}}^{\infty} \frac{dF_{\Theta_p}(\upsilon\theta_{in})}{d\upsilon} f_{\Theta_{in}}(\theta_{in})\, d\theta_{in}}_{I'_2} \tag{B.2}$$

We use the same $S(x)$ and limits as in Section 5.4, this gives $R(x) = \frac{1}{q_p}\frac{dF_{\Theta_p}(\upsilon\theta_{in})}{d\upsilon}$, where, $q_p = \max\{\frac{dF_{\Theta_p}(\upsilon\theta_{in})}{d\upsilon}\}$. The bounds are on I'_1 and I'_2 are

$$q_pF_{\Theta_{in}}(N_0+\lambda_4) - q_pF_{\Theta_{in}}(N_0) \le I_1 \le q_pF_{\Theta_{in}}(\theta^*_{in}) - q_pF_{\Theta_{in}}(\theta^*_{in}-\lambda_4) \tag{B.3}$$

$$0 \le I_2 \le q_pF_{\Theta_{in}}(\theta^*_{in}+\lambda_5) - q_pF_{\Theta_{in}}(\theta^*_{in}) \tag{B.4}$$

where $\lambda_4 = \frac{1}{q_p}\int_{N_0}^{\theta^*_{in}} \frac{dF_{\Theta_p}(\upsilon\theta_{in})}{d\upsilon} d\theta_{in}$ and $\lambda_5 = \frac{1}{q_p}\int_{\theta^*_{in}}^{\infty} \frac{dF_{\Theta_p}(\upsilon\theta_{in})}{d\upsilon} d\theta_{in}$. Summing up I_1 and I_2 leads to (B.5).

$$q_pF_{\Theta_{in}}(N_0+\lambda_4) - q_pF_{\Theta_{in}}(N_0) \le f_\Upsilon(\upsilon) \le q_pF_{\Theta_{in}}(\theta^*_{in}+\lambda_5) - q_pF_{\Theta_{in}}(\theta^*_{in}-\lambda_4) \tag{B.5}$$

It is important to note that for any given υ the above integrals and expressions are often known. From (B.5), the relaxed upper bound is:

$$f_{\Upsilon}(\upsilon) \leq q_p \tag{B.6}$$

Bibliography

[1] United States Frequency Allocations, [Online] Available: http://www.ntia.doc.gov/osmhome/allochrt.pdf

[2] Federal Communications Commission (FCC), "Facilitating Opportunities for Flexible, Efficient, and Reliable Spectrum Use Employing Cognitive Radio Technologies," ET Docket No. 03-108, Mar. 2005.

[3] Cognitive Radio Technology, [Online] Available: http://www.ofcom.org.uk/research/technology/overview/emer_tech/cograd/cograd_main.pdf

[4] J. Mitola III, *Cognitive radio: An Integrated Agent Architecture for Software Defined Radio*, Ph.D. Thesis, KTH Royal Institute of Technology, Sweden, May 2000.

[5] S. Haykin, "Cognitive radio: Brain-empowered Wireless Communications," *IEEE J. Select. Areas Commun.*, vol. 23, pp. 201-220, Feb. 2005.

[6] I. F. Akyildiz, W.-Y. Lee, M. C. Vuran and S. Mohanty, "NeXt Generation/Dynamic Spectrum Access/Cognitive Radio Wireless Networks: A Survey," *Computer Networks*, vol. 50, pp. 2127-2159, 2006.

[7] IEEE Standard P1901.1/D01 (v 0.16), Standard Definitions and Concepts for Spectrum Management and Advanced Radio System Technologies (DRAFT), Jun. 2, 2006.

[8] A. Goldsmith, S. A. Jafar, I. Maric, and S. Srinivasa, "Breaking Spectrum Gridlock With Cognitive Radios: An Information Theoretic Perspective," *Proceedings of the IEEE*, vol. 97, no. 5, pp. 894-914, May 2009.

[9] Y. Han, A. Pandharipande and S. H. Ting, "Cooperative Decode-and-Forward Relaying for Secondary Spectrum Access," *IEEE Trans. Wireless Commun.*, vol. 8, no. 10, pp. 4945-4950, Oct. 2009.

[10] C.-X. Wang, X. Hong, H.-H. Chen, and J. Thompson, "On Capacity of Cognitive Radio Networks with Average Interference Power Constraints," *IEEE Trans. Wireless Commun.*, vol. 8, no. 4, pp. 1620-1625, Apr. 2009.

[11] A. Ghasemi and E. Sousa, "Fundamental Limits of Spectrum Sharing in Fading Environments," *IEEE Trans. on Wireless Commun.*, vol. 6, no. 2, pp. 649-658, 2007.

[12] V. Chandrasekhar, J. Andrews, and A. Gatherer, "Femtocell Networks: A Survey," *IEEE Commun. Mag.*, vol. 46, no. 9, pp. 59-67, Sep. 2008.

[13] D. L.-Perez, A. Valcarce, G. de la Roche, and J. Zhang, "OFDMA Femtocells: A Roadmap on Interference Avoidance," *IEEE Commun. Mag.*, vol. 47, no. 9, pp. 41-48, Jun. 2009.

[14] G. Gur, S. Bayhan, and F. Alagoz, "Cognitive Femtocell Networks: An Overlay Architecture for Localized Dynamic Spectrum Access [Dynamic Spectrum Management]," *IEEE Wireless Commun.*, vol. 17, no. 4, pp. 62-70, Aug. 2010.

[15] "Interference Management in UMTS femtocell," FemtoForum, Dec. 2008.

[16] V. Chandrasekhar, M. Kountouris, and J. G. Andrews, "Uplink Capacity and Interference Avoidance for Two-Tier Femtocell Networks," *IEEE Trans. Wireless Commun.*, vol. 8, no. 7, pp. 3498-3509, July 2010.

[17] Y. Kim, and G. de Veciana, "Understanding the Design Space for Cognitive Networks," in *Proc. IEEE WiOpt, 2010*, pp. 418-423, 2010.

[18] S.-M. Cheng, W. C. Ao, and K.-C. Chen, "Downlink Capacity of Two-Tier Cognitive Femto Networks," in *Proc. IEEE PIMRC 2010*, pp. 1303-1308, Sept. 2010.

[19] G. L. Stüber, *Principles of Mobile Communication.* 2^{nd} ed. Norwell, MA, USA: Kluwer Academic Publishers, 2001.

[20] D. S. Mitrinović, J. E. Pečarić and A. M. Fink, *Classical and New Inequalities in Analysis*, vol. 61, Kluwer Academic Publishers, Dordrecht, Boston and London, pp. 311-331, 1993.

[21] L. Wu, K. Niu, Z. He, W. Xu, and J. Li, "Ergodic Capacity of Dual-Hop Transmissions over Composite Multipath/Shadowing," *IET Electronic Lett.*, vol. 45, no. 1, 2009.

[22] H. A. Suraweera,, P. J. Smith, and M. Shafi, "Capacity Limits and Performance Analysis of Cognitive Radio With Imperfect Channel Knowledge," *IEEE Trans. Veh. Tech.*, vol. 59, no. 4, pp. 1811-1822, May 2010.

[23] T. Weiss and F. Jondral, "Spectrum Pooling: An Innovative Strategy for the Enhancement of Spectrum Efficiency," *IEEE Commun. Mag.*, vol. 42, pp. S8-S14, Mar. 2004.

[24] S. Srinivasa and S. A. Jafar, "Cognitive Radios for Dynamic Spectrum Access-The Throughput Potential of Cognitive Radio, A Theoretical Perspective," *IEEE Commun. Mag.*, vol. 45, no. 5, pp. 73-79, May. 2007.

[25] J. Mehdi, *Stochastic Models in Queueing Theory.* Academic Press, San Diego: CA, 1991.

[26] M. Raspopovic, C. Thompson, and K. Chandra, "Performance Models for Wireless Spectrum Shared by Wideband and Narrowband Sources," in *Proc. IEEE MILCOM*, pp.1-6, Oct. 2005.

[27] M. Raspopovic, and C. Thompson, "Finite Population Model for Performance Evaluation Between Narrowband and Wideband Users in the Shared Radio Spectrum," in*Proc. IEEE DySPAN*, pp. 340-346, Apr. 2007.

[28] Y. Xing, R. Chanddramouli, S. Mangold, and S. Shankar, "Dynamic Spectrum Access in Open Spectrum Wireless Networks," *IEEE J. Sel. Areas Commun.*, vol. 24, pp. 626-636, Mar. 2006.

[29] C.-T. Chou, S. Shankar N, H. Kim, and K. G. Shin, "What and How Much to Gain by Spectrum Agility," *IEEE J. Sel. Areas in Commun.*, vol. 25, no.3, pp. 576-588, Apr. 2007.

[30] F. Capar, I. Martoyo, T. Weiss and F. Jondral, "Comparison of Bandwidth Utilization for Controlled and Uncontrolled Channel Assignment in a Spectrum Spooling System," in *Proc. IEEE VTC Spring*, pp. 1069-1073, May 2002.

[31] P. K. Tang, Y. H. Chew, L. C. Ong, and M. K. Haldar, "Performance of Secondary Radios in Spectrum Sharing with Prioritized Primary Access," in *Proc. IEEE MILCOM 2006*, pp.1-7, 23-25 Oct. 2006.

[32] P. K. Tang, and Y. H. Chew, "On the Modeling and Performance of Three Opportunistic Spectrum Access Schemes," *IEEE Trans. Veh. Tech.*, vol. 59, no. 8, Oct. 2010.

[33] S. Huang, X. Liu, and Z. Ding, "Opportunistic Spectrum Access in Cognitive Radio Networks," in *Proc. IEEE INFOCOM* , pp. 1427-1435, Apr. 2008.

[34] G. Yuan, R. C. Grammenos, Y. Yang, and W. Wang, " Performance Analysis of Selective Opportunistic Spectrum Access With Traffic Prediction," *IEEE Trans. Veh. Tech.*, vol. 59, no. 4, May. 2010.

[35] J. Park et al., "To Buffer or to Switch: Design of Multichannel MAC for OSA Ad Hoc Networks," in *Proc. IEEE DySPAN*, pp. 1-10, 2010.

[36] Y. Song and J. Xie, "Proactive Spectrum Handoff in Cognitive Radio Ad Hoc Networks based on Common Hopping Coordination," in *Proc. IEEE INFOCOMM*, pp. 1-2, 2010.

[37] S.-U Yoon and E. Ekici, "Voluntary Spectrum Handoff: A Novel Approach to Spectrum Management in CRNs," in *Proc. IEEE ICC*, pp. 1-5. 2010.

[38] X. Zhu, L. Shen and T.-S. P. Yum, "Analysis of Cognitive Radio Spectrum Access with Optimal Channel Reservation," *IEEE Commun. Lett.*, vol. 11, pp. 304-306, Apr. 2007.

[39] H. Al-Mahdi, M. A. Kalil, F. Liers, and A. Mitschele-Thiel, "Increasing Spectrum Capacity for Ad Hoc Networks using Cognitive Radios: An Analytical Model," *IEEE Comm. Lett.*, vol. 13, no. 9, Sept. 2009.

[40] W. Ahmed, J. Gao, and M. Faulkner, " Comments on "Analysis of Cognitive Radio Spectrum Access with Optimal Channel Reservation"," *IEEE Trans. Wireless Commun.*, pp. 4488-4491, vol. 8, no. 9, Sept. 2009.

[41] Y. Zhang, "Dynamic Spectrum Access in Cognitive Radio Wireless Networks," in *Proc. IEEE ICC*, pp. 4927-4932, May 2008.

[42] J. M.-Bauset, V. Pla, and D. Pacheco-Param, "Comments on Analysis of Cognitive Radio Spectrum Access with Optimal Channel Reservation," *IEEE Commun. Lett.*, vol. 13, no. 10, Oct. 2009.

[43] S.-S Tzeng, "Call admission Control Policies in Cellular Wireless Networks with Spectrum Renting," *Comp. Commun.*, no. 32, pp. 19051913, 2009.

[44] J. M.-Bauset, et al., "Admission Control and Interference Management in Dynamic Spectrum Access Networks," *EURASIP J. Wireless Commun. and Net.*, Article ID 708029, 2010.

[45] S. M. Kannappa, and M. Saquib, "Performance Analysis of a Cognitive Network with Dynamic Spectrum Assignment to Secondary Users," in *Proc. IEEE ICC*, pp. 1-5, May 2010.

[46] J. Heo, et al., "Mathematical Analysis of Secondary User Traffic in Cognitive Radio System," in *Proc. IEEE VTC-Fall*, pp. 1-5, Sept. 2008.

[47] D. Xue, H. Yu, X. Wang, and H.-Hwa Chen, "Adoption of Cognitive Radio Scheme to Class-based Call Admission Control," in *Proc. IEEE ICC*, pp. 1-5, Jun. 2009.

[48] R. Ramjee, R. Nagarajan and D. Towsley, "On Optimal Call Admission Control in Cellular Networks," in *Proc. IEEE INFOCOMM*, vol. 1, pp. 43-50, 1996.

[49] Y. Zhang, "Spectrum Handoff in Cognitive Radio Networks: Opportunistic and Negotiated Situations," in *Proc. IEEE ICC*, pp. 1-5, 2009.

[50] S. Tang, and B. L. Mark, "Modeling and Analysis of Opportunistic Spectrum Sharing with Unreliable Spectrum Sensing," *IEEE Trans. Wireless Commun.*, vol. 8, no. 4, Apr. 2009.

[51] L.-C. Wang, and C. Anderson, "On the performance of Spectrum handoff for Link Maintenance in Cognitive Radio," in *Proc. IEEE ISWPC*, pp. 670-674. May 2008.

[52] D. Willkomm, J. Gross, and A. Wolisz, “Reliable link Maintenance in Cognitive Radio Systems,” in *Proc. IEEE DySPAN*, pp. 371-378, Nov. 2005.

[53] M. A. Khalil, H. Al-Mahdi, and A. Mitschele-Thiel, “Spectrum Handoff Reduction for Cognitive Radio Adhoc networks,” in *Proc. IEEE ISWCS*, pp. 1036-1040, Sept. 2010.

[54] P. Lin, T. Lin, and C. Wang, “Performance Analysis of a Cross-Layer Handoff Ordering Scheme in Wireless Networks,” *IEEE Trans. Wireless Commun.*, vol. 7, no. 12, Dec. 2009.

[55] J.-M. Chung, C. H. Kim, J.-H. Park, J. Shin and D. Kim, “Optimal Channel Allocation for Cognitive Radios,” *IET Lett.*, vol. 46, no. 11, Mar. 2010.

[56] B. Wang, Z. Ji, and K. J. R. Liu, “Primary-Prioritized Markov Approach for Dynamic Spectrum Access,” in *Proc. IEEE DySPAN*, pp. 507-515, Apr. 2007.

[57] L. Luo, and S. Roy, “Analysis of Dynamic Spectrum Access with Heterogeneous Networks: Benefits of Channel Packing Scheme,” in *Proc. IEEE GLOBECOM*, pp.1-7, Dec. 2009.

[58] Z. Ma, Z. Cao, and W. Chen, “A Fair Opportunistic Spectrum Access (FOSA) Scheme in Distributed Cognitive Radio Networks,” in *Proc. IEEE ICC*, pp. 4054-4058, May 2008.

[59] U. Wiggins, R. Kannan, V. Chakravarthy and A. V. Vasilakos, “Data-Centric Prioritization in a Cognitive Radio Network: A Quality-of-Service Based Design and Integration,” in *IEEE Proc. DySPAN*, pp. 111, Oct. 2008.

[60] C. Gosh, S. Chen, D. P. Agarwal and A. M. Wyglinski, “Priority Based Spectrum Allocation for Cognitive Radio Networks Employing NC-OFDM Transmission,” in *Proc. IEEE MILCOM*, pp. 15, Oct. 2009.

[61] V. K. Tumuluru, P. Wang, and D. Niyato, "Performance Analysis of Cognitive Radio Spectrum Access with Prioritized Traffic," To Appear in *Proc. IEEE ICC 2011.*

[62] W. Ahmed, J. Gao, and M. Faulkner, "Channel Allocation for Fairness in Opportunistic Spectrum Access Networks," in *Proc. IEEE WCNC*, pp. 1-6, 18-21 Apr. 2010.

[63] W. Ahmed, J. Gao, H. Zhou and M. Faulkner, "Throughput and Proportional Fairness in Cognitive Radio Network," in *Proc. ATC*, pp. 248-252, 12-14 Oct. 2009.

[64] Federal Communications Commission (FCC), "Revision of Part 15 of the Commissions Rules Regarding Ultra-Wideband Transmission Systems," ET Docket 98-153, Apr. 2002.

[65] M. Aljuaid, and H. Yanikomeroglu, "Investigating the Gaussian Convergence of the Distribution of the Aggregate Interference Power in Large Wireless Networks," *IEEE Trans. Veh. Tech.*, pp. 4418-4424, Nov.2010.

[66] A. Hasan and J. G. Andrews, "The Guard Zone in Wireless Adhoc Networks," *IEEE Trans. Wireless Commun.*, vol. 6, no. 3, pp. 897-906, Mar. 2007.

[67] X. Hong; C.-X. Wang, and J. Thompson, "Interference Modeling of Cognitive Radio Networks," in *Proc. IEEE VTC-Spring*, pp.1851-1855, May 2008.

[68] A. Papoulis, *Probability, Random Variable, and Stochastic Process,* New York: McGraw Hill, 1984.

[69] A. Ghasemi and E. S. Sousa, "Interference Aggregation in Spectrum-Sensing Cognitive Wireless networks," *IEEE J. of Sel. Topics in Signal Processing*, vol. 2, pp. 41-56, Feb. 2008.

[70] M. Aljuaid, and H. Yanikomeroglu, "Identifying Boundaries of Dominant Regions Dictating Spectrum Sharing Opportunities for Large Secondary Networks," in *Proc. IEEE PIMRC*, pp. 1521-1526, 2010.

[71] A. Rabbachin et al., "Cognitive Network Interference," *IEEE J. Sel. Areas in Commun.*, vol. 29, no. 2, pp. 480-493, Feb. 2011.

[72] G. Samoradnitsky and M. Taqqu, *Stable Non-Gaussian Random Processes.* Chapman and Hall, 1994.

[73] K. W Song, M. Tercero, and J. Zander, "Aggregate Interference in Secondary Access with Interference Protection," *IEEE Commun. Lett.*, vol. 15, no. 6, pp. 629-631, Jun. 2011.

[74] Y. Zhao, D. Raymond, C. da Silva, J. H. Reed, and S. F. Midkiff, "Performance Evaluation of Radio Environment Map-Enabled Cognitive Spectrum Sharing Networks," in *Proc. IEEE MILCOM*, pp. 1-7, Oct. 2007.

[75] M. F. Hanif, M. Shafi, and P. J. Smith, "Performance of Cognitive Radio Systems with Imperfect Radio Environment Map Information," in *Proc. IEEE AusCTW*, pp. 61-66, 2009.

[76] L.-C Wang, and A. Chen, "Effects of Location Awareness on Concurrent Transmissions for Cognitive Ad Hoc Networks Overlaying Infrastructure-Based Systems," *IEEE Trans. Mob. Comp.*, vol. 8, no. 5, May 2009.

[77] Y. Zhao, "Overhead Analysis for Radio Environment Mapenabled Cognitive Radio Networks," in *IEEE Workshop on SDR*, pp. 18-25, Sept. 2006.

[78] M. Vu, N. Devroye, and V. Tarokh, "On the Primary Exclusive Region of Cognitive Networks," *IEEE Trans. Wireless Commun.*, vol. 8, no. 7, Jul. 2009.

[79] R. Menon, R. M. Buehrer, and J. H. Reed, “Outage Probability Based Comparison of Underlay and Overlay Spectrum Sharing Techniques,” in *Proc. IEEE DySPAN*, pp. 101-109, Nov. 2005.

[80] R. Menon, R. M. Buehrer, and J. H. Reed, “Impact of Exclusion Region and Spreading in Spectrum Sharing Adhoc Networks,” in *Proc. IEEE TAPAS*, Aug. 2006

[81] V. Mordachev and S. Loyka, “On Node Density - Outage Probability Tradeoff in Wireless Networks,” *IEEE J. on Sel. Areas in Commun.*, vol. 27, no. 7, pp. 1120-1131, Sept. 2009.

[82] Y. Wen, S. Loyka, and A. Yongacoglu, “The Impact of Fading on the Outage Probability in Cognitive Radio Networks,” in *Proc. VTC-Fall*, pp. 1-5, Sept. 2010.

[83] M. G. Khoshkholgh et al., “Impact of the Secondary Network on the Outage Performance of the Primary Service in Spectrum Sharing,” in *Proc. IEEE ICC*, pp. 1-5, May. 2010

[84] R. Dahama, K. W. Sowerby, and G. B. Rowe, “Outage Probability Estimation for Licensed Systems in the presence of Cognitive Radio Interference,” in *Proc. IEEE VTC*, 2009.

[85] R. Dahama, K. W. Sowerby, and G. B. Rowe, “Adjacent Channel Operation of Portable Unlicensed Devices inside DTV Service Contours,” in *Proc. IEEE WCNC*, Apr. 2010.

[86] A. Bagayoko, P. Tortelier, and I. Fijalkow, “Impact of Shadowing on the Primary Exclusive Region in Cognitive Networks,” in *Proc. Europ. Wireless Conf*, pp. 105-110. 2010.

[87] J.-M. Dricot et al., "Primary Exclusive Region and Optimality of the Link-Level Throughput of Cognitive Terminals," *in Proc. PIMRC Workshops*, 2010.

[88] 3GPP. Evolved Universal Terrestrial Radio Access (E-UTRA); Physical Layer Measurements, Sept. 2009.

[89] Dong-Chan Oh et al., "Cognitive Radio Based Femtocell Resource Allocation," in *Proc. ICTC* , pp. 274 - 279, Nov. 2010.

[90] A. Ghosh, et al. *Fundamentals of LTE*. Prentice Hall Commun. Engg. and Emerg. Tech. Series, 2010.

[91] Y.-Y. Li and E. S. Sousa, "Cognitive Uplink Interference Management in 4G Cellular Femtocells," in *Proc. IEEE PIMRC*. pp. 1-5, Sept. 2010.

[92] Y.-Y. Li et al., "Cognitive Femtocell in 3G network," in *Proc. IEEE PIMRC*. pp.1-5, Sept. 2009.

[93] Z. Bharucha et al., "Dynamic Resource Partitioning for Downlink Femto-to-Macro-Cell Interference Avoidance," *EURASIP J. on Wireless Commun. and Net.*, vol. 2010, Article no. 143413.

[94] J. Perez-Romero, O. Sallent, R. Agusti, and L. Guipponi, "A Novel on-Demand Cognitive Pilot Channel Enabling Dynamic Spectrum Allocation," in *Proc. IEEE DySPAN*, Apr. 2007.

[95] M. Mueck et al., "Smart Femtocell Controller Based Distributed Cognitive Pilot Channel," in *Proc. CROWNCOM*, pp. 1 - 5, Jun. 2009.

[96] J. Jin, and B. Li, "Cooperative Resource Management in Cognitive WiMAX with Femto Cells," in *Proc. INFOCOM*, pp. 1-9, Mar. 2010.

[97] S.-M. Cheng et al. "Efficiency of a Cognitive Radio Link with Opportunistic Interference Mitigation," *To Appear in Trans. on Wireless Commun.*

[98] S.-M. Cheng, W. C. Ao, and C. K.-C. Chen, "Downlink capacity of Two Tier Cognitive Femto Networks," in *Proc. IEEE PIMRC*, pp. 1303- 1308, Sept. 2010.

[99] F. Pantisano, K. Ghaboosi, M. Bennis and M. Latva-Aho, "Interference Avoidance via Resource Scheduling in TDD Underlay Femtocells," in *Proc. IEEE PIMRC*, pp. 175-179, Sep. 2010.

[100] A. Adhikary et al., "Cognitive Femtocells: Breaking the Spatial Reuse Barrier of Cellular Systems," in *Proc. ITA*, pp. 1-10, Mar. 2011.

[101] J. Hansen, and M. Reitzner, "Electromagnetic Wave Propagation and Inequalities for Moments of Chord Lengths," *Advances in Applied Probability*, vol. 36, no. 4, pp. 987-995, 2004.

[102] A. Annamal, and C. Tellambura, "Cauchy-Schwarz Bound on the Generalized Marcum Q-Function with Applications," *Wirel. Commun. Mob. Comput.*, vol. 1, no. 2, pp. 243-253.

[103] J. F. Steffensen, "On Certain Inequalities between Mean Values and their Application to Actuarial Problems," *Skand. Aktuarietidskr.*, pp. 82-97, 1918.

[104] P. R. Mercer, "Extensions of Steffensen's Inequality," *Journal Mathematical Analysis and Applications*, vol. 246 (1), pp. 325-329, 2000.

[105] S.-He Wua, and H. M. Srivastavab, "Some Improvements and Generalizations of Steffensen's Integral Inequality," *Applied Mathematics and Computation*, vol. 192, no. 2, pp. 422-428, Sept. 2007.

[106] P. Cerone, "On Applications of the Integral of Products of Functions and its Bounds," RGMIA: *Journal of Inequalities in Pure and Applied Mathematics*, vol. 6, no. 4, pp. 1-18, 2003.

[107] P. Cerone, "On Some Generalisation Of Steffensen's Inequality and Related Results," *Journal of Inequalities in Pure and Applied Mathematics*, vol. 2, no. 3, Article 28, 2001.

[108] P. Cerone, "Special functions: Approximations and Bounds," *Applicable Analysis and Discrete Mathematics*, vol. 1, no. 1, pp. 72-91, 2007.

[109] K. A. Hamdi, "Capacity of MRC on Correlated Rician Fading Channels," *IEEE Trans. on Commun.*, vol. 56, no. 5, May 2008.

[110] O. Waqar, M. Ghogho, and D. McLernon, "Tight Bounds for Ergodic Capacity of Dual-Hop Fixed-Gain Relay Networks under Rayleigh Fading," *IEEE Commun. Lett.*, vol. 15, no. 4, Apr. 2011.

[111] W. Ahmed, J. Gao, H. Zhou and M. Faulkner, "Goodput and Channel Allocation," in *Proceedings Personal Indoor and Mobile Radio Communications PIMRC*, pp. 476-480, 13-16 Sept. 2009.

[112] W. Ahmed, J. Gao, and M. Faulkner, "Performance Evaluation of a Cognitive Radio Network with Exponential and Truncated Usage Models," in *Proceedings International Conference on Wireless and Pervasive Computing*, pp. 1-5, 11-13 Feb. 2009.

[113] J. Gao, W. Ahmed, J. Yang, and M. Faulkner, "Throughput Comparison in Cognitive Radio Networks," in *Proceedings of Electrical Engineering/Electronics Computer Telecommunications and Information Technology (ECTI-CON)*, pp. 748-751, 19-21 May 2010.

[114] W. Ahmed, M. Faulkner, and J. Gao, "Opportunistic Spectrum Access in Cognitive Radio Network," *Chapter 9 in Foundation of Cognitive Radio Systems*, pp. 189-214, 2012, ISBN 978-953-307-643-0.

[115] W. Li, and Y. Fang, "Performance Evaluation of Wireless Cellular Networks with Mixed Channel Holding Times," *IEEE Trans. Wireless Commun.*, vol. 7, no. 6, pp. 2154-2160, Jun. 2008.

[116] D. Hong and S. Rappaport, "Traffic Model and Performance Analysis for Cellular Mobile Radio Telephone Systems with Prioritized and Nonprioritized Handoff Procedures," *IEEE Trans. Veh. Technol.*, vol. 35, pp. 77-92, Aug. 1986.

[117] H. M. Antia, *Numerical Methods for Scientists and Engineers*, 2$^{\text{nd}}$ ed., Birkhuser Basel, 2002

[118] S. M. Ross, *Introduction to Probability and Statistics for Engineers and Scientists.* 3rd ed. Academic Press, 2004.

[119] W. Ahmed, J. Gao, S. Saleem, and M. Faulkner, "An Access Technique for Secondary Network in Downlink Channels," *Proceedings of IEEE Personal Indoor and Mobile Radio Communication (PIMRC)*, pp. 423-427, Sept. 2011.

[120] W. Ahmed, M. Faulkner, J. Gao, and S. Saleem, "An Access Architecture for Secondary Femtocells in Downlink channels," *To be Submitted in IEEE Transactions on Wireless Communications.*

[121] W. Ahmed, and M. Faulkner, "An Approximate PDF of the Distance Between Uniformly Distributed Points in a Circle," *To be Submitted in Institute of Engineering and Technology Letter.*

[122] Jörg Eberspächer, H.-J Vögel, C. Bettstetter, and C. Hartmann. *GSM: Architecture, Protocols and Services,* 3rd ed. Wiley-Blackwell, 2009.

[123] M. Rahnema, *UMTS Network Planning, Optimization, and Inter-Operation with GSM,* illustrated ed. Wiley, 2007

[124] IEEE P802.11 Wireless LANs, "TGn Channel Models," IEEE 802.11-03/940r4, 2004-05-10.

[125] M. Gudmundson, "Correlation Model for Shadow Fading in Mobile Radio Systems," *Electron. Lett.*, vol. 27, pp. 2145-2146, Nov. 1991.

[126] S. Kotz, N. Balakrishnan, and N. L. Johnson, *Continuous Multivariate Distribution:Models and Applications*, vol. 1, 2^{nd} ed. New York: Wiley, pp. 251-348, 2000.

[127] J. Gai, *A Computational Study of Bivariate Normal probability function*, Master of Sci. Project, Queen's University, Kingston, Dec. 2001. [Online]. Available: www.mast.queensu.ca/ web/Papers/jing-project.ps

[128] Z. Drezner and G. O. Wesolowsky, "On the Computation of the Bivariate Normal Integral," *J. of Stat. Comp. and Sim.*, vol. 35, pp. 101-107, 1990.

[129] Abramowitz, Milton; Stegun, and Irene A., *Handbook of Mathematical Functions with Formulas, Graphs, and Mathematical Tables*, eds. (1972), New York: Dover Publications.

[130] D. Skraparlis, Magnus Sandell, V. K. Sakarellos, A. D. Panagopoulos, and J. D. Kanellopoulos, "On the Effect of Correlation on the Performance of Dual Diversity Receivers in Lognormal Fading," *IEEE Comm. Lett.*, vol. 14, no. 11, Nov. 2010.

[131] S. Atapattu, C. Tellambura, and H. Jiang, "Representation of Composite Fading and Shadowing Distributions by using Mixtures of Gamma Distributions," in *in Proc. of IEEE (WCNC)*, pp. 1-5, Apr. 2010.

[132] N. B. Mehta, J. Wu, A. F. Molisch, and J. Zhang, “Approximating a Sum of Random Variables with a Lognormal,” *IEEE Trans. Wireless Commun.*, vol. 6, pp. 2690-2699, July 2007.

[133] C. Tellambura et al., “Performance Analysis of Wireless Systems from the MGF of the Reciprocal of the Signal-to-Noise Ratio,” *To Appear in IEEE Commun. Lett.*

[134] M. Alamgir, M. Faulkner, P. Conder, and P. Smith, “Modifed Criterion of Hypothesis Testing for Signal Sensing in Cognitive Radio,” in *Proc. CROWNCOMM 2009.*

[135] X. Hong, C.-X. Wang,, and J. Thompson, “Uplink Cell Capacity of Cognitive Radio Networks with Peak Interference Power Constraints,” in *Proc. ICCCAS*, pp. 372 - 377, 2008.

[136] D. Blumenfeld, *Operations Research Calculations Handbook*, 2nd ed., CRC Press, Dec. 2009.

[137] V. Alagar, “The Distribution of the Distance Between Random Points,” *J. of Appl. Prob.*, vol. 13, no. 3, 1976.

[138] A. P. Prudnikov, Yu. A. Brychkov, and O. I. Marichev, *Integral and Series: Special Functions*, vol. 2, Gordon and Breach Science Publisher, 1986.

[139] E. Onur, C. Ersoy, and H. Delic, “Analysis of Target Detection Probability in Randomly Deployed Sensor Networks,” *IEEE Comm. Lett.*, vol. 11, no. 10, Oct. 2007.

[140] A. P. Prudnikov, Yu. A. Brychkov, and O. I. Marichev, *Integral and Series: More Special Functions*, vol. 3, Gordon and Breach Science Publisher, 1986.

[141] I. A. Ibragimov, “On the Composition of Unimodal Distributions,” Theory of Probability and Its Applications 1, 1956 pp. 255-260.

[142] A. Abdi and M. Kaveh, “On the Utility of Gamma PDF in Modelling Shadow fading (Slow Fading),” in *Proc. IEEE VTC*, vol. 3, pp. 2308-2312, May 1999.

[143] S. Al-Ahmadi and H. Yanikomeroglu, “On the Approximation of the Generalized-K Distribution by a Gamma Distribution for Modeling Composite Fading Channels,” *IEEE Trans. Wireless Commun.*, vol. 9, no. 2, pp. 706-713. Feb. 2010.

[144] A. Mosleh, and G. Apostolakis, “Some Properties of Distributions Useful in the Study of Rare Events,” *IEEE Trans. on Reliability, vol. R-31, no. 1, Apr. 1982*

[145] A. Azzalini, “A Class of Distributions which Includes the Normal Ones,” *Scand. J. Statist.*, vol. 12, no. 2, pp. 171-178, 1985.

[146] A. J. Coulson, A. G. Williamson and R. G. Vaughan, “A Statistical Basis for Lognormal Shadowing Effects in Multipath Fading Channels,” *IEEE Trans. Comm.*, vol. 46, no. 4, 1998.

[147] W. Ahmed, J. Gao, D. Lai, and M. Faulkner, “On Generalized SINR bounds: A Steffensen’s Inequality Approach,” *To be Submitted in IEEE Transactions on Wireless Communications.*

[148] K. A. Hamdi, “On the Statistics of Signal-to-Interference Plus Noise Ratio in Wireless Communications,” *IEEE Trans. Commun.*, pp. 3199-3204, vol. 57, no. 11, Nov. 2009.

[149] I. S. Gradshteyn and I. M. Ryzhik, *Table of Integrals, Series and Products,* 6th ed. San Diego: CA, Academic Press, 2000.

[150] N. Balakrishnan and V. B. Nevzorov, *A Primer on Statistical Distributions.* John Wiley & Sons, 2003.

[151] Generalized Gamma Distribution [Online] Available: `http://www.http://functions.wolfram.com/GammaBetaErf/Gamma3/`

[152] M. D. Springer, *The Algebra of Random Variables.* New York: Wiley, 1979

[153] A. Goldsmith, *Wireless Communications*, Cambridge University Press, 2005.